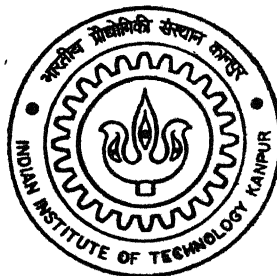# CHARACTERISTICS OF Cu ELECTRODEPOSITED ON TEXTURED Ni-Co ALLOY SUBSTRATE

By

Bijayani Panda

DEPARTMENT OF MATERIALS AND METALLURGICAL ENGINEERING

INDIAN·INSTITUTE OF TECHNOLOGY· KANPUR
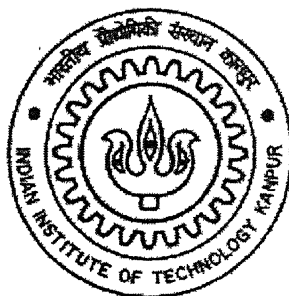
AUGUST, 2003

CHARACTERISTICS OF Cu ELECTRODEPOSITED ON TEXTURED Ni-Co ALLOY SUBSTRATE

*A thesis submitted in partial fulfillment of the
Requirements for the Degree of*

MASTER OF TECHNOLOGY

By

Bijayani Panda

to the

DEPARTMENT OF MATERIALS AND METALLURGICAL ENGINEERING

INDIAN INSTITUTE OF TECHNOLOGY, KANPUR-208016

AUGUST, 2003

CERTIFICATE

This is to certify that the work contained in the thesis entitled **Characteristics of Cu electrodeposited on textured Ni-Co alloy substrate** by Bijayani Panda (Roll No-Y120605) has been carried out under my supervision and to the best of my knowledge this work has not been submitted elsewhere for a degree.

Date: 31- 7 -03

Dr.R.K Ray

(Professor)

Department of Materials & Metallurgical

Engineering

Indian Institute of Technology

Kanpur

ACKNOWLEDGEMENT

Bijayani Panda

CONTENTS

LIST OF FIGURES

LIST OF TABLES

ABSTRACT

An attempt has been made to study the effect of deposition parameter (as current density) and the texture of the underlying Ni-Co alloy substrate on the characteristics of the electrodeposited copper film. For this purpose, a total of five Ni-Co alloys, Ni-10Co, Ni-20Co, Ni-30Co, Ni-40Co and Ni-60Co cold rolled to 95% reduction were taken. Out of the total number of cut pieces from any alloy, one half were subjected to annealing heat treatment at 800°C for 1 hour. Acid Copper Sulfate solution was used to plate the Ni-Co alloy plates (with copper plate as anode) at four different current densities of 1, 10, 30 and 50 mA/cm^2. The thickness of the electrodeposit was measured from the weight increase of the cathode after deposition. No difference was found in the thickness of the electrodeposited layer, for either the cold rolled or the annealed substrates. The chemical compositions of the substrates also do not seem to have any effect on the thickness of the electrodeposited Cu layer. X-ray diffraction of the copper layer on the Ni-Co substrate showed that for the cold rolled substrate Cu(111) and Ni(220) peaks are most intense and for the annealed substrate the Cu(111) and Ni(200) peaks as most intense, the intensity of the Ni peaks decreasing with increasing current density. From SEM, the surface topographies showed that the grain size of the copper deposit decreases with the increase in current density from 1mA/cm^2 to 50mA/cm^2. On increasing the current density, the average roughness value of Cu on annealed Ni-Co alloys decreases as compared to cold-rolled alloys.

CHAPTER 1

INTRODUCTION

Electroplating on articles is widely carried out for purposes such as appearance, protection, special surface properties and engineering or mechanical properties. Electroplating is an electrodeposition process which requires that the coating layer should be adherent to the basis metal during the useful life of the object. Because of the relative simplicity of obtaining highly purified copper metal and copper salts, copper has been a favorite of academic research, since studies can be made on highly pure materials without complications introduced by impurities or the necessity of using additives to obtain satisfactory deposits. The most widely used copper bath for electroplating is the copper sulfate bath.

In the present work, five Ni-Co alloys (Ni-10Co, Ni-20Co, Ni-30Co, Ni-40Co and Ni-60Co) in cold rolled and annealed condition have been used as substrates for electrodeposition of Cu. The textures of Ni-Co alloys have been studied previously. As the Co concentration increases, the SFE decreases drastically (for pure Ni, the SFE is 130mJ/m^2). Pure Ni shows a rolling texture of copper or pure metal type, in which the Cu {112}<111>, S {123}<634> and Bs {110}<112> are equally strong. In the Ni-Co alloys there is a texture transition from the copper type to the α-brass type at a cobalt content of around 40%. In annealed Ni-Co alloys having low SFE, the Bs texture transforms to {332}<113>. The compositions having higher magnitude of SFE (10, 20, 30%Co) yield {100}<001> cube texture. The intermediate composition Ni-40Co exhibits some amount of recrystallized cube texture with some amount of twin of cube texture {122}<212>.

Electrodeposited films have textures, which influence their electronic, magnetic, optical and other properties and are closely linked with their microstructures and surface morphologies. For example, the crystallographic texture of zinc layer deposited on steel influences the application properties such as deformation and friction behaviour and corrosion resistance. Hence it is necessary to understand how the texture of the substrate and the deposition conditions influence the property of the electrodeposited layer. In the present work, an attempt has been made to study the effect of deposition parameter (as

current density) and the texture of the underlying Ni-Co alloy substrate on characteristics of the electrodeposited copper film.

CHAPTER 2
LITERATURE REVIEW

2.1. Fundamentals of electroplating

Electroplating is defined as the "electrodeposition of an adherent metallic coating upon an electrode for the purpose of securing a surface with properties or dimensions different from those of the basis metal". The key word in the definition of electroplating is *adherent*. In the other two principal applications of electrodeposition –electrorefining and electrowinning- the deposit need be only sufficiently adherent to the cathode so that it does not fall off during the operation, whereas in electroplating the deposit becomes an integral part of the work and is expected to adhere to the basis metal during the useful life of the object.

2.1.1. Purpose of electroplating

The purposes for which articles are electroplated are (1)appearance, (2)protection, (3)special surface properties, or (4)engineering or mechanical properties.

Decorative plating is applied to enhance the appearance of the articles. For example, a thin coating of a metal such as chromium gives a pleasing appearance. Other electroplated metals used for decorative effects include gold, silver, brass, bronze, nickel, copper, and rhodium. *Protective plating* is applied to protect the substrate from corrosion. The common copper/nickel/chromium composite applied to automotive hardware, zinc coating to steel (to prevent it from rusting) and tin coating on steel cans for food and beverages are few of the examples of protective plating. Plating for *special surface properties* cannot be characterized by generalities: each use has its own particular reason for being. Light reflection is a surface property, which can be modified by coating; both silver and rhodium are used for this application. Gold and palladium plating are used for reducing the contact resistance between mating electrical and electronic assemblies. *Engineering and mechanical properties* that are of interest include hardness and wear resistance. This last category might be considered a subclass of the previous one, in that in both cases modification of physical properties is the aim of the coating process. They

are separated because in most of (not all) cases coatings for so-called engineering uses are thicker than the former, often quoted in millimeters (mm) rather than micrometers (μm). For example, chromium in thicknesses far greater than those used for decorative purposes, is used to face gun barrels and to form dies, rolls for papermaking machinery, etc.

2.1.2. Plating bath

The plating bath is practically always an aqueous solution containing a compound of the metal to be deposited. Nonaqueous solutions, in which the solvents may be an organic or inorganic liquid or a fused salt, are hardly of any commercial use; the only present exceptions are the plating of aluminum from an organic electrolyte, and refractory metals, such as tantalum, niobium, zirconium and tungsten plated from fused electrolytes.

Plating baths are of two general types; *acid* and *alkaline* Acid baths usually are solutions of relatively simple salts with little complex formation; alkaline baths are by their very nature complex, since the metal is contained in the anion. *"Neutral"* baths are sometimes added as a third type. They have a pH range of about 5 to 8, and they may be solutions of simple salts, as with nickel, or of complex ions as in the various pyrophosphate solutions.

2.1.3. Deposit Growth

The usual formulation of a metal deposition process, $M^{n+} + ne^- = M$ represents only the total stoichiometry of the reaction and does not take into account any intermediate steps between the beginning and the end of the process. Metals do not deposit as continuous sheets from one part of the cathode to the others. Metal ions, carrying with them their accompanying ligands (water molecules or complexing ions), attach themselves at certain preferred sites, losing in the process some of the water or other ligands, forming bonds with the cathode surface while their charges are partially neutralized.

These adions diffuse over the surface to various irregularities in the surface such as kinks, edges, or steps, where they are now incorporated into the metal lattice. As these

growth sites travel across the face of the crystal, monatomic growth layers are produced; they grow until they encounter adsorbed impurities, where they agglomerate to form growth stacks consisting of several layers. This lateral growth proceeds until several neighboring lattices meet to form a boundary at the contact lines; the individual structures thus formed are called *grains*. Further growth now proceeds outward, and the thickness of the deposit is thus built up.

2.1.4. Epitaxy

The structure of the basis metal often has an effect on that of the elctrodeposit, depending on a variety of factors. If the interatomic distances in the lattice plane of the substrate match those of the lattice plane of the deposit, the structure of the substrate may be continued into that of the deposit. This is called *epitaxy*, or *epitaxial growth*. Plating conditions often determine whether epitaxy will occur; if these conditions result in high overvoltages, produced, for example, by high current densities or some bath additives, three-dimensional nuclei may be formed which tend to overcome the relationship between the substrate and deposit. Conversely, elevated bath temperatures and low current densities, which permit the migration of atoms to sites where they can be incorporated into the existing structure, favor epitaxy.

2.1.5. Adhesion

Except for the special case of electroforming, in which it is desired to strip the electrodeposit from the substrate, electrodeposits are applied with the expectation that they will adhere to the substrate during the useful life of the article; and if proper operating practice is followed, this will be true. The first layer of deposited atoms engages the lattice forces of the substrate; the strength of the bond is approximately the same as that of the basis metal unless there is a major mismatch between the two lattices.

2.2. Fundamentals of Copper Plating

As would be expected from its position in the emf series, there is no difficulty in electroplating copper from aqueous solution. In fact, one of the problems is to prevent the formation of immersion deposits on less noble metals $Cu^{2+} + M \longrightarrow Cu + M^{2+}$. Such

immersion deposits are usually nonadherent and powdery. Such deposits can be avoided by reducing the activity of the copper ion by complexing it. The complexing agent universally used for this purpose is cyanide ion. There are several reasons why copper is used as a plating metal in large tonnages.

Because of the relative simplicity of obtaining highly purified copper metal and copper salts, copper has also been a favorite of academic research, since studies can be made on highly pure materials without the complications introduced by impurities or the necessity of using additives to obtain satisfactory deposits.

2.2.1. Applications for copper are [1] :

- As a coating prior to nickel-chrome.

- To eliminate deep scratches in base metal by heavy plating followed by polishing.

- Brazing.

- Repair.

- Electroforming.

- Drawing lubricant.

2.2.2. Properties of copper electrodeposits

- Bright.

- Ductile.

- Easily buffed.

- Conductivity (only exceeded by silver).

- Easily machined.

Three types of copper baths are in general use: *cyanide, acid (sulfate or fluoborate)*, and the *pyrophosphate* complex bath. Since in the present case, electroplating of copper on the five Ni-Co alloys was carried out from acid copper bath, only the acid copper plating has been discussed below.

2.2.3. Acid copper plating

Acid copper baths are based on copper(II) salts [2]. The acid copper solutions are very simple in composition, consisting only of a copper(II) salt and the corresponding acid, i.e., copper sulfate plus sulfuric acid, or copper fluoborate plus fluoboric acid. Such solutions produce a dense mat deposit; for some of the newer "bright acid copper" baths, proprietary addition agents and a small amount of chloride ion are added to sulfate bath. With these additions, the copper sulfate bath can be made to produce bright and leveling deposits. Copper(II) sulfate is available as the pentahydrate, $Cu(SO)_4.5H_2O$. Copper (II) fluoborate, $Cu(BF_4)_2$, is available only in the form of a solution concentrate, containing about 45% $Cu(BF_4)_2$ and some excess boric acid to prevent the formation of fluorides by hydrolysis.

Although copper(II) ions form weak complexes with sulfate, essentially the Cu^{++} ion in these baths is the simple aquo-ion and may be regarded as uncomplexed. Fluoborate solutions have not been studied extensively from the academic standpoint, but the fluoborate ion is known to be a very poor complexing agent, and the Cu^{++} ion in this solution is most likely also the simple aquo ion.

Excessive acid is needed in both baths for producing satisfactory deposits. These acids account for the high conductivity of the baths. Anode and cathode efficiencies are nearly 100 percent at practical current densities. The copper sulfate bath requires excess acid to improve conductivity (as stated earlier) and to prevent hydrolysis of the copper salts, precipitating copper hydroxide (or hydrated copper oxide). Increased copper concentration leads to increased resistivity of the bath, and cathode polarization increases somewhat when the copper concentration is above 1M (63 g/L Cu or 250 g/L $CuSO_4.5H_2O$). If the copper sulfate concentration is less than about 60 g/L, the deposit quality may deteriorate slightly. Sulfuric acid decreases the solubility of copper sulfate by *common ion effect*. Many addition agents are used for the copper sulfate bath for special purposes: increasing the limiting current density, reducing treeing, grain refining, or smoothing. Many brightening agents have been developed, including thiourea and some sulfur containing compounds. **Table 2.1** shows the composition and properties of a typical copper sulfate bath.

Table 2.1. Composition and properties of copper sulfate bath

	Average		Limits	
	g/L	Molarity	g/L	Molarity
Copper sulfate, $CuSO_4.5H_2O$	188	0.75	150-250	0.6-1.0
Cu as metal	48	0.75	38-63.5	0.6-1.0
Sulfuric acid, H_2SO_4	75	0.76	45-110	0.45-1.12
Temperature, ^{o}C	32-43		18-60	
Cathode cd, A/m^2	300-5000 depending on conditions			
Anode cd, A/m^2	to 1700			
Specific gravity, $25^{o}C$	1.165		1.115-1.21	
Resistivity, $\mu\Omega$-cm	4.2-4.3		-	

Copper anodes in sulfate solutions may become coated with films containing finely divided copper and copper oxide particles. Disproportionation (a redox reaction in which some atoms of a single element in a reactant are oxidized and others are reduced)[1] of Cu(I) to metal and Cu(II) ions may also lead to fine particles in the anode, causing intergranular corrosion and cathode roughness; any impurities such as arsenic, tellurium, selenium, lead and silver are insoluble and may lead to similar difficulties. Bagging of anodes is one method of avoiding the transfer of such articles to the cathode. Addition of phosphorus, in amounts from 0.02 to 0.04 percent, is claimed to increase the tenacity of the anode film and prevent the dislodgement of particles into the solution.

2.3. Effect of Processing Parameters on the nature of electrodeposited layer

2.3.1. Effect of Current Density

A number of research works have been published in the field of the effect of processing parameters on the nature and morphology of electrodeposited copper layer. Copper is being considered the material for semiconductor metallization because of its better conductivity, higher corrosion resistance in high temperature [7, 8, 9]. Cu electroplating process is characterized by excellent gap filling, high deposition rate, low temperature processing, system simplicity and process controllability [10]. Kim and Hong [11] have investigated the microstructures and textures of copper films deposited by electroplating on the WN diffusion barrier with the variation of deposition conditions by using a copper sulfate solution. In this study Cu was electrodeposited on WN coated silicon wafer. The bath solution used for copper plating was composed of $CuSO_4$ (160-200 g/l) H_2SO_4 (60-80 g/l). A silicon wafer with WN CVD coated was used for plating. Using a current density of $4A/dm^2$, $8 A/dm^2$ and $12A/dm^2$, it was found that the size of the surface grains decreased with increasing current density (**Fig. 2.1**).

In the study carried out by Cho and Szpunar [12], the influence of electroplating conditions on the texture and surface morphology of electrodeposits was investigated. The surface morphology for different current density (1, 50, 100 & 1000 mA/cm^2) were studied. It was found that a rough morphology is produced at a low current density and the surface of electrodeposits is more smooth as the current density increases. In other words, the surface morphology of electrodeposits is strongly affected by substrate texture
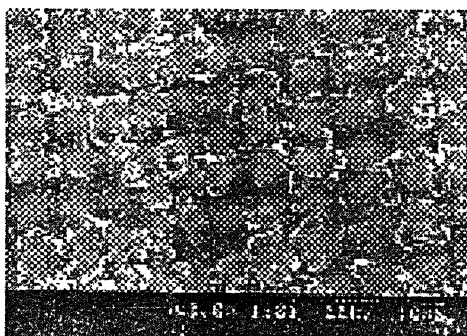
(a)
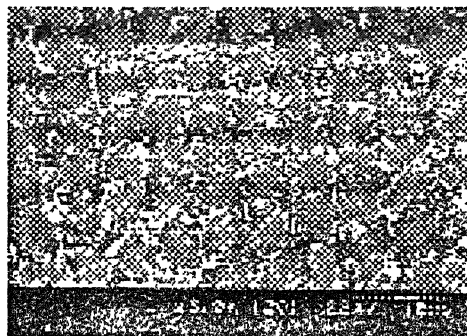
(b)
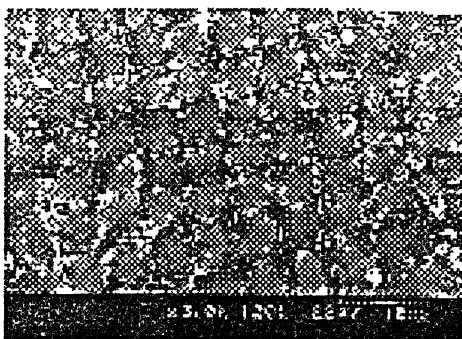
(c)

Fig. 2.1. Surface morphologies of copper electrodeposits with the change of current density. **(a)** 4A/dm^2, **(b)** 8A/dm^2, **(c)** 12A/dm^2 [11]

at low current density, however, the deposit surface is more smooth at high current density where the effect of substrate texture is negligible. The results obtained demonstrated that an increase of current density during electroplating will allow to generate more smooth surface morphology which is beneficial for better filling in the trench. Blauwe, De Boeck, Bollen and Timmermans [13] have focused on the influence of the electrodeposition processing parameters as current density on the zinc layer deposited on steel.

Electrogalvanised steel is used extensively in the automotive industry. Hence, the coating must be compatible with the fabrication process of the car body. The crystallographic texture of the zinc layer deposited on steel influences the application properties such as deformation and friction behavior and the corrosion resistance [14]. So it is necessary to understand what the optimum texture is and which process parameter have significant influence. These experiments show that the change in current density results in the change of the texture of the electrodeposited zinc layer. A higher current density involves an increase of percentage of high angle pyramidal and prismatic planes (**Fig. 2.2**). The graphs of the samples from laboratory electroplating show that the increase of prismatic and high angle pyramidal planes with higher current density is compensated by the decrease of the basal and low angle pyramidal planes. **Figs. 2.3, 2.4, 2.5** and **2.6** show the photographs of some typical zinc coating morphologies. They clearly reflect the change in morphology with increasing amount of basal planes. Above about 70% basal planes, the morphology changes drastically: more hexagonal zinc crystal plates grow parallel to the steel substrate.

Park and Szpunar [15] have demonstrated that the morphology and texture of zinc coatings significantly changes with current density. As the current density increases from 30 to 300mA/cm^2, the coating surface evolves from the morphology of hexagonal platelets and ridges to the pyramidal morphology, while the texture changes from the texture of the basal {0001} fiber and pyramidal {1013}non-fiber component (**Fig. 2.7a**) to the pyramidal {101X} fiber texture(**Fig. 2.7c & d**). Other deposition parameters were kept constant.
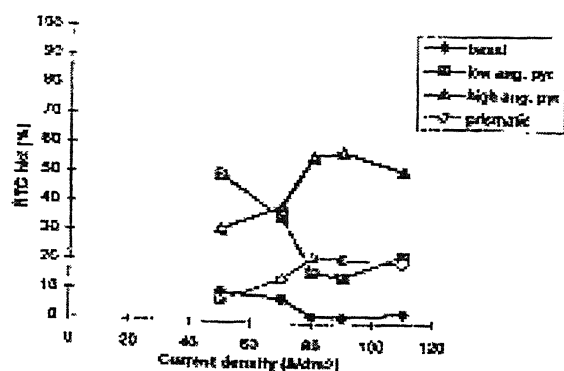
Fig. 2.2. Influence of the current density on the electrodeposited zinc texture on steel substrate [13]
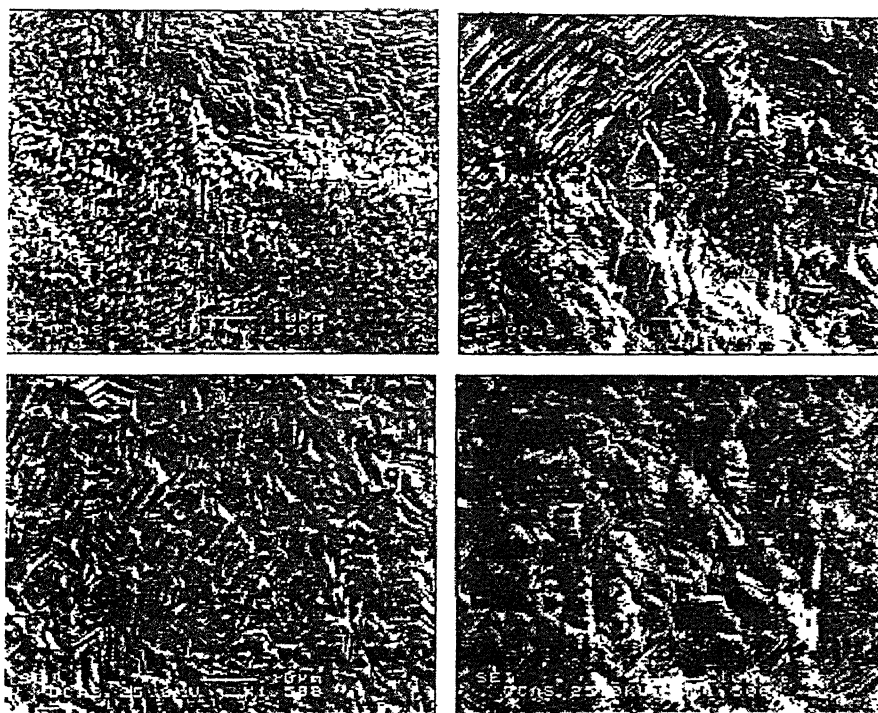
Figs. 2.3, 2.4, 2.5, 2.6. SE- images of Zinc coatings with 18% (upper left), 39% (upper right), 53% (below left) and 73% (below right) basal planes [13]
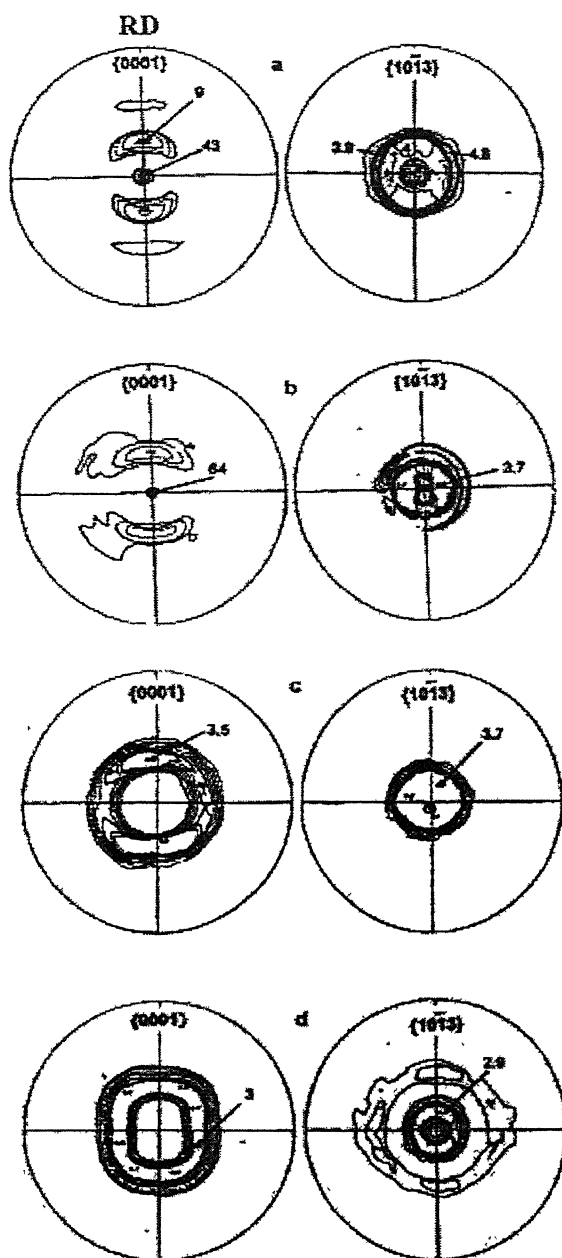
Fig. 2.7. The pole figures of zinc electrodeposited coatings deposited at different current density: **(a)** 30, **(b)** 300, **(c)** 400, **(d)** 500 mA/cm^2. The basal component completely disappears while the non-fiber pyramidal component evolves to fiber at high current density [**15**].

Correlation is found between the morphology and texture of zinc coatings. The morphology of hexagonal ridges represents the {1013} pyramidal non-fiber texture, while the morphology of hexagonal platelets represents the {0001} basal fiber texture. The morphology of pyramidal grains represents the {101X} pyramidal fiber texture.

2.3.2. Effect of pH

Park and Szpunar [15], have studied the influence of pH of the bath on the texture of the electrogalvanized zinc coatings. The electrodeposition was carried out in a bath of Zinc sulfate and the pH was controlled in the range between 1 to 5 by adding sulfuric acid or sodium hydroxide. The substrate was prepared from commercially cold rolled low carbon steel sheet and an electrolytic zinc plate was used as an anode.

In the above study it was demonstrated that the coating texture is sensitive to the pH of the bath. On the basis of the experimental results, it was concluded that the basal texture is predominant at low pH value, whereas the pyramidal texture is the main component at high pH values.

2.3.3. Effect of electrolyte speed

The change in electrolyte speed is also found to have an influence on the coating texture. In the zinc coating (on steel substrate) produced by laboratory electroplating [15], it is demonstrated that there is an increase in amount of basal and low angle pyramidal planes with higher electrolyte speed.

2.4. Effect of Substrate Texture on the nature of Electrodeposited layer
2.4.1. Determination of Texture

Stating the crystallographic orientation of each and every crystallite belonging to a polycrystalline material is very difficult. So it is customary to use statistical description instead. X-ray diffraction methods are now widely used to yield a collective determination of orientation over a large number of crystals. The material is first subjected to X-ray diffraction, and the intensity vs. angle data is recorded. The diffracted intensity data obtained from X-ray techniques are corrected for background intensity and adsorption. These are then normalized relative to intensity level of a random specimen.

Then these dataset are transformed from a linear scale to a polar plot, which is the pole figure. The dataset may then be represented by the use of either conventional or inverse pole figure or by means of mathematical functions.

There are certain defined directions in a specimen. In rolled sheet, for example, reference is given with respect to rolling direction (RD) and the sheet plane normal (ND). The pole figures must also contain some reference directions and these are usually chosen so that they correspond to the above defined directions in the specimen.

Pole figures are nothing but the stereographic projections, which show the distribution of particular crystallographic directions in the assembly of grains belonging to the metal. It is considered that the sheet is situated at the center of an imaginary sphere or the stereographic sphere with orthogonal reference direction as x, y and z –axis. The orientation of a single grain in the sample can be represented by plotting its three {100} poles at the appropriate angular positions relative to the reference directions. In reality all the poles concerned are projected on to the equatorial plane to produce a stereographic projection. The experimental procedure of the pole figure construction is briefly shown in **Fig. 2.8**.

There are a few limitations of pole figure. Although exhibiting all the texture components of a material, in a pole figure, the pole of particular texture is not pin pointed, rather it is scattered throughout a zone and it becomes difficult to distinguish them perfectly. The resolution of pole figure is poor. Also, it gives only some qualitative idea about the strength of a particular texture component.

In order to overcome these problems another technique is frequently applied. The data is represented numerically, which is known as *orientation distribution function* (ODF). It is easily understood that a frame of three mutually perpendicular axes can be superimposed on another frame of three mutually perpendicular axes. The same principle is followed here; the specimen frame as shown in **Fig. 2.9a**, is superimposed on the crystallographic frame by means of three successive rotations as shown in **Fig. 2.9b**.

The three rotations given to the frame are as follows:

1. A first rotation Φ_1 around ND transforms TD and RD into the new directions TD_1 and RD_1 respectively. Φ_1 has to have such a value that RD_1 will be perpendicular to the plane formed by ND and [001].

2. A second rotation Φ around the new direction RD$_1$ with Φ having such a value that ND transforms into [001] and TD to TD$_2$.

3. The third rotationΦ$_1$ with Φ$_2$ having such value that RD$_1$ transforms into [100] and TD$_2$ to [010].

Φ$_1$, Φ and Φ$_2$ completely represent the orientation of a particular texture. For every set of {hkl} <uvw> values, there is exactly one set of Φ$_1$, Φ, Φ$_2$ values. These three angles are represented in a three dimensional space where the three mutually perpendicular axes are the Φ$_1$, Φ, Φ$_2$ values varying from 0° to 90°. This three dimensional box is known as orientation space (**Fig. 2.9c**) and is widely used for texture notation [16].

The texture determination from ODF is by far more popular as it has better resolution, as stated earlier and also it allows the quantitative measurement of the strength of a particular texture component in volume fraction.

2.4.2. Rolling Textures of Nickel-Cobalt Alloys

The chemical compositions of the Ni-Co alloys (in weight percent) taken for the experiment work are given in **Table 3.1**. Both the nominal and detailed compositions of each alloy are shown in that table. For higher stacking fault energy, the stacking fault width is very low, and the stacking faults are easily constricted. In this situation, the cross-slip becomes easier and the material undergoes slip deformation rather than twinning. When the deformation is governed by slip mode, the deformation texture is generally copper type {112}<111>. For example, pure copper, pure nickel or nickel with low amount of cobalt, etc. The material with lower SFE predominantly exhibits Bs type of texture. For lower SFE, the stacking fault width is much greater, which makes it difficult to create any constriction within the stacking fault region and cross-slip becomes difficult. As a result of it, the critical resolved shear stress (CRSS) for twin becomes lower than that of slip and the plastic deformation is essentially governed by twinning process. In Ni-Co alloy system, the SFE significantly decreases on increasing the Co percentage (**Fig. 2.10**). Accordingly it is observed that the Cu component of rolling texture gradually decreases from pure nickel to Ni-30Co. Ni-40Co shows a transition from Cu type to Bs type rolling texture, and Ni-60Co alloy predominately exhibits Bs type texture.
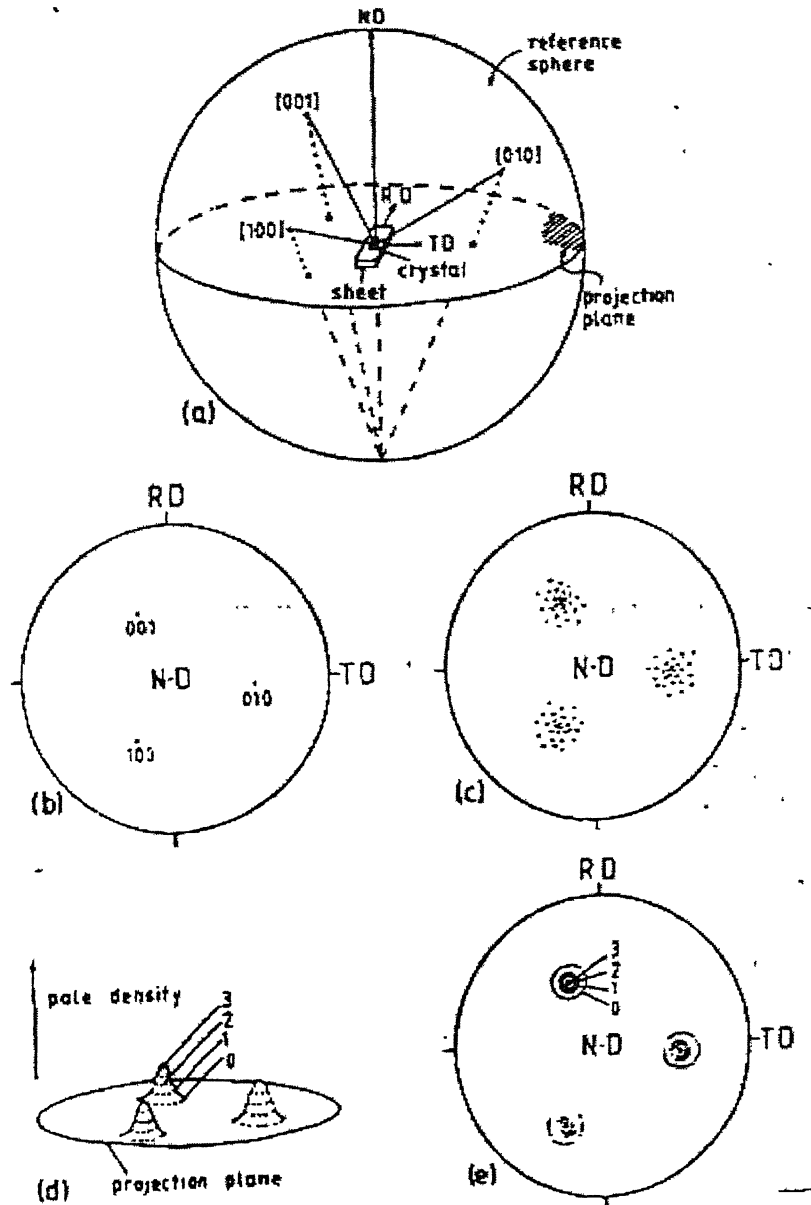
Fig. 2.8. **(a)** Position of sheet at the center of the stereographic sphere, **(b)** (100) Pole figure, **(c)** clustering of pole figure in certain areas revealing presence of preferred orientation or texture, **(d)** and **(e)** pole density as contour lines on the stereographic projection [Ref: **M. Hatherly and W.B. Hutchinson, 'An Introduction to Textures in Metals', p. 6, (1973), University of Birmingham, UK]**
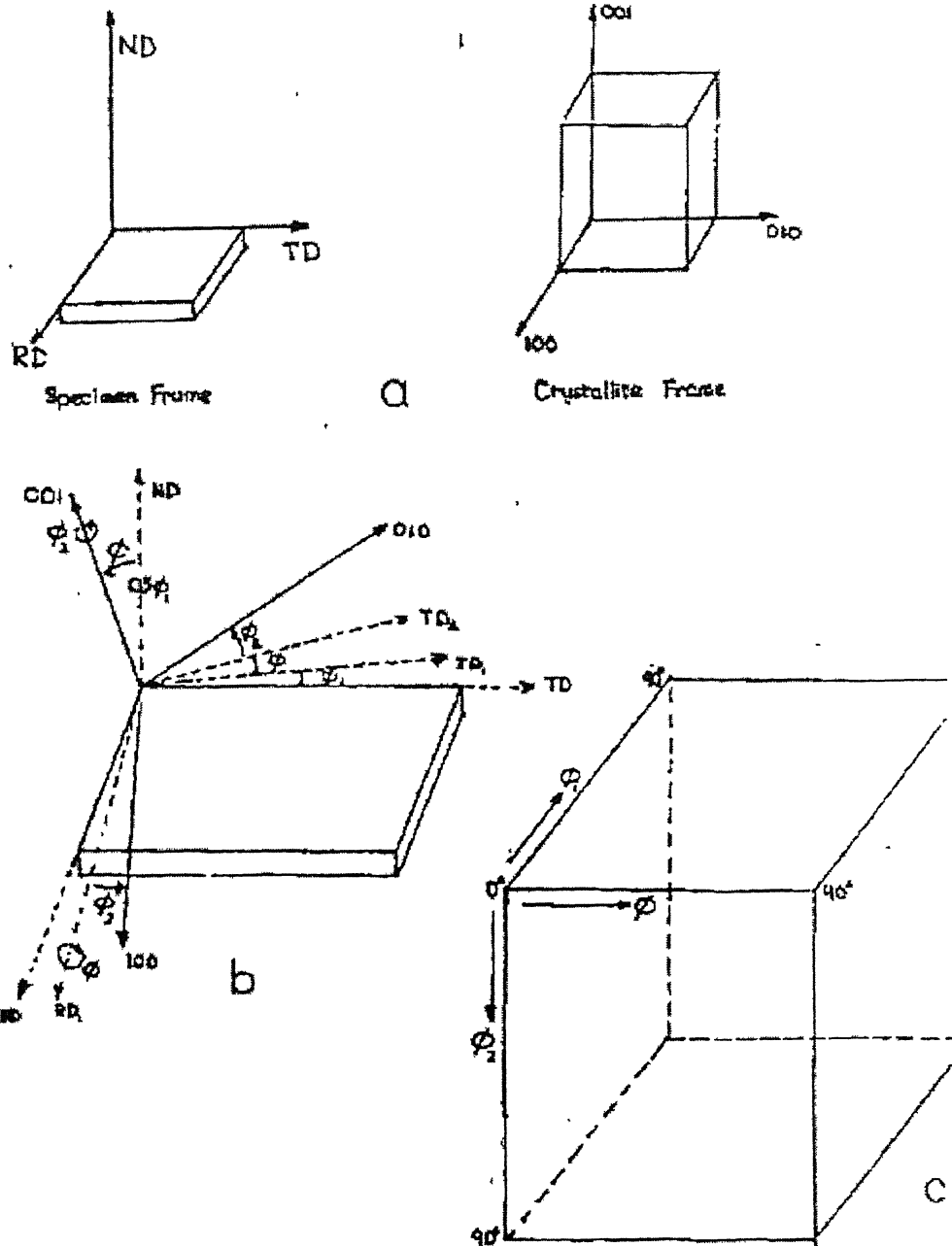
Fig.2.9. **(a)** Specimen frame and crystallite frame **(b)** The three rotations for superimposing crystallite frame on reference frame **(c)** Orientation space [**Ref: M. Hatherly and W.B. Hutchinson, 'An Introduction to Textures in Metals', p.6, (1973), University of Birmingham, UK**].
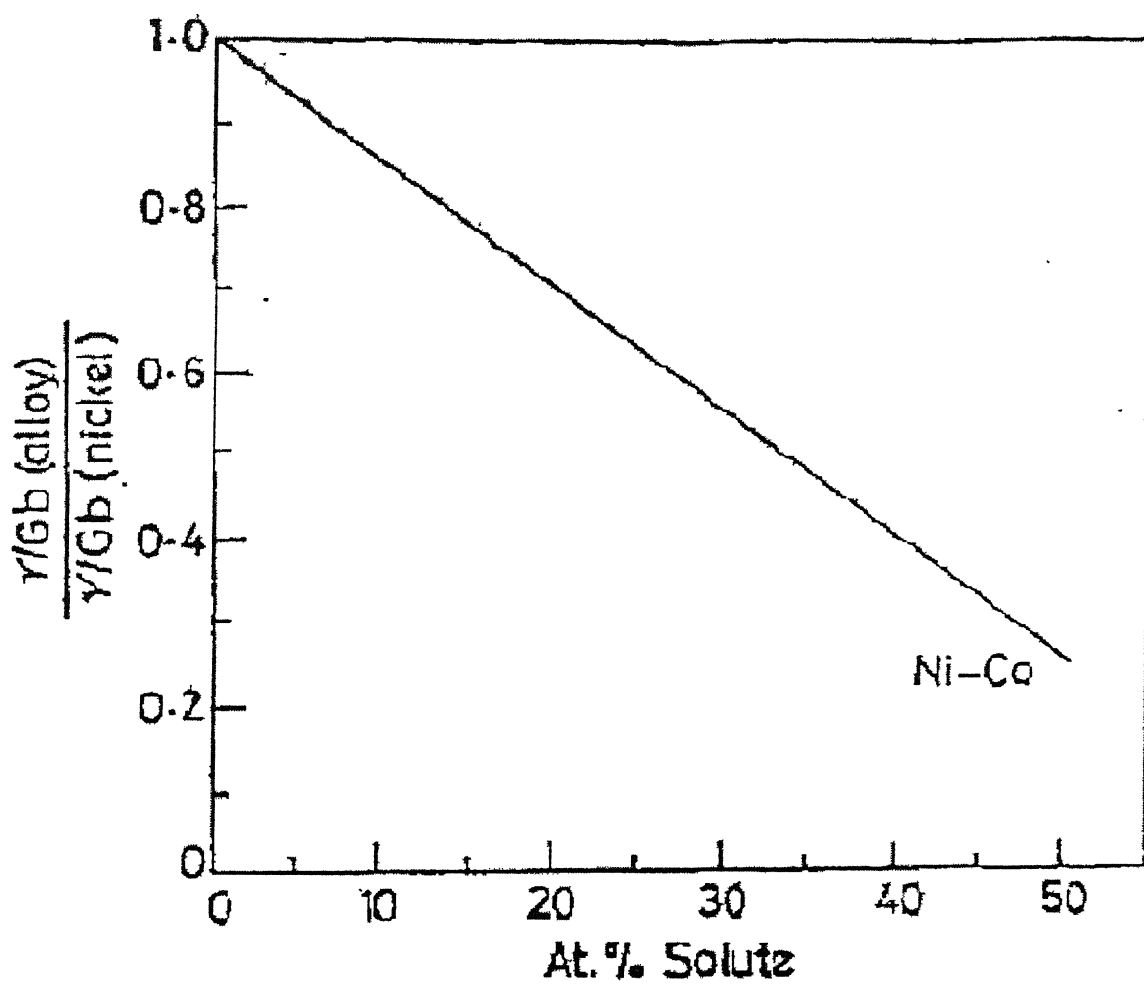
Fig. 2.10. Effect of composition on Stacking Fault Energy

It was also observed by Ray [17] that Cu type texture decreases with increasing amount of deformation. In case of Ni-40Co alloy, the intensity of Cu type texture remarkably decreased from 40% cold rolling to 95% cold rolling. The starting materials were cold-rolled by an amount of 95% reduction, textures of pure Ni **Fig 2.11(a)** and all the five Ni-Co alloys **2.11(b-f)** are shown by pole figures.

It is clear from the pole figures that the rolling textures of alloys b, c and d (with upto 30% Co) are rather similar to that of pure Ni (**Fig. 2.11a**). The rolling texture of the alloy f (with up to 60% Co) shows an α-brass or alloy type, whereas the texture of the alloy e (with 40%Co) shows features common to those of both the pure metal and alloy-type. Presumably in the Ni-Co alloys there has been a texture transition from copper type to the α-brass type at cobalt content of around 40%.

A total of nine major and minor texture components have been identified in pure Ni and the five Ni-Ço alloys under study from the analysis from ODF data. The standard nomenclature for the nine components and their {hkl}<uvw>, Φ_1, Φ, Φ_2 values as used by Ray [17], Hirsch and Lüke [18] and Virnich [19] are given in **Table 2.2.**
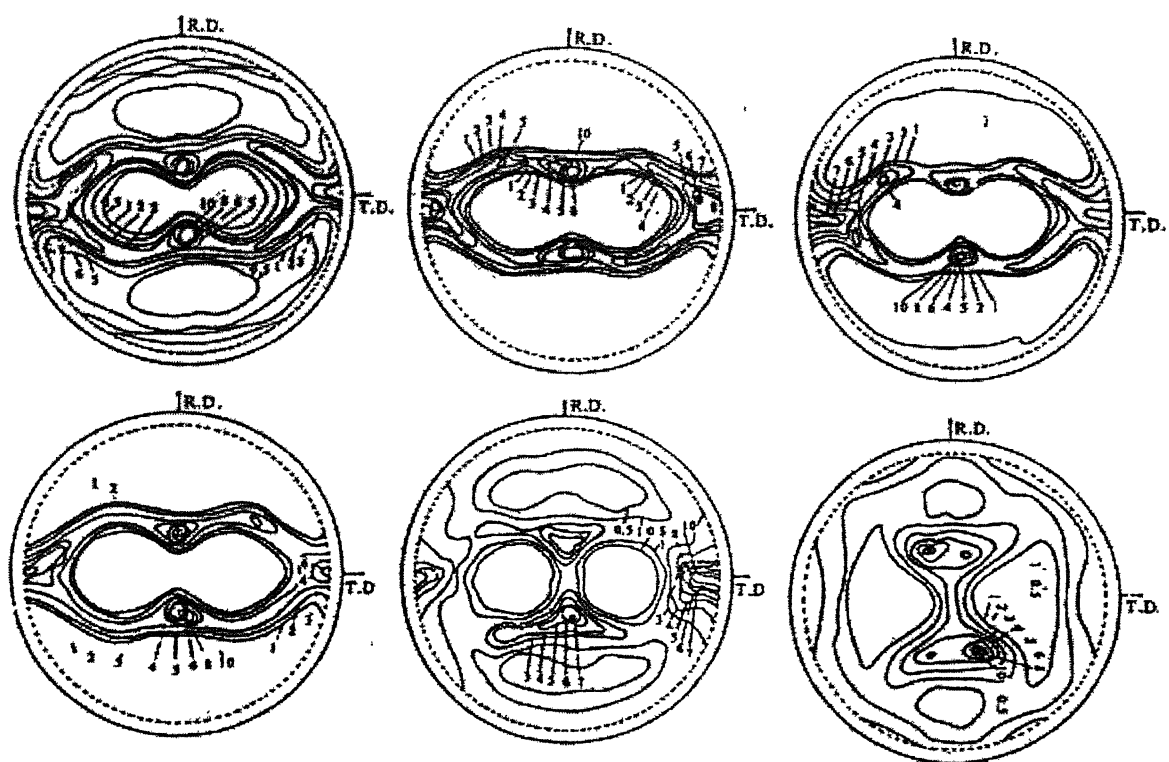
Fig. 2.11. {111}Pole figures showing the rolling textures of: **(a)** pure Ni; **(b)** Ni-10Co; **(c)** Ni-20Co; **(d)** Ni-30Co; **(e)** Ni-40Co; **(f)** Ni-60Co.

Table 2.2. Details of components identified in Ni-Co alloys

Name of Component	Symbol	{hkl}<uvw>	Φ_1, Φ, Φ_2
Copper	Cu	{112}<111>	(90, 35, 45)
Copper Twin-I	Twin Cu-I	{255}<511>	(11, 46, 74)
Goss	G	{011}<100>	(0, 45, 0)
S	S	{123}<634>	(59, 37, 63)
Brass	Bs	{011}<211>	(35, 45, 0)
Brass-Goss (auxiliary component)	B/G[1]	{011}<511>	(20, 45, 0)
P-(B_{ND}) (auxiliary component)	P(B_{ND})[2]	{011}<111>	(47, 45, 0)
Copper Twin-II	Twin Cu-II	{233}<311>	(23, 50, 56)
Brass-S (auxiliary component)	B/S[3]	{168}<211>	(45, 40, 75)

Cu Component

Out of the above components, the intensity of Cu component shows a steady increase in intensity with deformation in pure Ni and alloys of 10%, 20% and 30%Co. A transition in the nature of the Cu component is observed for 40%Co as stated previously and its intensity starts to decrease beyond 70% deformation leading to its complete absence in 60%Co. Cu is the most intense component in all cases except in Ni-40Co 95% and Ni-60Co. At high deformations of 90% and 95% a fall in intensity of this component is only observed beyond Co additions of 30%. Thus Ni-40 Co shows a transition of Cu component at high deformations of 90% and 95% , leading to its complete absence in Ni-60Co.

Twin Cu-I Component

The twin Cu-I component makes its appearance in the various alloys only after 90% deformation. It is completely absent in Ni-60Co. This component shows increase in intensity with deformation upto 30%Co, intensity slightly decreases in case of Ni-40Co beyond 90% deformation and it is completely absent in Ni-60Co. Thus twin Cu-I shows a transition with Co content. At any particular deformation this component does not show any change in intensity with Co addition.

G Component

The G component shows constant intensity in all alloys irrespective of % deformation. The intensity values are very low for the G component. For any particular deformation, intensity of the G component is maximum in case of Ni-40Co and at 95% deformation it is maximum in Ni-60Co.

S Component

The S component shows a steady increase in intensity with deformation for all alloys upto Ni-40Co, but at Ni-60Co the intensity stays at a constant value and does not change with the degree of rolling. Position wise the S component shows a considerable spread in Ni-60Co about the ideal orientation. At high deformation of 90% and 95%, an intensity fall is observed beyond 30%Co additions, same as that for the Cu component.

Bs Component

The Bs component also registers an increase in intensity with deformation for alloys upto 40Co with major increase for higher deformations of 90% and 95%. The

intensity shows a marked increase from 40% to 60%Co at any particular deformation. Bs is the most intense component in Ni-60Co and in Ni-40Co at 95% deformation.

B/G Component

The B/G component shows almost constant intensity with deformation in the various alloys. At any particular deformation it shows a slight increase in intensity with alloy additions upto Ni-40Co and then rises sharply to Ni-60Co.

P(B$_{ND}$)Component

P(B$_{ND}$) is completely absent in Ni-60Co. In pure Ni it is present upto 90% deformation but in other Ni-Co alloys it is only present till 70% deformation. It maintains an intensity about 5 times random in the various cases and does not show any trend of change with % deformation or wt% Co.

B/S Component

This component is absent in Ni-60Co. This intensity increases with deformation becoming as strong as the S and Bs component. At a particular deformation intensity of this component does not show any considerable variation with alloy additions upto 40% Co.

Twin Cu II

This component is only present in Ni-60Co and increases in intensity with deformation.

2.4.3. Annealing Textures of Nickel Cobalt Alloys

On annealing a deformed material, the rolling texture completely or partially changes to a new texture, which is the recrystallization or annealing texture. It is also observed that there is a one-to-one correspondence between the rolling texture and annealing texture. So it is can be inferred that the ultimate annealing texture of the material is dependent on the following factors:

(a) Deformation mode

(b) Degree of deformation

(c) Temperature at which the rolling is carried out

(d) Stacking fault energy

(e) Critical resolved shear stress for slip and twinning.

When the cold worked metal is annealed, the Cu type texture essentially changes to cube texture {100}<001>. This is a familiar phenomenon for the pure f.c.c. metals like Cu, Ni etc. except Al. The reverse effect is observed in case of Bs type rolling texture. On recrystallization it does not yield Cu type texture. In a series of Ni-Co alloys, it has already been observed that the compositions having higher magnitude of SFE (0, 10, 20 and 30% Co) yield cube texture. Composition of low SFE (Ni-60Co) does not yield cube texture, rather the Bs texture transforms to {332}<113> type texture. The intermediate composition Ni-40Co exhibits some amount of recrystallized cube texture along with some amount of twin of cube texture {122}<212>.

The formation of cube texture is not a desirable one so far as the material property is concerned. The formation of cube texture is a very fast process and just after the starting of recrystallization, the complete material immediately becomes highly anisotropic. But the reason for the dominating characteristic of cube texture and its actual origin is still not known. The pole figure of recrystallized texture and 95% cold rolled pure copper of the same have been shown in **Fig. 2.12 & 2.13** from which it is clearly observed that in the cold deformed alloy, a high density of material is oriented within a range of orientations near $(211)[1\bar{1}\bar{1}]$. In addition, substantial amount of material is also oriented near $(110)[1\bar{1}2]$ to $(100)[00\bar{1}]$. One of the theories of recrystallization says that the nucleus of recrystallization texture remains in the cold rolled structure itself as small crystallites, and during the course of recrystallization they just grow by consuming the highly strained region. This is the strain induced boundary migration theory (Block theory), which says that the nucleus of the cube texture should be present in the deformed structure itself, and it is observed that a small amount of material having orientations very near to the cube (100)[001] is also present. **Fig. 2.12** shows that most of the material has cube orientation for fully recrystallized alloy. The twin related component of the cube texture also appeared, around $(221)[2\bar{1}\bar{2}]$. In addition small amounts of materials are also found having orientation spread over from $(531)[2\bar{3}1]$ to $(553)[5\bar{2}\bar{5}]$.
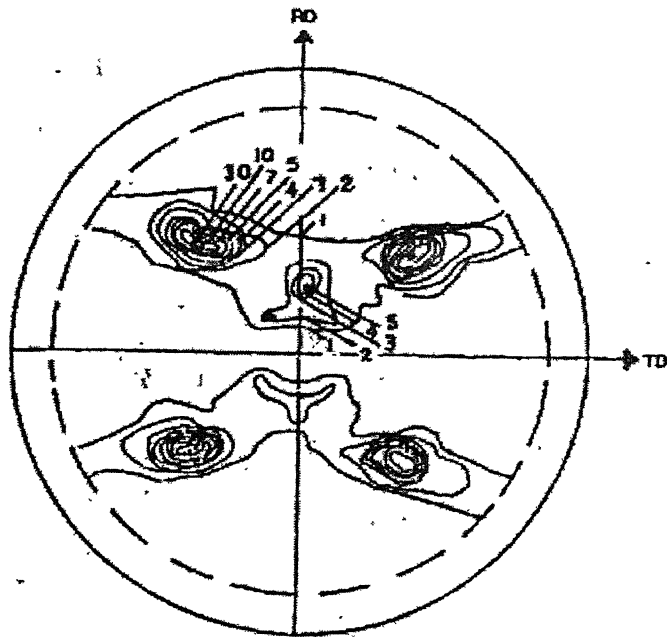
Fig. 2.12. Cube type annealing Texture
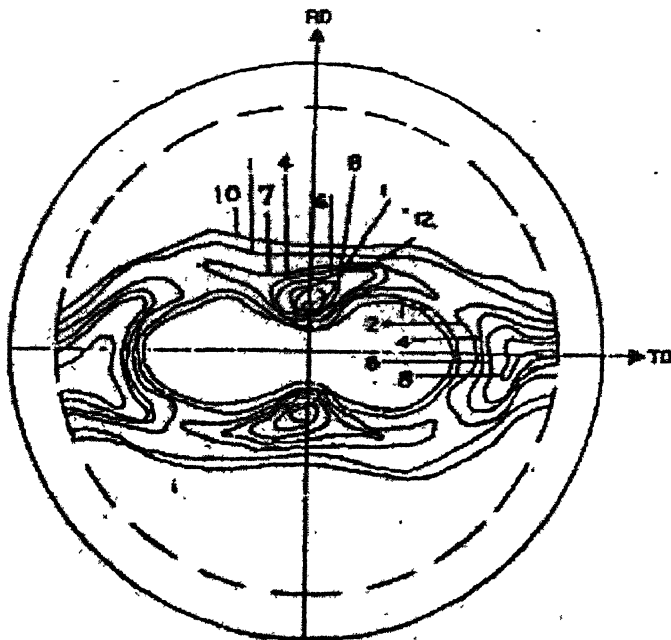
Fig. 2.13. Cu type rolling Texture

2.4.4. Effect of Substrate Texture on:

2.4.4.1. Morphology of electrodeposited layer

Electrochemical deposition techniques are utilized increasingly in the fabrication of micro-components, for example Cu-interconnects [20-24], mainly because they represent inexpensive alternatives to physical or chemical vapour deposition techniques. One of the parameters of major importance for the fabrication of micro-components is the influence of the substrate on the microstructure that develops in the electrodeposited layer. Somers [25] has carried out experiment in which Cu layers were electrodeposited from an acidic copper electrolyte onto two distinct substrate materials important for micro-component industry: an Au layer with a pronounced <111>-texture, and a nano-crystalline Ni-P layer. Au and Ni-P deposited on Si-wafers were used as substrate for deposition of copper. All depositions were carried out at a current density of $3A/dm^2$.

The evolution of surface topography, and morphology in the layers were investigated with SEM and TEM respectively. Distinct surface topographies, as obtained from Scanning Electron Micrographs, were observed for Cu layers deposited on the Au and Ni-P substrates. Deposition onto the Au substrate resulted in a very smooth surface of all Cu layers, whereas the Ni-P substrate caused an irregular surface for 3-μm-thick layers of Cu. For the 12-μm-thick Cu layers on top of Au and on top of Ni-P the opposite tendency is observed: the smoothest surface is obtained for Cu on top of Ni-P (**Fig. 2.14**).

From TEM studies it was found that the morphology of the Cu grains on the Au specimen changes considerably with distance from the Au /Cu interface. At various locations the grains close to the interface with Au are roughly equiaxed with a grain size of less than 0.5μm. At 2-4μm into the Cu deposit, **Fig.2.15a**, the grains are still predominantly equiaxed, but with a grain size of around 1μm. A clear changeover to columnar, highly twinned, grains (**Fig. 2.15b**) occurs at this depth, the columnar twinned morphology persists to the surface of the deposit. The column boundaries are orientated within about 20° of the growth direction. Secondly, at the Au/Cu interface cavities are seen that vary between 2 and 10nm and they do not appear to be restricted to a single plane at the interface, but they occur over a zone of about 20nm in thickness (**Fig. 2.16a**). Secondly, the Au/Cu interface is seen not to be planar, but shows 'mounds' (**Fig. 2.16b**). On the other hand the Cu grains are approximately equiaxed both near to the interface

(a) 3 μm Cu on Au   10 μm

(c) 12 μm Cu on Au   10 μm

(b) 3 μm Cu on NiP   10 μm
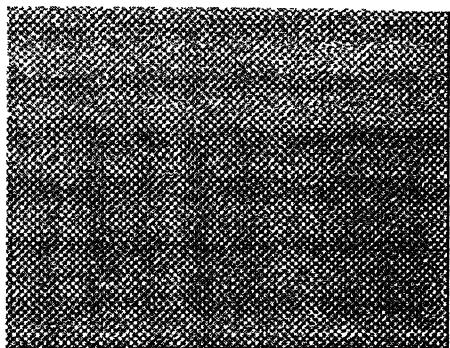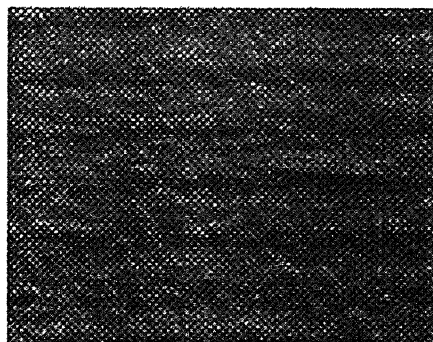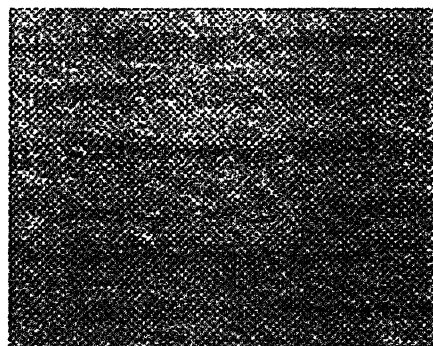
(d) 12 μm Cu on NiP   10 μm

Fig. 2.14. SEM micrographs showing the topography of as-deposited Cu layers of 3μm **(a)** and **(b)** and 12μm copper **(c)** and **(d)** deposited onto a substrate of Au **(a)** and **(c)** and Ni-P **(b)** and **(d)** [25].
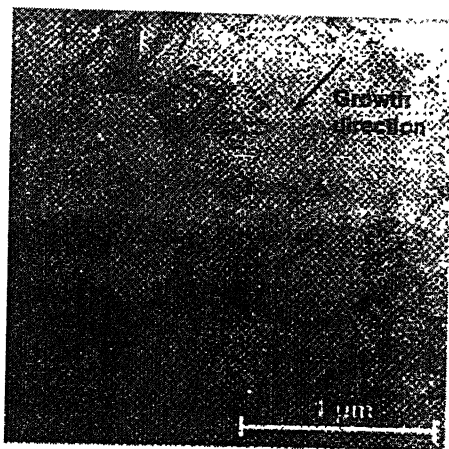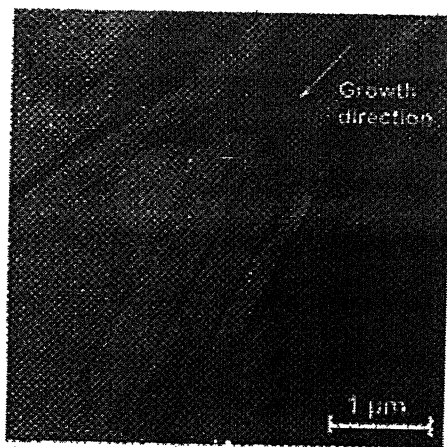
(a)   (b)

Fig. 2.15. TEM micrographs of Cu on Au. In **(a)** which is obtained in the Cu layer at 2-3 μm away from the Au/Cu interface, the Cu grains are equiaxed. In **(b)**, which was obtained at 10 μm away from the Au/Cu interface, the Cu grains are strongly columnar with many twins oriented both parallel and inclined to the direction of growth of the layer. The surface of the Cu layer, in the bottom left corner of the micrograph, is strongly faceted.
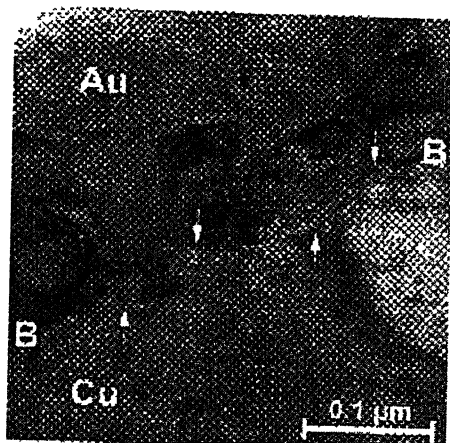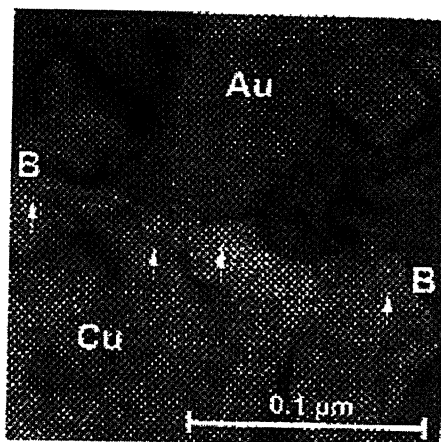
(a)   (b)

Fig.2.16. TEM micrographs of Cu on Au, showing cavities (arrowed) at the Au/Cu interface. **(a)** The approximately circular cavities are seen to occur in a narrow band parallel to the interface. **(b)** The Au/Cu interface is shown to be non-planar and to have 'mounds' on the scale of the Au grains. [25]

and well into the deposit. Secondly, the interface between Ni-P and Cu is extremely planar, and there is no indication of cavities at, or near to, this interface.

2.4.4.2. Thickness of Electrodeposited layer

Park and Szpunar [15] have shown that there is a significant effect of texture of underlying substrate on the coating with increase in coating thickness. As stated earlier, they have studied the zinc coatings on steel. The substrate was commercially cold rolled low carbon steel sheet and electrodeposition was carried out from a zinc sulfate bath. In the above experiment it was observed that the pyramidal texture disappears as the coating thickness increases from 0.6 to 100μm. It was suggested that the formation of the pyramidal non-fiber texture {1013} is due to the influence of the substrate. Based upon this suggestion, it was inferred that the strong pyramidal texture for the thin coatings are induced by the influence of the substrate. A decrease in pyramidal texture intensity with a thickness increase indicates that the influence of the substrate is weaker.

As the coating thickness increases, the morphology of the zinc coatings evolves from the sub-micron sized particles to the thin hexagonal ridges, then to the packets of thicker hexagonal platelets and finally to the hexagonal columnar crystals. Other parameters, pH and current density were kept constant.

The microstructural evolution of electroplated Cu films with thickness values ranging from 0.89 to 3.0μm have been investigated by Pérez-Prado and Vlassak [26]. Here copper thin films of different thickness were deposited onto <100> Si single crystal substrates. Bare Si substrates were first coated with a 1000 Å LPCVD SiN, film and a 200 Å PVD TaN barrier layer. Cu films were then deposited to various thicknesses by means of a standard electroplating process used in semiconductor industry [27-28]. Immediately prior to electroplating, a very thin Cu layer was sputter deposited onto the TaN to act as a seed layer for the electroplating process.

The microstructure of the electroplated Cu films was found to be highly dependent on film thickness. **Fig. 2.17** shows the grain structures for Cu films, 3.0μm (**Fig. 2.17a**), 1.81μm (**Fig. 2.17b**) and 0.89μm (**Fig. 2.17c**) thick. The texture of the Cu films varies significantly with film thickness. As shown in **Fig. 2.18**, the texture of the 3.0 μm film is formed by <111>, <100> and <110> fibers, as well as a strong random component. **Fig.**

2.18a shows a cross-section through the X-ray ODF at constant Φ_1, in which the three fiber components are indicated. The maximum intensities corresponding to the <111>, <100> and <110> fibers are 16, 8 and 5 respectively. The presence of a significant amount of grains with random orientations can be best appreciated in Fig. **2.18b**, where the discrete (111), (200) and (220) pole figures derived from the EBSD measurements have been represented. Good agreement between the micro and macro-textures indicates that there is no significant texture gradient across the film thickness.

As the film thickness decreases, the <111> fiber becomes stronger and the random component decreases. **Fig. 2.19** shows the texture of the 0.89μm film, which is clearly dominated by a sharp <111> fiber. The predominance of <111> oriented grains can be appreciated in **Fig. 2.19a**, in which the macrotexture of the 0.89μm film has been represented by means of a cross-section at constant Φ_1 through the ODF. The intensity of the <111> fiber component has increased with respect to that of the 3.0 μm film reaching a value of 32. The intensities of the <100> and <110> fiber components are now 8 and 3, respectively. The X-ray texture data are consistent with the microtexture presented in **Fig. 2.19b**.

2.4.4.3. Texture of Electrodeposited layer

The texture of electroplated layer is found to be strongly dependent on the underlying substrate texture. Much work has been carried out to investigate the effect of substrate texture on the texture of the electrodeposit. Park and Szpunar [15] have shown that when the coating thickness is very less, the formation of pyramidal non-fiber texture in the zinc coating on steel is due to the influence of the substrate. A decrease in pyramidal texture intensity with a thickness increase indicates that the influence of the substrate is weaker.

The texture of electroplated Cu is highly depended on the characteristics of underlying barrier and seed layers in Damascene process. A smooth and strongly textured Cu seed layer is needed to promote the development of highly textured, large grains in the electroplated Cu film [29]. If the seed layer has a strong (111) texture, the electroplated Cu film also has a strong (111) texture as illustrated in **Fig. 2.20**, in which
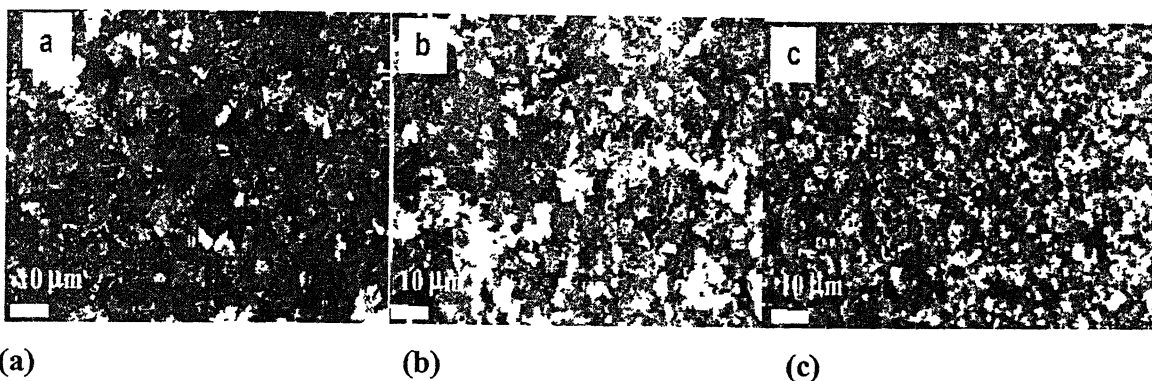
Fig. 2.17. SEM micrographs showing microstructure of the Cu thin films after deposition. Backscattered electron imaging mode.(a) 3.0 μm (b) 1.81 μm (c) 0.89 μm [26]

▲ <111>

■ <100>

● <110>

(a)   (b)
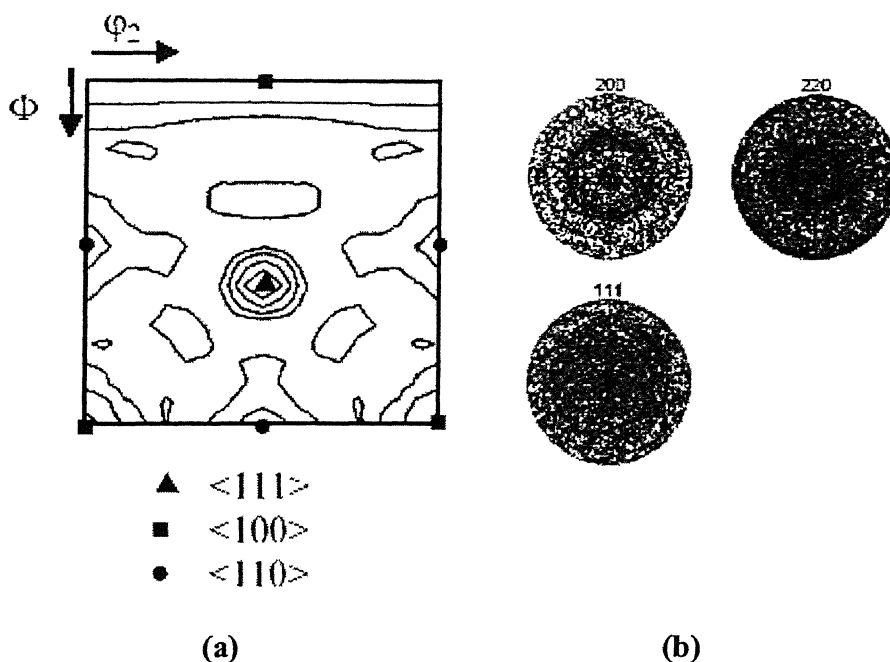
Fig. 2.18. Texture of 3.0 μm copper thin films. **(a)** Macrotexture: Φ_1= constant section of the ODF (levels: 1, 4, 8, 12, 16) **(b)** Microtexture: (200), (220) and (111) discrete pole figures [26]
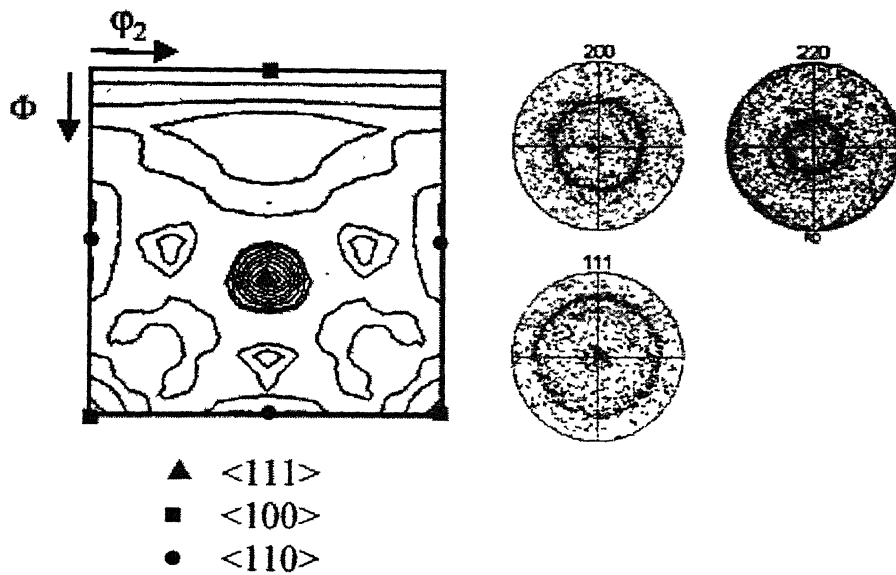
Fig. 2.19. Texture of the 0.89 μm thick Cu film. **(a)** Macrotexture: Φ_1= constant section of the ODF (level: 1, 4, 8, 12, 16, 20, 24, 28, 32); **(b)** Microtexture: (200), (220), and (111) discrete pole figures [**26**].

Table 2.3. Summary of Film Characteristics

Cu	Underlayer	Sample	Film Structure	$I_{(111)}/I_{(200)}$
Seed Layer Only	Ta	#1-s	Sputtered Cu/Ta	64.6
		#2-s	Sputtered Cu/Ta	1.9
		#3-s	Sputtered Cu/Ta	34.5
		#4-s	Sputtered Cu(air break)/Ta	4.0
	TiN	#5-s	Sputtered Cu/TiN/Ti	4.1
		#6-s	Sputtered Cu/TiN/Ti	16.7
		#7-s	CVD Cu/TiN/Ti	2.0
With Electroplated Cu	Cu/Ta	#1-p	Electroplated Cu on #1-s	24.3
		#2-p	Electroplated Cu on #2-s	9.8
		#3-p	Electroplated Cu on #3-s	56.9
	Cu/TiN	#5-p	Electroplated Cu on #5-s	2.4
		#6-p	Electroplated Cu on #6-s	34.4
		#7-p	Electroplated Cu on #7-s	3.7

the datum represents an electroplated Cu film and the corresponding Cu seed layer. The Cu seed layers were deposited under different conditions to achieve different texture and surface conditions. As shown in **Table 2.3**, a strongly textured seed layer promotes the growth of a similar texture in the electroplated film. The (111) texture is quite weak for samples #5-p and #7-p.

In the study carried out by Cho and Szpunar[12], pure polycrystalline copper substrate samples which have different textures were taken as follows: (i)po6, weak (110) texture, (ii)po8, strong (100) texture and (iii)po9, strong (100) and (111) texture. The change in maximum intensity are plotted and shown in **Fig. 2.21**. In specimen that has a weak (110) texture, there is no clear difference in the maximum intensity as current density increased. However, in the specimen which has a strong (100) texture, the highest maximum intensity is for the current density $1mA/cm^2$ and this intensity decreases as the current density increases. In the specimen having strong (100) and (111) texture, the texture data is scattered.

2.5 Objective of my work

In the present study, an attempt has been made to study the effect of current density and the texture of underlying substrate on the electrodeposited copper. Five Ni-Co alloys, Ni-10Co, Ni-20Co, Ni-30Co, Ni-40Co & Ni-60Co were used in the cold rolled (95%) and annealed condition as substrate for the electrodeposition. The five alloys have different textures in cold rolled and annealed conditions. Their textures have been previously evaluated. The objective of the present study was to find out any correlation between the texture of the substrate on the morphology, surface roughness and the texture of the electrodeposited copper layer and to find out the overall effect of current density on the above parameters.
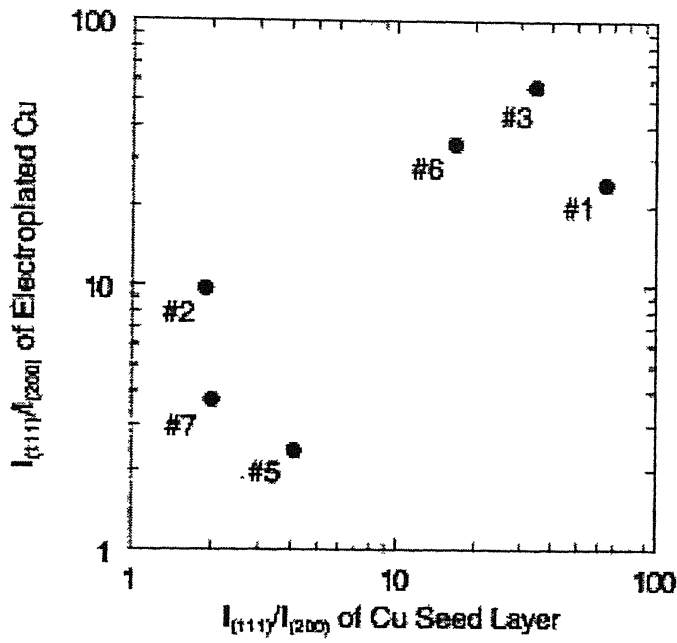
Fig. 2.20. Correlation between textures of seed layer and electroplated Cu film [29].
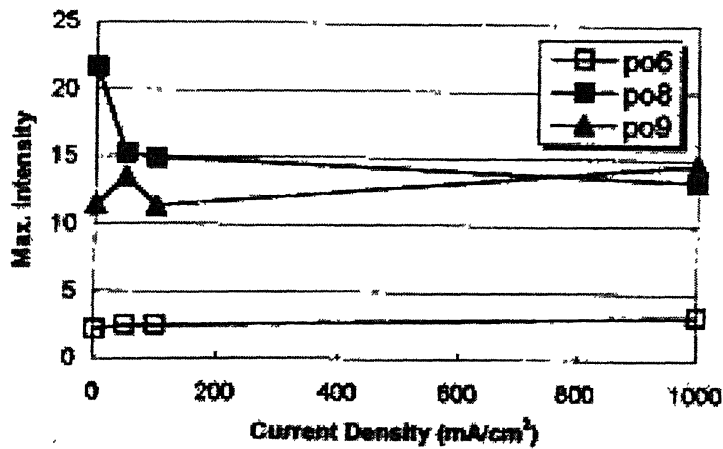
Fig. 2.21. Maximum intensity of inverse pole figure in electroplated copper as a function of current density (po6, po8 and po9 specimens) [29]

CHAPTER 3
EXPERIMENTAL PROCEDURE

For the present investigation, five Ni-Co binary alloys were selected on which copper was electroplated. The chemical compositions of the alloys (in wt%) used in the present study are given in **Table 3.1**. Both the nominal and detailed compositions of each alloy are shown in that table. A total of five Ni-Co alloys, Ni-10Co, Ni-20Co, Ni-30Co, Ni-40Co and Ni-60Co were melted under vacuum. Segregation was avoided by magnetic stirring during melting. The ingots were cold rolled 50% to a thickness of 10mm and then homogenization annealed in vacuum at 1150^0C for 24 hours. These were then again cold rolled 50% and annealed at 1100^0C for a period of 3 hours to yield the starting materials of almost random texture and a grain size of 0.1 mm.

3.1. Cold Rolling

The starting materials were then cold-rolled by an amount of 95% reduction, using a laboratory rolling mill having 250 mm diameter rolls. Strips cut from the thick sheets were cold rolled. The directions of the strips were reversed end to end after each pass. In between any two successive passes, the strips were dipped into cold water bath to minimize any unwanted rise in temperature. The change in thickness after each pass was noted. In order that homogeneous deformation throughout the specimens might be achieved, the ratio of the length of contact with the rolls to specimen thickness was maintained at a value greater than unity[30]. Reproducible texture was found over almost the whole of the thickness except in a very narrow zone near the outermost surface. From each specimen, material was etched off from one side up to the mid-thickness section on which all texture measurements were carried out. These cold rolled alloys were made available for the purpose of this thesis work along with the relevant texture plots.

Table 3.1. Chemical compositions of Ni-Co alloys (wt%)

Alloy nominal composition		Detailed composition (wt%)					
		Co	C	S	Si	Cu	Ni
A	Ni-10Co	11.15	0.006	0.003	0.03	0.03	Bal.
B	Ni-20Co	22.85	0.007	0.003	0.06	0.03	Bal.
C	Ni-30Co	30.90	0.006	0.003	0.03	0.03	Bal.
D	Ni-40Co	41.05	0.006	0.004	0.03	0.03	Bal.
E	Ni-60Co	60.50	0.006	0.004	0.06	0.03	Bal.

3.2. Recrystallization anneal

From the cold rolled strips of the five alloys, samples of dimensions 14 mm x 25 mm were cut. Out of the total number of cut pieces from any alloy, one half were subjected to annealing heat treatment at 800°C for 1 hour in a Horizontal Tube furnace using argon atmosphere for complete recrytallization. After heat treatment, the samples were cooled in the furnace. The textures measured from the recrystallized samples were also made available for the purpose of this study. All the textures, for both cold worked and recrystallized samples, were in the form of pole figures.

3.3. Material preparation for electroplating

3.3.1. Organic degreasing

The cold-rolled and annealed samples were cleaned first with an organic solvent and then with an alkali solvent. The organic solvent used for the removal of greases and waxes in the present case was Trichloroethylene (C_2HCl_3). The metal was immersed in the liquid and gently scrubbed with a swab for 5-10 minutes to ensure effective degreasing.

3.3.2. Alkali degreasing

Samples cleaned with organic solvents were again subjected to degreasing in an alkali solution. The composition of the alkali solution is given below. The temperature of the solution was kept at 70-90°C and degreasing was carried out for 10-30 minutes.

Alkali degreasing solution:

NaOH	20-30 g/l
Na_2CO_3	25-30 g/l
Na_2SiO_3	3-10 g/l

3.4. Electroplating

Additive-free acid copper plating solution was used for plating, which was composed of $CuSO_4.5H_2O$ (188 g/l) and H_2SO_4 (75 g/l). The experimental Ni-Co alloy plates of dimension 14 mm x 25 mm were used as cathode after careful surface preparation. High purity copper metal plates were used as anode. The distance between

cathode and anode was maintained at 6 cm. Four different current densities of 1, 10, 30 and 50 A/cm^2 were used for plating and the bath temperature was kept at room temperature. The bath was stirred at constant speed and controlled to maintain a pH of 3.0. Time of electroplating was kept constant at 10 minutes for each case. Each of the five Ni-Co alloys (both cold-rolled and annealed) was electroplated at the four different current densities as stated above. After deposition, the Ni-Co alloy plate was washed and dried carefully.

3.5. Measurement of thickness of deposit

The thickness of the electrodeposit was measured from the weight increase of the cathode after deposition, using the relationship:

$$t = W/\rho A$$

where t is the thickness of the deposit , W is the increase in weight of the cathode plate after electrodeposition, ρ is the density of copper and A is the surface area of the cathode.

3.6. X-ray diffraction

X-ray diffraction of the electrodeposited copper layer on the Ni-Co substrate was carried out using a SIEFERT IS0-DEBYEFLEX 2002 X-ray diffractometer equipped with a Cu-tube. Samples of 14 mm x 25 mm were scanned in a 2θ range of 35° to 150° at a sweep rate of 3°/ minute. The three most important peaks from each phase were analyzed and these values were matched with the values in the relevant ASTM index cards for textureless pure copper and pure nickel.

3.7. Scanning electron microscopy

The surface topographies of the Cu layers on the annealed and cold rolled Ni-Co alloy substrates were investigated with a JEOL JSM 840A Scanning electron microscope, operating at 15KV accelerating voltage, using the secondary electron signal. The specimens were investigated in the as-deposited condition without any additional preparation.

3.8. Surface roughness measurements

In order to look at the effects of current density and the substrate texture on the Cu electrodeposit, the surface roughness measurement was carried out using a FEDRAL SURFANALYZER 5000. The cut-off for all the measurements was 0.8 mm. Drive speed of probe was 0.25 mm/sec and the probe range was +/- 50 microns. The main roughness parameters measured under the present case were R_a (central line average), R_q (root mean square value), and R_y (peak to valley height). Out of the three parameters, the central line average was used for comparing the relative roughness of the electrodeposited layer as function of the current density as well as the composition of the Ni-Co substrates.

CHAPTER 4

RESULTS AND ANALYSIS

4.1. Measurement of thickness of deposit

The thicknesses of copper deposits on the Ni-10Co alloy as a function of the current density, in both annealed as well as cold rolled conditions are shown in **Fig. 4.1(a)**. Similarly, for Ni-20Co, Ni-30Co, Ni-40Co and Ni-60Co alloys, the thicknesses of the electroplated copper layers are plotted in **Figs. 4.1(b)-4.1(e)**. As expected, the thickness of the electroplated copper layer increases with the increase in current density for all the alloys. There is hardly any difference in the thickness of the electrodeposited layer, for either the cold rolled or the annealed substrates. The chemical compositions of the substrates also do not seem to have any effect on the thickness of the electrodeposited Cu layer.

4.2. XRD Results

4.2.1. Cold rolled Ni-Co alloy substrate

The XRD pattern of the electrodeposited Cu layers on Ni-Co alloy, cold rolled 95%, are shown in **Fig. 4.2- 4.6**. As stated previously, four different current densities, 1, 10, 30 and 50 mA/cm^2, were used to electrodeposit copper over the alloys. The X-ray data are also represented in a tabular manner in **Table 4.1- 4.5**. The examination of any of the XRD patterns has indicated the presence of diffraction lines from both the electrodeposited Cu as well as from the Ni-Co alloy substrate. The three most intense lines for each of the above phases in the patterns are represented in terms of the d-values and relative intensities.

Ni-10Co alloy substrate

The (111), (200) and (220) peaks of both Ni-10Co and copper have been shown in the XRD plots (**Fig. 4.2**). At a current density of 1mA/cm^2, out of the Cu peaks, (111) peak is most intense. At a current density of 10mA/cm^2, the (220) line of copper is most intense followed by (111) and (200) lines. Hence, there is a change in order of relative intensities for the three lines as compared to that at 1mA/cm^2. The same order is followed

at current densities of 30mA/cm^2 and 50 mA/cm^2 as far as the relative intensities of the (111), (200) and (220) peaks of Cu are concerned.

The (220) peak of Ni-10Co is most intense for the electroplated alloy at all current densities. But there is a decrease in the peak intensities of all the three lines as we move from lower to higher current density. This is expected as the effect of the Ni-10Co substrate decreases as the thickness of copper deposit increases. At 50mA/cm^2, the Cu (220) peak is most pronounced as compared to all other peaks of copper as well as Ni-10 Co.

Ni-20Co alloy substrate

Similarly the cold rolled Ni-20Co alloy electroplated with copper shows the same trend at 1mA/cm^2 as for Ni-10Co substrate; diffraction from (111) planes of Cu are most intense, with lower intensities of (200) and (220) lines. At 10 mA/cm^2 also the Cu (111) peak is most intense. At 30 and 50 mA/cm^2, the (220) peaks for copper are most intense (see **Fig. 4.3**). The diffraction peaks from Ni-20Co substrate are also shown in the plot. The intensity due to diffraction from (220) plane of Ni-20Co is most intense as compared to the other two peaks at all current densities. As in Ni-10Co alloy, the peak due to (220) planes of copper are most pronounced as compared to all other peaks from copper as well as Ni-20Co at 50mA/cm^2.

Ni-30Co alloy substrate

A similar trend is observed in the XRD pattern of Cu electrodeposited on the Ni-30Co alloy. The Cu(111) peak has maximum intensity when the current density is 1mA/cm^2. At the other three current densities, Cu(220) lines have maximum intensity (see **Fig. 4.4**). The lines from Ni-30 Co here have a common trend, with the (220) line being most intense at all current densities. When we compare the intensities of each of the three peaks obtained from the Ni-30Co substrate, we find that the intensity of each peak decreases as the current density increases from 1mA/cm^2 to 50 mA/cm^2. At a plating current density of 50mA/cm^2, the Cu(220) peak is most intense, as compared to all other peaks of Cu and Ni-30Co.

Ni-40Co alloy substrate

Here again, out of the several XRD peaks of copper, the Cu(111) is the most intense at $1mA/cm^2$. At 10, 30 and 50 mA/cm^2 Cu (220) is more intense followed by (111) and (200) peaks. The XRD plots for the above case are shown in **Fig. 4.5**.

As in the previous cases, the effect of substrate decreases as the current density of electrodeposition increases. This is marked by a decrease in the intensities of the respective peaks from the substrate with increase in current density. The (220) peaks of Ni-40Co have maximum intensity for all current densities. Of all the lines due to copper as well as Ni-40Co, (220) peak due to Cu shows maximum intensity at $50mA/cm^2$. All other lines have very low intensities at this current density.

Ni-60Co alloy substrate

For the Ni-60Co alloy, the peaks obtained are of similar nature as in all other Cu plated cold rolled Ni-Co alloys (**Fig. 4.6**). The (111) peak of Cu is most intense at $1mA/cm^2$. At higher current densities (10, 30 & $50mA/cm^2$) the Cu(220) peaks becomes most intense. The (220) peak for Ni-60Co substrate is most intense for all current densities. However, all the peaks of Ni-60Co decrease in intensity with increasing current density.

4.2.2. Annealed Ni-Co alloy substrate

Ni-Co alloys annealed at $800^{\circ}C$ for 1 hour were similarly electroplated with copper under similar conditions as the cold rolled alloys. The alloys were electroplated at four current densities, as stated above. The XRD plots for the annealed Ni-Co alloys electroplated with copper have been shown in **Fig. 4.7-4.11**. The XRD data are also represented in a tabular manner in **Table 4.6-4.10**. The three most intense lines of both electrodeposited Cu and the Ni-Co alloy substrate are presented in the table and plot.

Ni-10Co alloy substrate

The annealed Ni-10Co alloy electroplated with Cu shows the peaks of both Cu and Ni-10Co solid solution. At $1mA/cm^2$ and $10mA/cm^2$ current densities, out of the Cu lines, (111) has the highest intensity. At $30mA/cm^2$, Cu (220) has highest intensity out of the other two copper lines. Similar result is obtained at $50mA/cm^2$. The variation of intensity of the copper lines with respect to current density, are thus, similar to that obtained for the cold rolled alloys.

However, the Ni-10Co lines show a pattern different from that of the cold rolled alloys. Here, the (200) peaks of Ni-10Co are more intense in contrast to the (220) peaks in the cold rolled alloy. For all current densities starting from 1mA/cm^2 to 50 mA/cm^2, the same pattern is obtained. Of all the lines of Cu and Ni-10Co, the Cu (220) line becomes more pronounced at 50 mA/cm^2.

Ni-20Co alloy substrate

The XRD plots of Cu plated annealed Ni-20Co give similar results as for the annealed Ni-10Co alloy. The Cu (220) and Ni-Co (200) peaks intensities are high at all current densities except at 1mA/cm^2 where the Cu (111) and Ni-Co (200) peaks show maximum intensities.

Ni-30Co alloy substrate

The XRD plots of Cu plated annealed Ni-30Co give similar results as the other two cases explained above. At 1mA/cm^2 and at 10mA/cm^2, Cu(111) and Ni(200) are most intense and at higher current densities of 30 and 50 mA/cm^2, Cu(220) and Ni(200) are most intense.

Ni-40Co alloy substrate

The XRD plots for annealed Ni-40Co alloy with copper plating show the Cu (111) and Ni-Co (200) lines as the most intense ones at 1 and 10mA/cm^2. With increasing current density, the Cu(220) and Ni(200) peaks are the most intense ones. At 50 mA/cm^2 the Cu (220) peak is the only prominent line; all other lines of Cu and Ni-Co have very low intensities.

Ni-60Co alloy substrate

As above, here also at 1mA/cm^2 and 10mA/cm^2, the (111) diffraction peak of Cu is most intense. For higher current density, the Cu (220) is most intense out of all other peaks of Cu. Out of the peaks from Ni-60Co, the (200) peak is most intense at all current density but the intensity of the peaks from Ni-60Co substrate decreases as the current density increases showing the decrease in the effect of substrate with increasing current density.

All the above diffraction peaks have been compared with the ASTM index cards for textureless pure Ni and pure Cu (**Table 4.11a** and **b**).
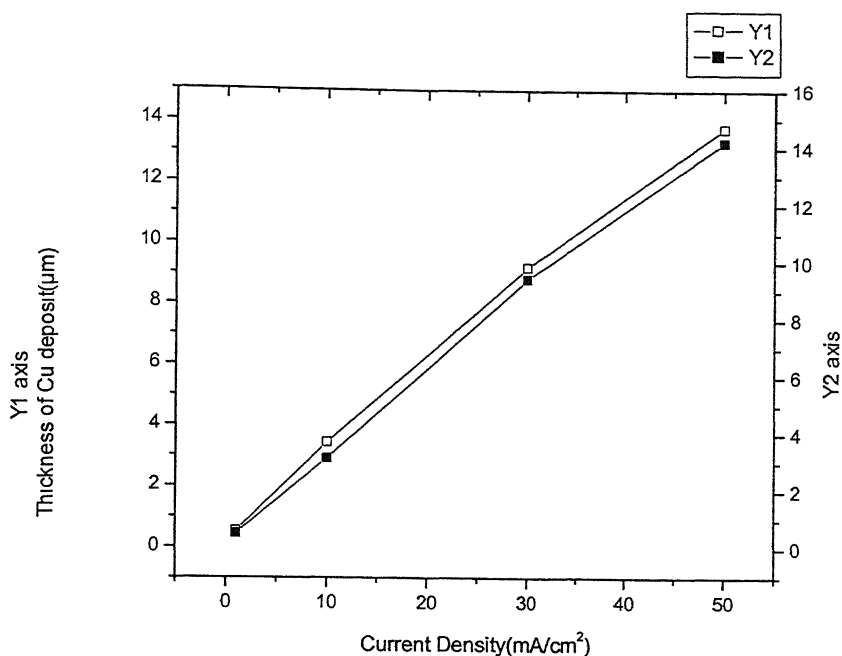
Fig. 4.1(a). Thickness of Cu deposit on cold rolled (Y1 axis) and annealed (Y2 axis) Ni-10Co alloy substrate as a function of current density.
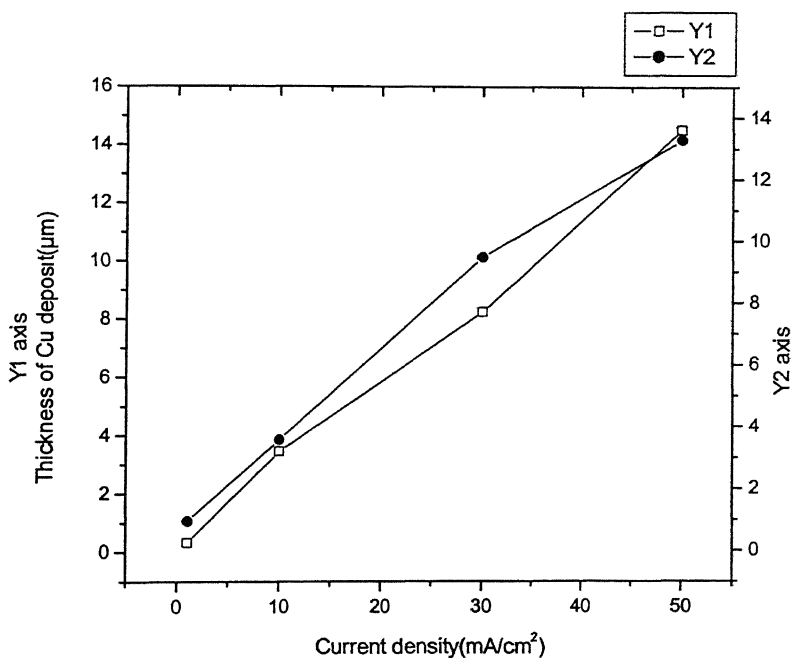
Fig. 4.1(b). Thickness of Cu deposit on cold rolled (Y1 axis) and annealed (Y2 axis) Ni-20Co alloy substrate as a function of current density.

46
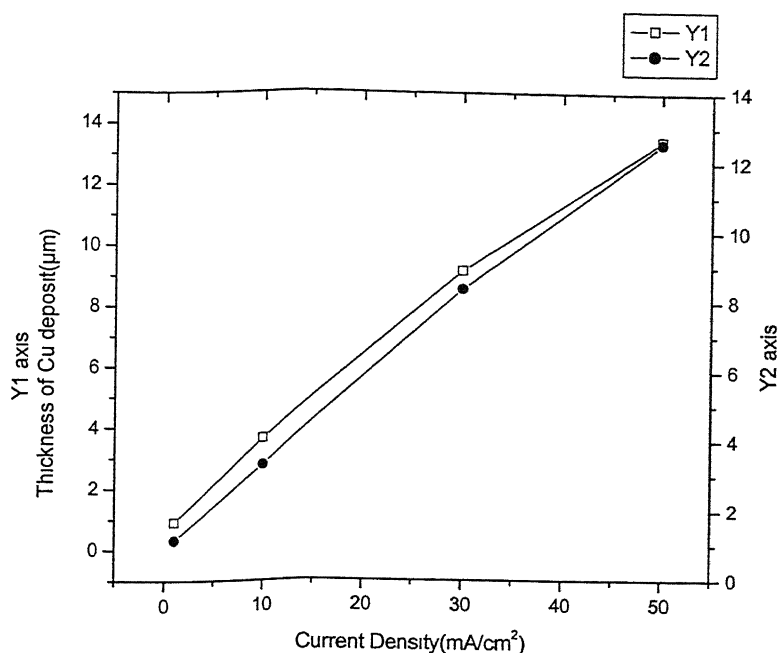
Fig. 4.1(c). Thickness of Cu deposit on cold rolled (Y1 axis) and annealed (Y2 axis) Ni-30Co alloy substrate as a function of current density.
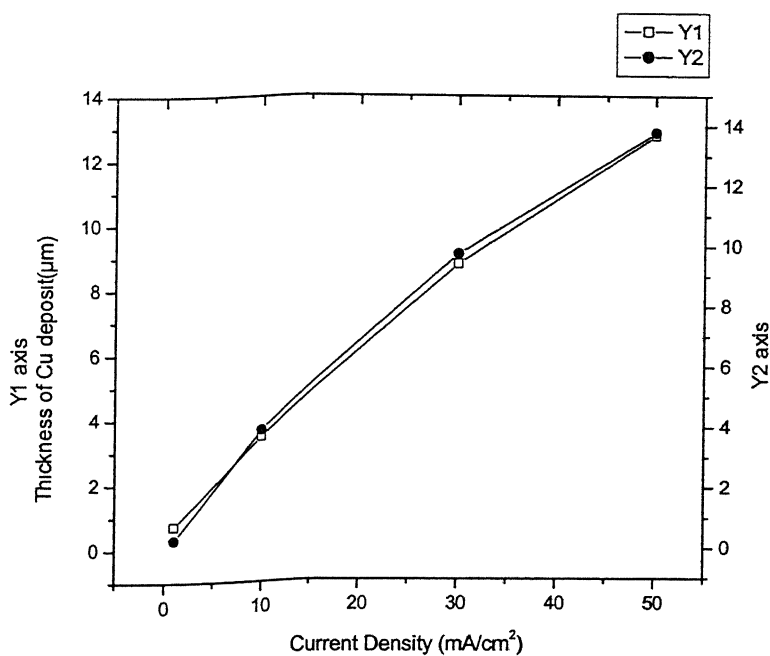
Fig. 4.1(d). Thickness of Cu deposit on cold rolled (Y1 axis) and annealed (Y2 axis) Ni-40Co alloy substrate as a function of current density.
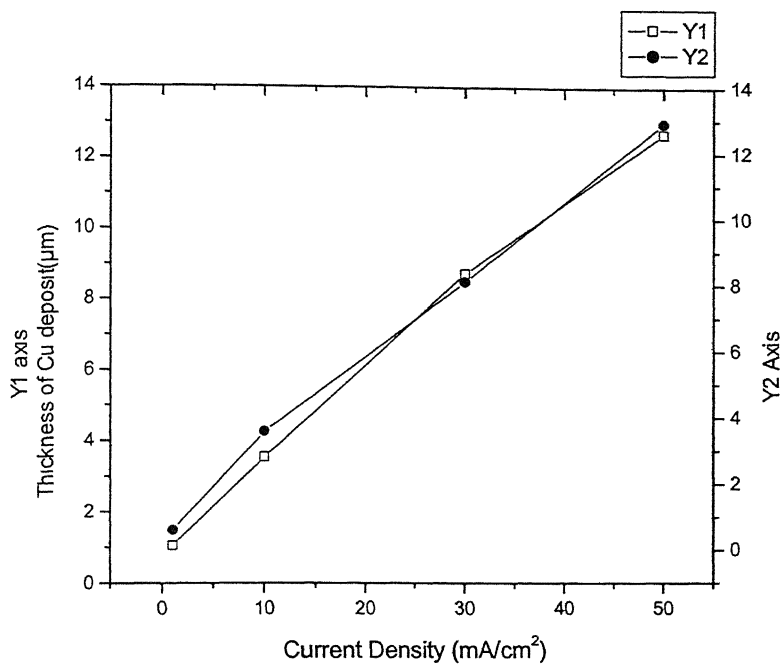
Fig. 4.1(e). Thickness of Cu deposit on cold rolled (Y1 axis) and annealed (Y2 axis) Ni-60Co alloy substrate as a function of current density.

Table 4.1. Relative intensities of diffraction peaks from Cu plated cold rolled Ni-10Co alloy electroplated at: (a) Current density = 1mA/cm^2

Lines of Cu					Lines of Ni-10 Co				
Relative Intensity	Angle	h	k	l	Relative Intensity	Angle	h	k	l
52.82	42	1	1	1	13	43	1	1	1
21.25	49	2	0	0	94	50.5	2	0	0
14.5	73	2	2	0	100	75.15	2	2	0

(b) Current density = 10mA/cm^2

Lines of Cu					Lines of Ni-10 Co				
Relative Intensity	Angle	h	k	l	Relative Intensity	Angle	h	k	l
41.71	43.09	1	1	1	14.44	44.32	1	1	1
31.07	50.15	2	0	0	75.06	51.4	2	0	0
93.63	74	2	2	0	74.53	76	2	2	0

(c) Current density = 30mA/cm^2

Lines of Cu					Lines of Ni-10 Co				
Relative Intensity	Angle	h	k	l	Relative Intensity	Angle	h	k	l
23.35	43.2	1	1	1	-	-	1	1	1
19.67	50.3	2	0	0	24	51.66	2	0	0
99.48	74	2	2	0	26.54	76	2	2	0

(d) Current density = 50mA/cm^2

Lines of Cu					Lines of Ni-10 Co				
Relative Intensity	Angle	h	k	l	Relative Intensity	Angle	h	k	l
33.76	43.2	1	1	1	-	-	1	1	1
25	50.3	2	0	0	20	52	2	0	0
100	74	2	2	0	18	76	2	2	0

Table 4.2. Relative intensities of diffraction peaks from Cu plated cold rolled Ni-20Co alloy electroplated at: (a) Current density =1mA/cm^2

Lines of Cu					Lines of Ni-20 Co				
Relative Intensity	Angle	h	k	l	Relative Intensity	Angle	h	k	l
39.4	43	1	1	1	13.5	44	1	1	1
26.4	50	2	0	0	87.3	51.4	2	0	0
18.6	73.98	2	2	0	100	76	2	2	0

(b) Current density = 10mA/cm^2

Lines of Cu					Lines of Ni-20 Co				
Relative Intensity	Angle	h	k	l	Relative Intensity	Angle	h	k	l
100	43.2	1	1	1	14.37	44.4	1	1	1
43.56	50.3	2	0	0	47.76	51.6	2	0	0
51.18	74	2	2	0	51.27	76	2	2	0

(c) Current density = 30mA/cm^2

Lines of Cu					Lines of Ni-20 Co				
Relative Intensity	Angle	h	k	l	Relative Intensity	Angle	h	k	l
25.43	43.3	1	1	1	-	-	1	1	1
21.77	50.5	2	0	0	24.17	52	2	0	0
99.82	74.1	2	2	0	29.72	76.2	2	2	0

(d) Current density = 50mA/cm^2

Lines of Cu					Lines of Ni-20 Co				
Relative Intensity	Angle	h	k	l	Relative Intensity	Angle	h	k	l
45.74	43	1	1	1	-	-	1	1	1
30.3	50.3	2	0	0	-	-	2	0	0
100	74	2	2	0	17.4	76	2	2	0

Table 4.3. Relative intensities of diffraction peaks from Cu plated cold rolled Ni-30Co alloy electroplated at: (a) Current density = 1mA/cm^2

Lines of Cu					Lines of Ni-30 Co				
Relative Intensity	Angle	h	k	l	Relative Intensity	Angle	h	k	l
54.09	42.3	1	1	1	18.4	43.36	1	1	1
31.2	49.4	2	0	0	100	50.7	2	0	0
23.64	73	2	2	0	87.73	75.3	2	2	0

(b) Current density = 10mA/cm^2

Lines of Cu					Lines of Ni-30 Co				
Relative Intensity	Angle	h	k	l	Relative Intensity	Angle	h	k	l
44.48	43	1	1	1	16.05	44.2	1	1	1
32.25	50.1	2	0	0	72.28	51.4	2	0	0
100	74	2	2	0	29.05	76	2	2	0

(c) Current density = 30mA/cm^2

Lines of Cu					Lines of Ni-30 Co				
Relative Intensity	Angle	h	k	l	Relative Intensity	Angle	h	k	l
20.77	43.3	1	1	1	-	-	1	1	1
17.17	50.4	2	0	0	13.79	52	2	0	0
99.68	74	2	2	0	17.01	76.3	2	2	0

(d) Current density = 50mA/cm^2

Lines of Cu					Lines of Ni-30 Co				
Relative Intensity	Angle	h	k	l	Relative Intensity	Angle	h	k	l
22.5	43.1	1	1	1	-	-	1	1	1
20	50.3	2	0	0	12	51.5	2	0	0
100	74	2	2	0	15.4	76	2	2	0

Table 4.4. Relative intensities of diffraction peaks from Cu plated cold rolled Ni-40Co alloy electroplated at: (a) Current density = 1mA/cm^2

Lines of Cu					Lines of Ni-40 Co				
Relative Intensity	Angle	h	k	l	Relative Intensity	Angle	h	k	l
40.83	43	1	1	1	17.54	44.1	1	1	1
25.35	50.2	2	0	0	49.82	51.3	2	0	0
19.66	74	2	2	0	98.7	76	2	2	0

(b) Current density = 10mA/cm^2

Lines of Cu					Lines of Ni-40 Co				
Relative Intensity	Angle	h	k	l	Relative Intensity	Angle	h	k	l
42.46	43.2	1	1	1	18.07	44.32	1	1	1
32.43	50.4	2	0	0	54.8	51.6	2	0	0
100	74.1	2	2	0	59.27	76.1	2	2	0

(c) Current density = 30mA/cm^2

Lines of Cu					Lines of Ni-40 Co				
Relative Intensity	Angle	h	k	l	Relative Intensity	Angle	h	k	l
20.37	43.2	1	1	1	-	-	1	1	1
18.91	50.4	2	0	0	12.53	51.5	2	0	0
99.86	74	2	2	0	16.57	76	2	2	0

(d) Current density = 50mA/cm^2

Lines of Cu					Lines of Ni-40 Co				
Relative Intensity	Angle	h	k	l	Relative Intensity	Angle	h	k	l
35	43	1	1	1	-	-	1	1	1
22.4	50.4	2	0	0	-	-	2	0	0
100	74	2	2	0	13	75.2	2	2	0

Table 4.5. Relative intensities of diffraction peaks from Cu plated cold rolled Ni-60Co alloy electroplated at: (a) Current density = 1mA/cm^2

Lines of Cu					Lines of Ni-40 Co				
Relative Intensity	Angle	h	k	l	Relative Intensity	Angle	h	k	l
20.37	43.2	1	1	1	-	-	1	1	1
18.91	50.4	2	0	0	12.53	51.5	2	0	0
99.86	74	2	2	0	16.57	76	2	2	0

(b) Current density = 10mA/cm^2

Lines of Cu					Lines of Ni-60 Co				
Relative Intensity	Angle	h	k	l	Relative Intensity	Angle	h	k	l
46.51	43.3	1	1	1	39.41	44.4	1	1	1
31.15	50.5	2	0	0	-	-	2	0	0
93.25	74.1	2	2	0	41.15	76	2	2	0

(c) Current density = 30mA/cm^2

Lines of Cu					Lines of Ni-60 Co				
Relative Intensity	Angle	h	k	l	Relative Intensity	Angle	h	k	l
22.08	43.3	1	1	1	13.14	44.4	1	1	1
19.98	50.5	2	0	0	-	-	2	0	0
99.5	74.2	2	2	0	18.33	76.14	2	2	0

(d) Current density = 50mA/cm^2

Lines of Cu					Lines of Ni-60 Co				
Relative Intensity	Angle	h	k	l	Relative Intensity	Angle	h	k	l
19	42.4	1	1	1	-	-	1	1	1
19.2	50	2	0	0	-	-	2	0	0
100	74	2	2	0	13.4	76	2	2	0

Table 4.6. Relative intensities of diffraction peaks from Cu plated annealed Ni-10Co alloy electroplated at: (a) Current density = 1mA/cm^2

Lines of Cu					Lines of Ni-Co10				
Relative Intensity	Angle	h	k	l	Relative Intensity	Angle	h	k	l
20.1	43.31	1	1	1	35.04	44.46	1	1	1
10.67	50.47	2	0	0	99.83	52	2	0	0
4.1	74.34	2	2	0	12.33	76.44	2	2	0

(b) Current density = 10mA/cm^2

Lines of Cu					Lines of Ni-Co10				
Relative Intensity	Angle	h	k	l	Relative Intensity	Angle	h	k	l
66.88	43.4	1	1	1	25.88	44.5	1	1	1
32.38	50.7	2	0	0	100	52	2	0	0
28.62	75	2	2	0	9.72	77	2	2	0

(c) Current density = 30mA/cm^2

Lines of Cu					Lines of Ni-Co10				
Relative Intensity	Angle	h	k	l	Relative Intensity	Angle	h	k	l
23.35	43.2	1	1	1	-	-	1	1	1
19.67	50.3	2	0	0	24	51.66	2	0	0
99.48	74	2	2	0	26.54	76	2	2	0

(d)Current density = 50mA/cm^2

Lines of Cu					Lines of Ni-Co10				
Relative Intensity	Angle	h	k	l	Relative Intensity	Angle	h	k	l
33.76	43.2	1	1	1	-	-	1	1	1
25	50.3	2	0	0	20	52	2	0	0
100	74	2	2	0	18	76	2	2	0

Table 4.7. Relative intensities of diffraction peaks from Cu plated annealed Ni-20Co alloy electroplated at: (a) Current density = 1mA/cm^2

Lines of Cu					Lines of Ni-20 Co				
Relative Intensity	Angle	h	k	l	Relative Intensity	Angle	h	k	l
34.6	43.4	1	1	1	22.84	44.4	1	1	1
16.73	50.5	2	0	0	100	51.7	2	0	0
9.11	74.3	2	2	0	6.16	76.3	2	2	0

(b) Current density = 10mA/cm^2

Lines of Cu					Lines of Ni-20 Co				
Relative Intensity	Angle	h	k	l	Relative Intensity	Angle	h	k	l
62.35	43.2	1	1	1	16.5	44.3	1	1	1
34.5	50.3	2	0	0	100	51.6	2	0	0
35.82	74	2	2	0	10.22	76	2	2	0

(c) Current density = 30mA/cm^2

Lines of Cu					Lines of Ni-20 Co				
Relative Intensity	Angle	h	k	l	Relative Intensity	Angle	h	k	l
52.23	43.3	1	1	1	16.27	44	1	1	1
44.83	50.4	2	0	0	63.67	51.6	2	0	0
98.78	74	2	2	0	15.29	76	2	2	0

(d) Current density = 50mA/cm^2

Lines of Cu					Lines of Ni-20 Co				
Relative Intensity	Angle	h	k	l	Relative Intensity	Angle	h	k	l
21.41	43.2	1	1	1	-	-	1	1	1
23.8	50.3	2	0	0	32	51.6	2	0	0
100	74	2	2	0	-	-	2	2	0

Table 4.8. Relative intensities of diffraction peaks from Cu plated annealed Ni-30Co alloy electroplated at: (a) Current density = 1mA/cm^2

Lines of Cu					Lines of Ni-30 Co				
Relative Intensity	Angle	h	k	l	Relative Intensity	Angle	h	k	l
74.77	43.3	1	1	1	46.55	44.4	1	1	1
42.87	50.5	2	0	0	100	51.7	2	0	0
20.66	74.3	2	2	0	16.64	76.4	2	2	0

(b) Current density = 10mA/cm^2

Lines of Cu					Lines of Ni-30 Co				
Relative Intensity	Angle	h	k	l	Relative Intensity	Angle	h	k	l
100	43.4	1	1	1	42.05	44.5	1	1	1
63.32	50.5	2	0	0	78.92	51.7	2	0	0
84.01	74.1	2	2	0	25.32	76	2	2	0

(c) Current density = 30mA/cm^2

Lines of Cu					Lines of Ni-30 Co				
Relative Intensity	Angle	h	k	l	Relative Intensity	Angle	h	k	l
24.95	43.3	1	1	1	10.68	44.3	1	1	1
25.4	50.35	2	0	0	15.69	51.6	2	0	0
99.34	74	2	2	0	10.67	76	2	2	0

(d) Current density = 50mA/cm^2

Lines of Cu					Lines of Ni-30 Co				
Relative Intensity	Angle	h	k	l	Relative Intensity	Angle	h	k	l
24.45	43.2	1	1	1	11.7	44.4	1	1	1
23	50.4	2	0	0	17	52	2	0	0
100	74	2	2	0	11	76	2	2	0

Table 4.9. Relative intensities of diffraction peaks from Cu plated annealed Ni-40Co alloy electroplated at: (a) Current density = 1mA/cm^2

Lines of Cu					Lines of Ni-40 Co				
Relative Intensity	Angle	h	k	l	Relative Intensity	Angle	h	k	l
67.9	43.3	1	1	1	100	44.3	1	1	1
41.56	50.4	2	0	0	95.19	52	2	0	0
19.35	74	2	2	0	44.5	76	2	2	0

(b) Current density = 10mA/cm^2

Lines of Cu					Lines of Ni-40 Co				
Relative Intensity	Angle	h	k	l	Relative Intensity	Angle	h	k	l
100	43.3	1	1	1	22.6	44.4	1	1	1
48.23	50.5	2	0	0	23.26	51.7	2	0	0
43.17	74.2	2	2	0	16.5	76.2	2	2	0

(c) Current density = 30mA/cm^2

Lines of Cu					Lines of Ni-40 Co				
Relative Intensity	Angle	h	k	l	Relative Intensity	Angle	h	k	l
27.8	43.3	1	1	1	11.83	44.16	1	1	1
25.13	50.38	2	0	0	13.29	51.52	2	0	0
98.87	74	2	2	0	11.25	76	2	2	0

(d) Current density = 50mA/cm^2

Lines of Cu					Lines of Ni-40 Co				
Relative Intensity	Angle	h	k	l	Relative Intensity	Angle	h	k	l
16.3	43.3	1	1	1	-	-	1	1	1
19	50.4	2	0	0	-	-	2	0	0
100	74	2	2	0	-	-	2	2	0

Table 4.10. Relative intensities of diffraction peaks from Cu plated annealed Ni-60Co alloy electroplated at: (a) Current density = 1mA/cm^2

Lines of Cu					Lines of Ni-60Co				
Relative Intensity	Angle	h	k	l	Relative Intensity	Angle	h	k	l
95.88	43.37	1	1	1	15.6	44.4	1	1	1
47.92	50.5	2	0	0	16.14	52	2	0	0
29.69	74	2	2	0	31.77	76	2	2	0

(b) Current density = 10mA/cm^2

Lines of Cu					Lines of Ni-60Co				
Relative Intensity	Angle	h	k	l	Relative Intensity	Angle	h	k	l
98.42	43.4	1	1	1	21.42	44.4	1	1	1
58.46	50.6	2	0	0	17.87	51.6	2	0	0
53.66	74.1	2	2	0	24.3	76.02	2	2	0

(c) Current density = 30mA/cm^2

Lines of Cu					Lines of Ni-60Co				
Relative Intensity	Angle	h	k	l	Relative Intensity	Angle	h	k	l
41.96	43.2	1	1	1	-	-	1	1	1
35.96	50	2	0	0	-	-	2	0	0
100	74	2	2	0	17	76	2	2	0

(d) Current density = 50mA/cm^2

Lines of Cu					Lines of Ni-60Co				
Relative Intensity	Angle	h	k	l	Relative Intensity	Angle	h	k	l
16.5	43.3	1	1	1	-	-	1	1	1
19	50.4	2	0	0	-	-	2	0	0
100	74	2	2	0	12	76	2	2	0

Table 4.11(a) ASTM index card for textureless pure Ni

04-0850

							Wavelength= 1.5405	

Ni

Nickel

2θ	Int	h	k	l
44.505	100	1	1	1
51.844	42	2	0	0
76.366	21	2	2	0
92.909	20	3	1	1
98.440	7	2	2	2
121.922	4	4	0	0
144.655	14	3	3	1
155.632	15	4	2	0

Nickel, syn

Rad.: CuKal   λ- 1.5405   Filter Ni   Beta   d-sp·

Cut off: Int : Diffract.   I/Icor :

Ref: Swanson, Tatge, Natl. Bur. Stand. (U.S.), Circ. 539, 1, 13 (1953)

Sys. Cubic   S.G.: Fm3̄m (225)

a: 3.5238   b.   c: A: C

α: β   γ.   Z: 4   mp·

Ref: Ibid.

Dx: 8.911   Dm·   SS/FOM: F₈ – 57(.0115 , 8)

Color: White
Pattern taken at 26 C   Sample obtained from Johnson Matthey
Company, Ltd CAS #   7440-02-0. Spectrographic analysis show
<0.01% each of Mg, Si and Ca. Cu type. Gold SuperGroup.
IC-disordered Group. PSC: cF4. See ICSD 64989 (PDF 87-712).
Mwt: 58.70. Volume[CD]: 43.76

Table 4.11(b) ASTM index card for textureless pure Cu

04-0836

							Wavelength= 1.5405	

Cu

Copper

2θ	Int	h	k	l
43.296	100	1	1	1
50.431	46	2	0	0
74.127	20	2	2	0
89.926	17	3	1	1
95.135	5	2	2	2
116.911	3	4	0	0
136.496	9	3	3	1
144.70	8	4	2	0

Copper, syn.

Rad.: CuKal   λ: 1.5405   Filter: Ni   Beta   d-sp:

Cut off: Int.: Diffract   I/Icor:

Ref: Swanson, Tatge, Natl. Bur. Stand. (U.S.), Circ. 539, 1, 15 (1953)

Sys.: Cubic   S.G.: Fm3̄m (225)

a: 3.6150   b: c: A: C.

α   β: γ: Z: 4   mp·1083

Ref: Ibid.

Dx: 8.935   Dm: 8.950   SS/FOM: F₈ – 89(.0112 , 8)

Color: Red
Pattern taken at 26 C. Sample from metallurgical laboratory of
NBS Gaithersburg, Maryland, USA. CAS #   7440-50-8. It had
been heated in an H2 atmosphere at 300 C. Impurities from
0.001-0.01%, Ag, Al, Ni, Fe, Si, Zn. Measured density and color
from Dana's System of Mineralogy. 7th Ed., I 99. Cu type. Gold
SuperGroup. IC-disordered Group. PSC: cF4. See ICSD-64699
(PDF 85-1326). Opaque mineral optical data on specimen from
unspecified locality. R3RX=60.65. Disp.=Std. VHN100=96-104.
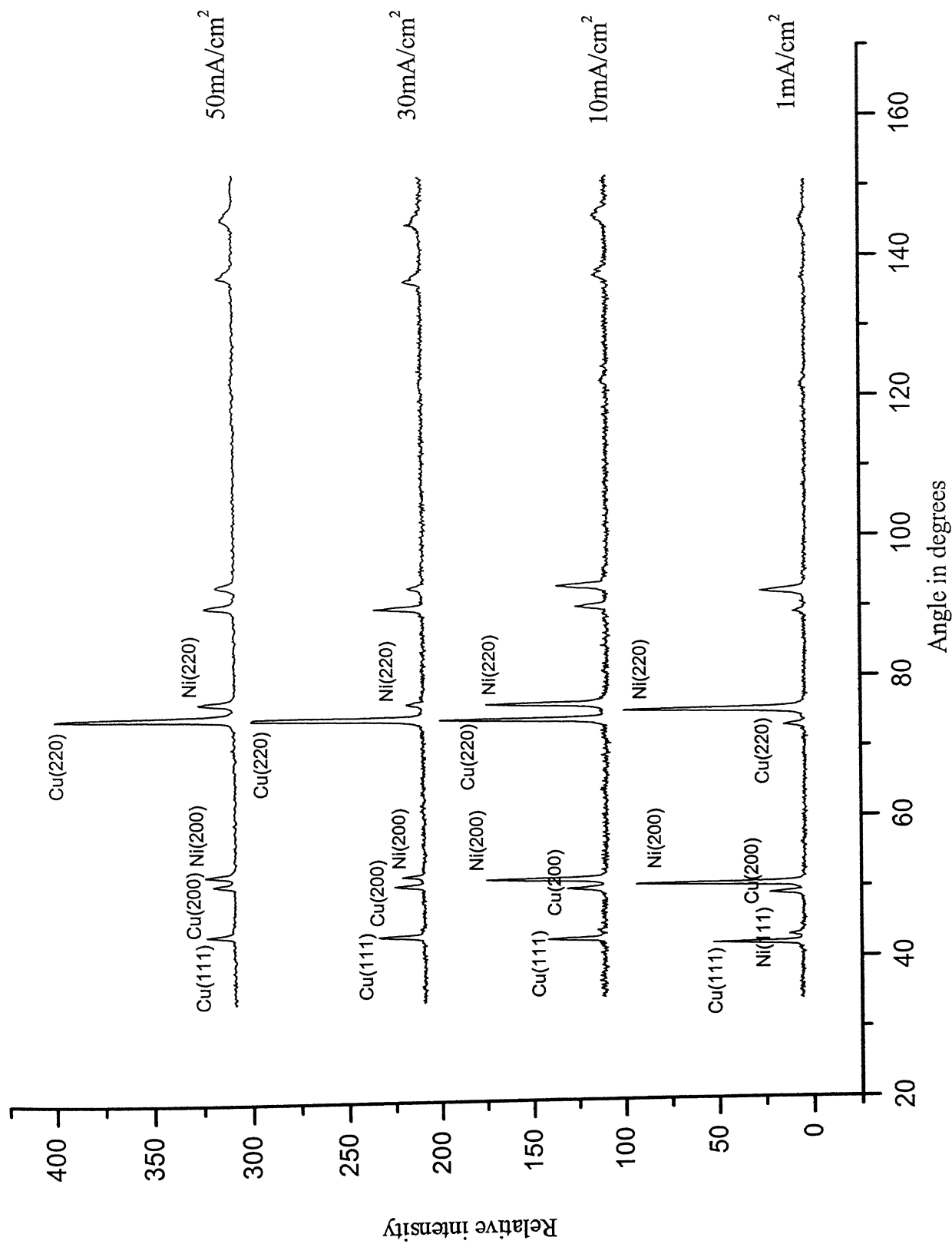Mwt: 63.55 Volume[CD]: 47.24.

Fig. 4.2. XRD plots of Cu plated cold rolled Ni-10Co alloy
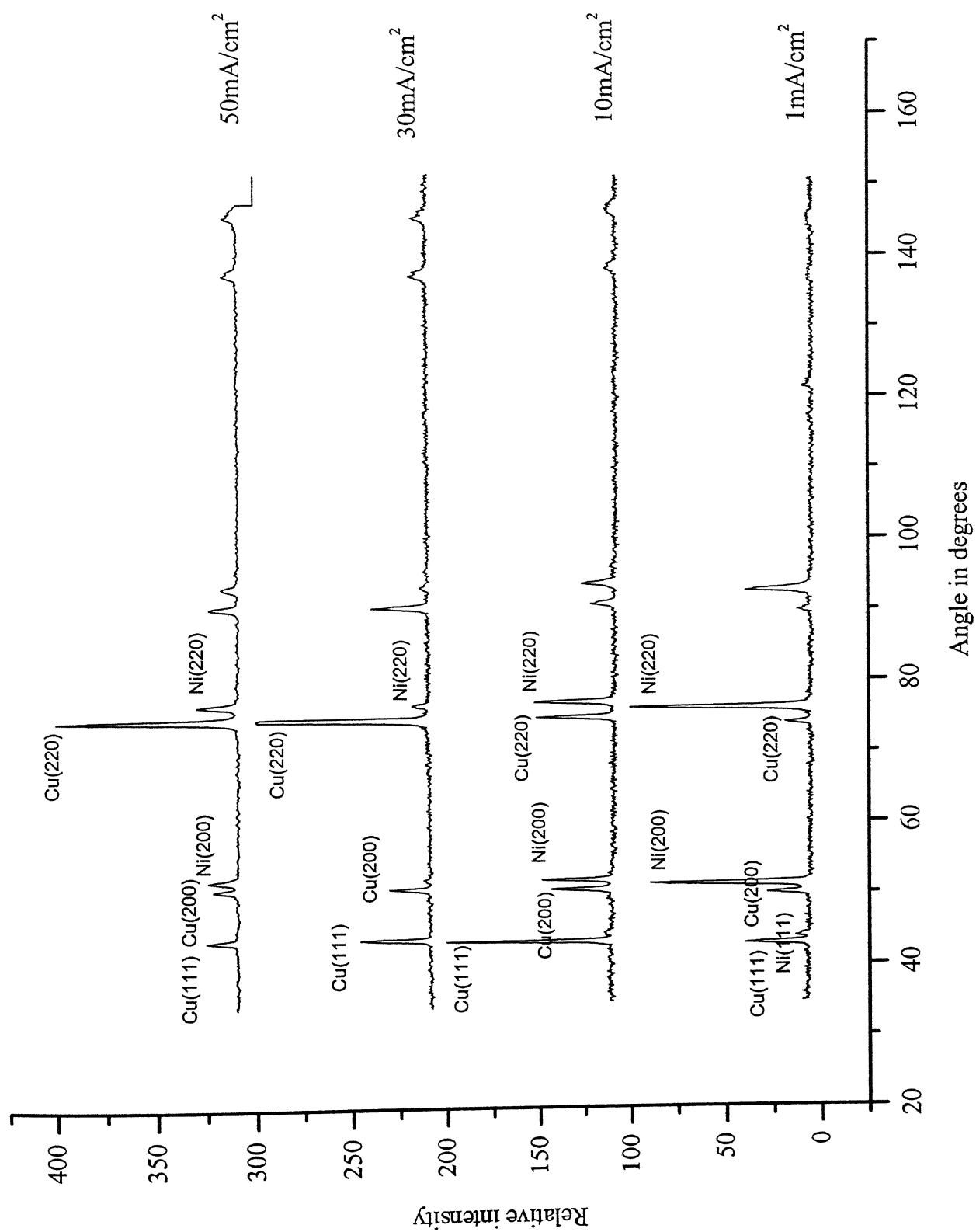
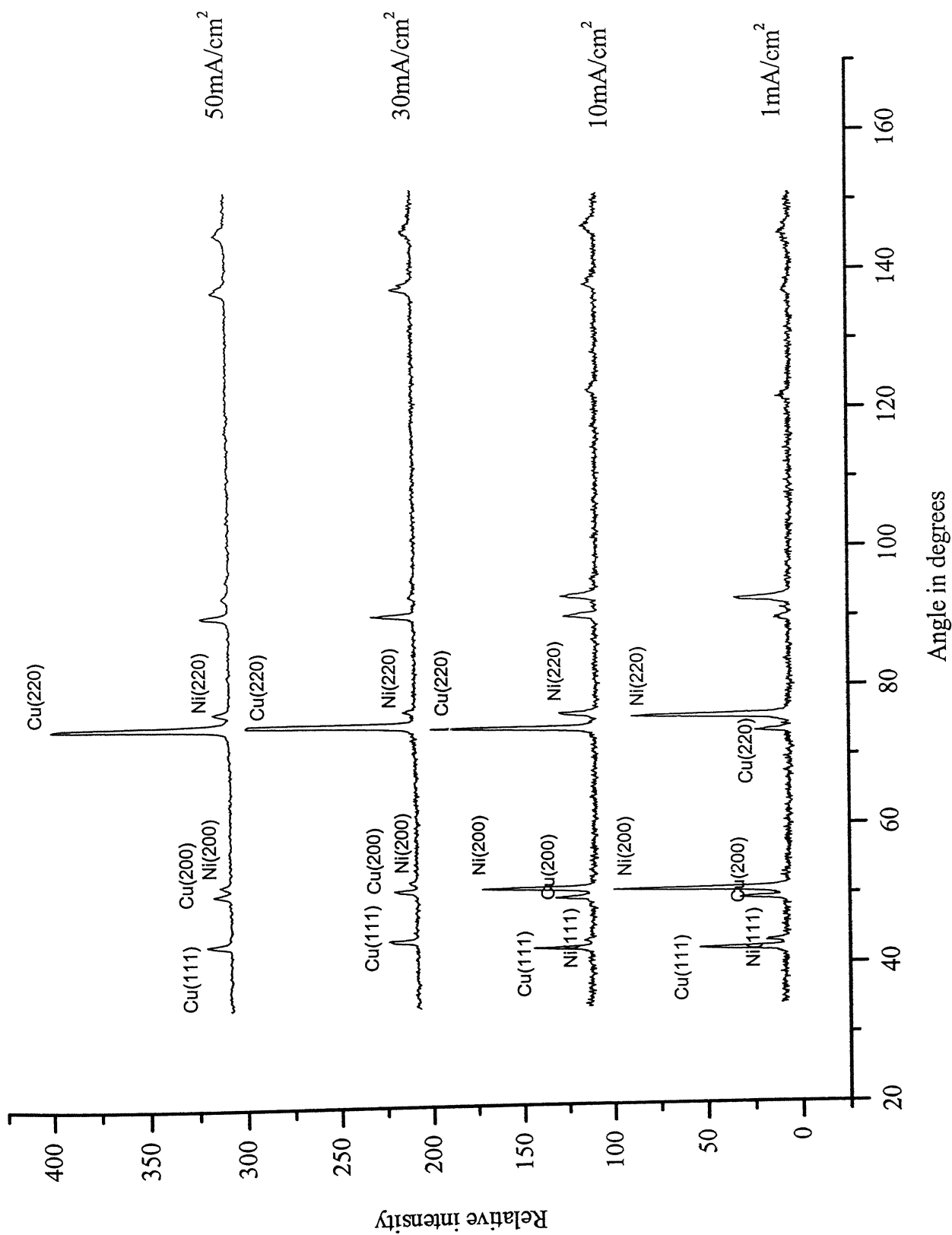**Fig. 4.3.** XRD plots of Cu plated cold rolled Ni-20Co alloy

61

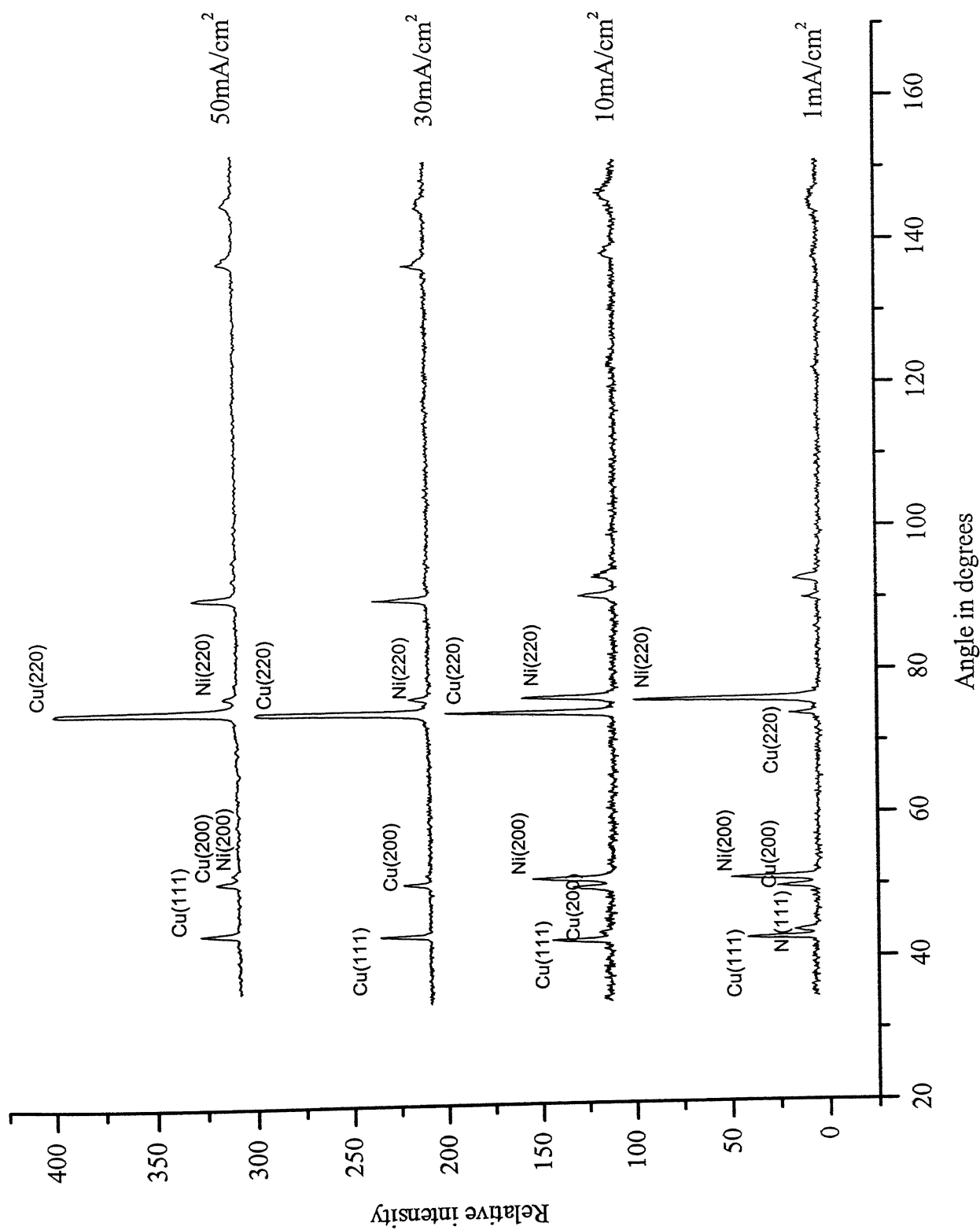**Fig. 4.4.** XRD plots of Cu plated cold rolled Ni-30Co alloy

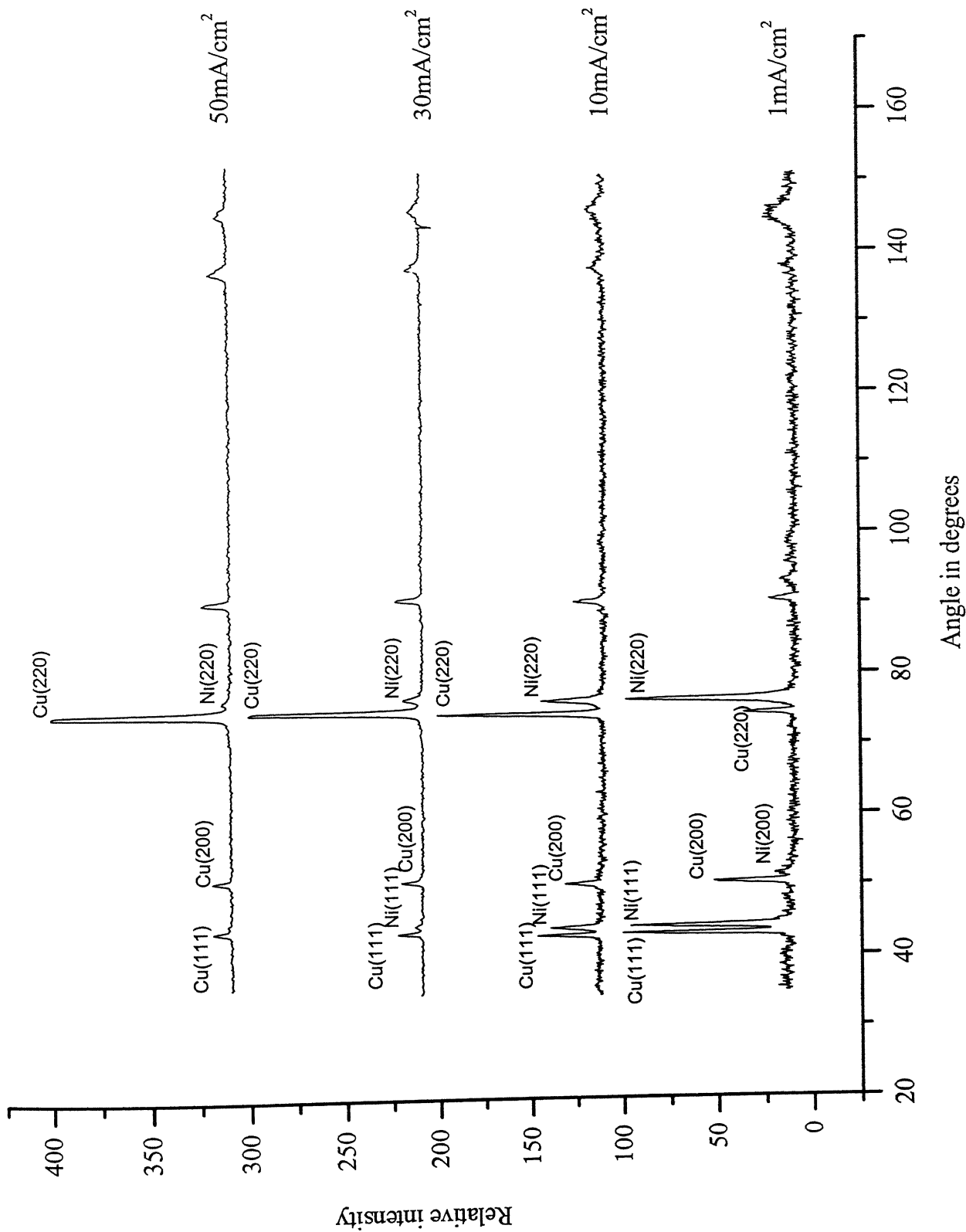**Fig. 4.5.** XRD plots of Cu plated cold rolled Ni-40Co alloy
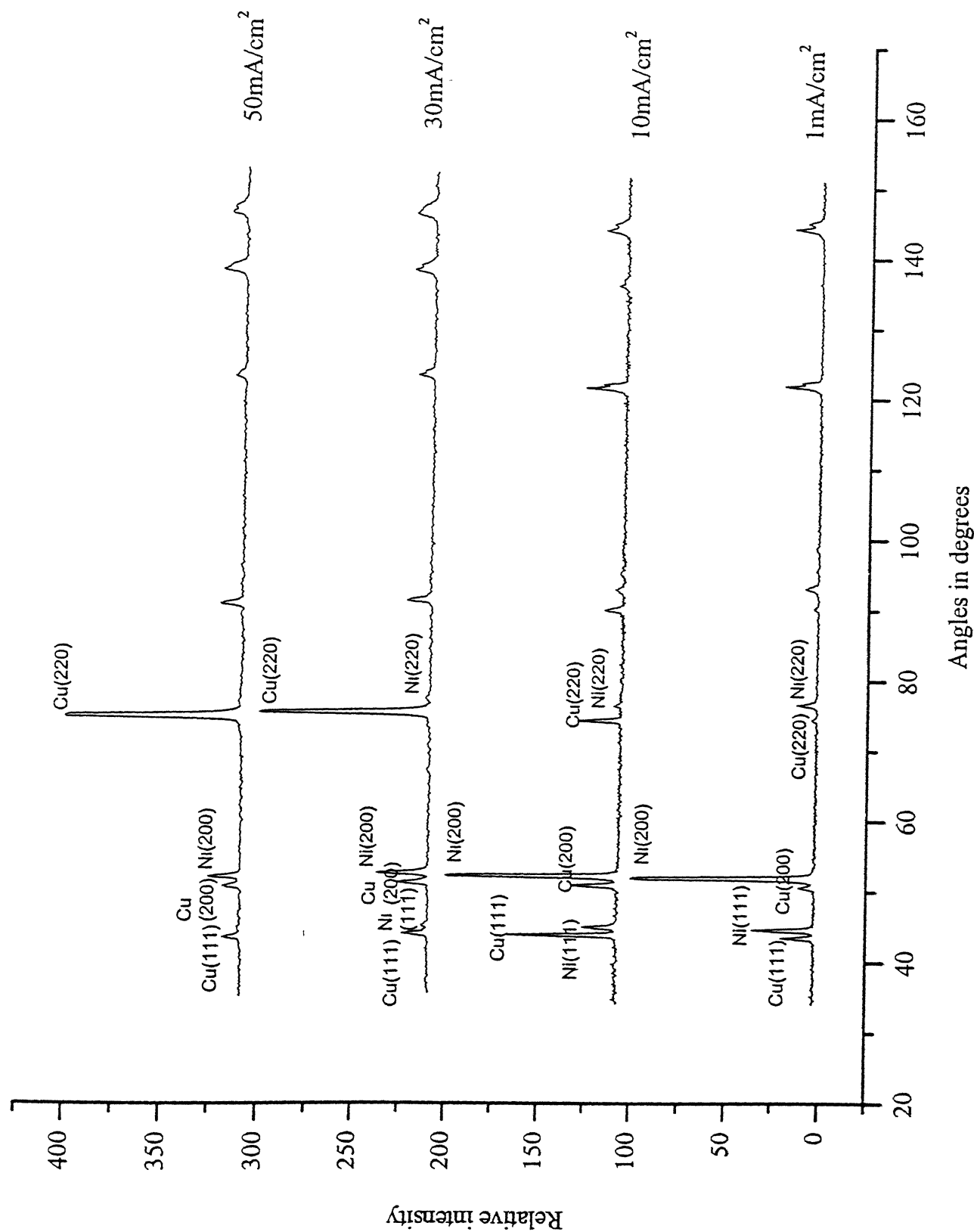
Fig. 4.6. XRD plots of Cu plated cold rolled Ni-60Co alloy

Fig. 4.7. XRD plots of Cu plated annealed Ni-10Co alloy
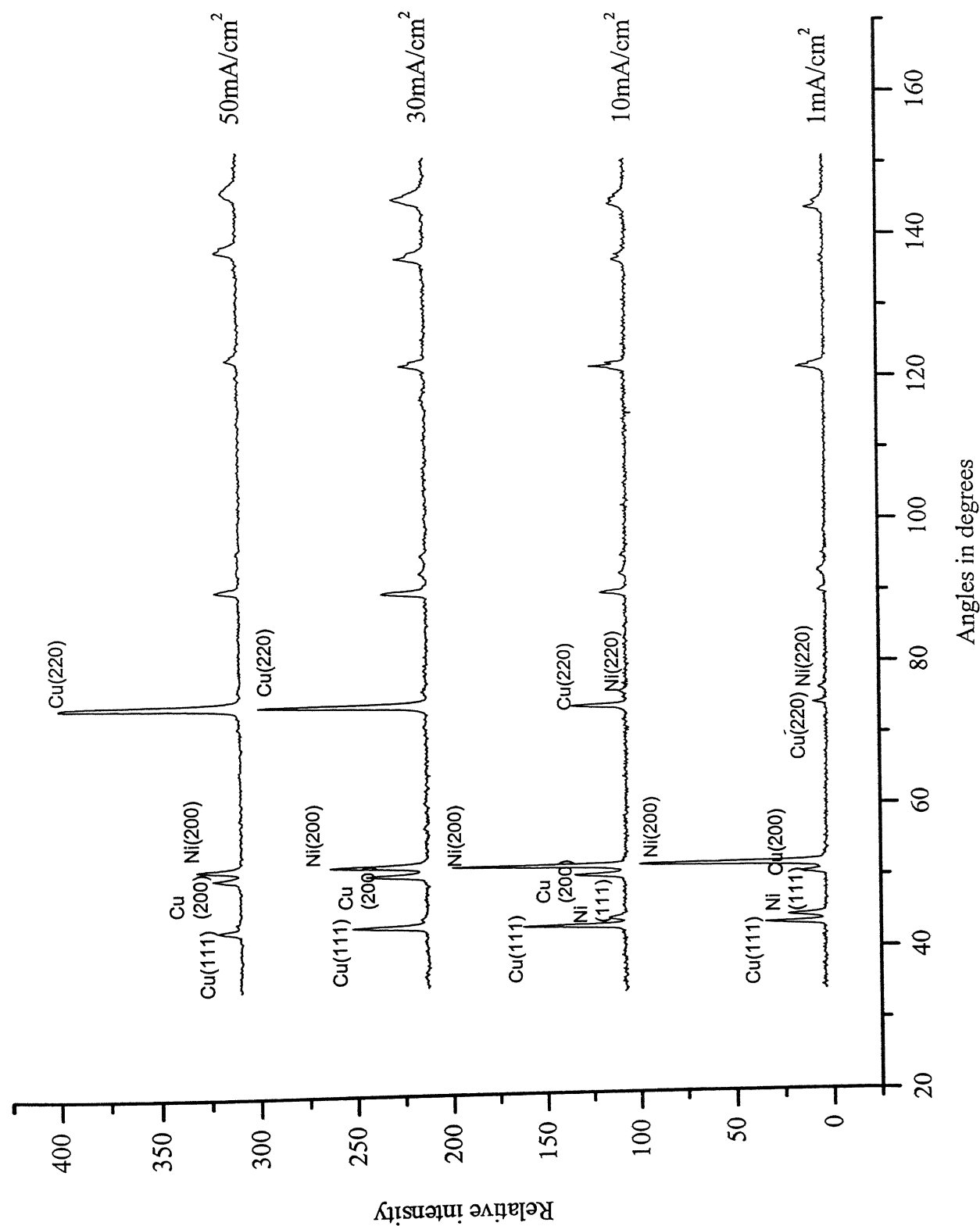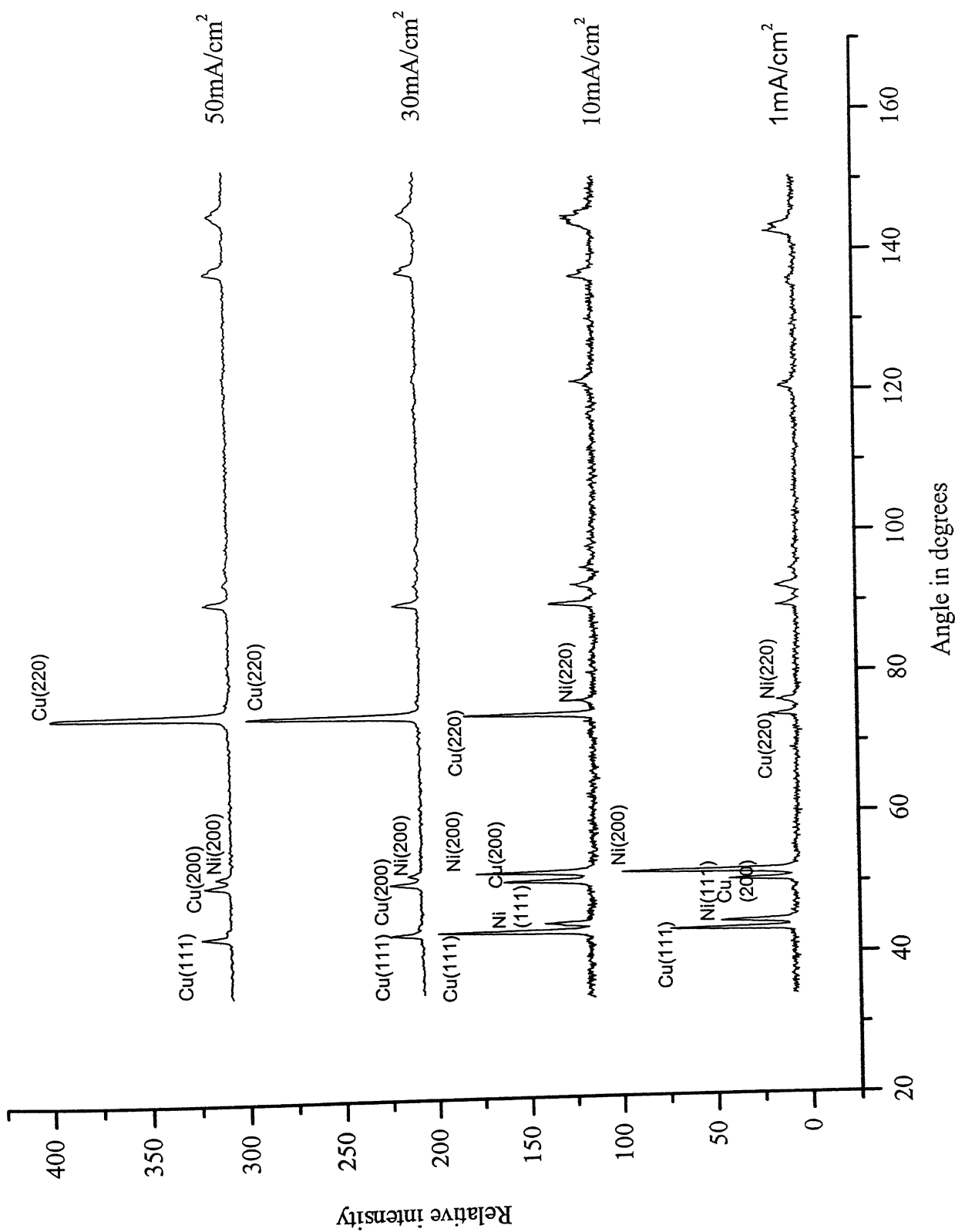
Fig. 4.8. XRD plots of Cu plated annealed Ni-20Co alloy
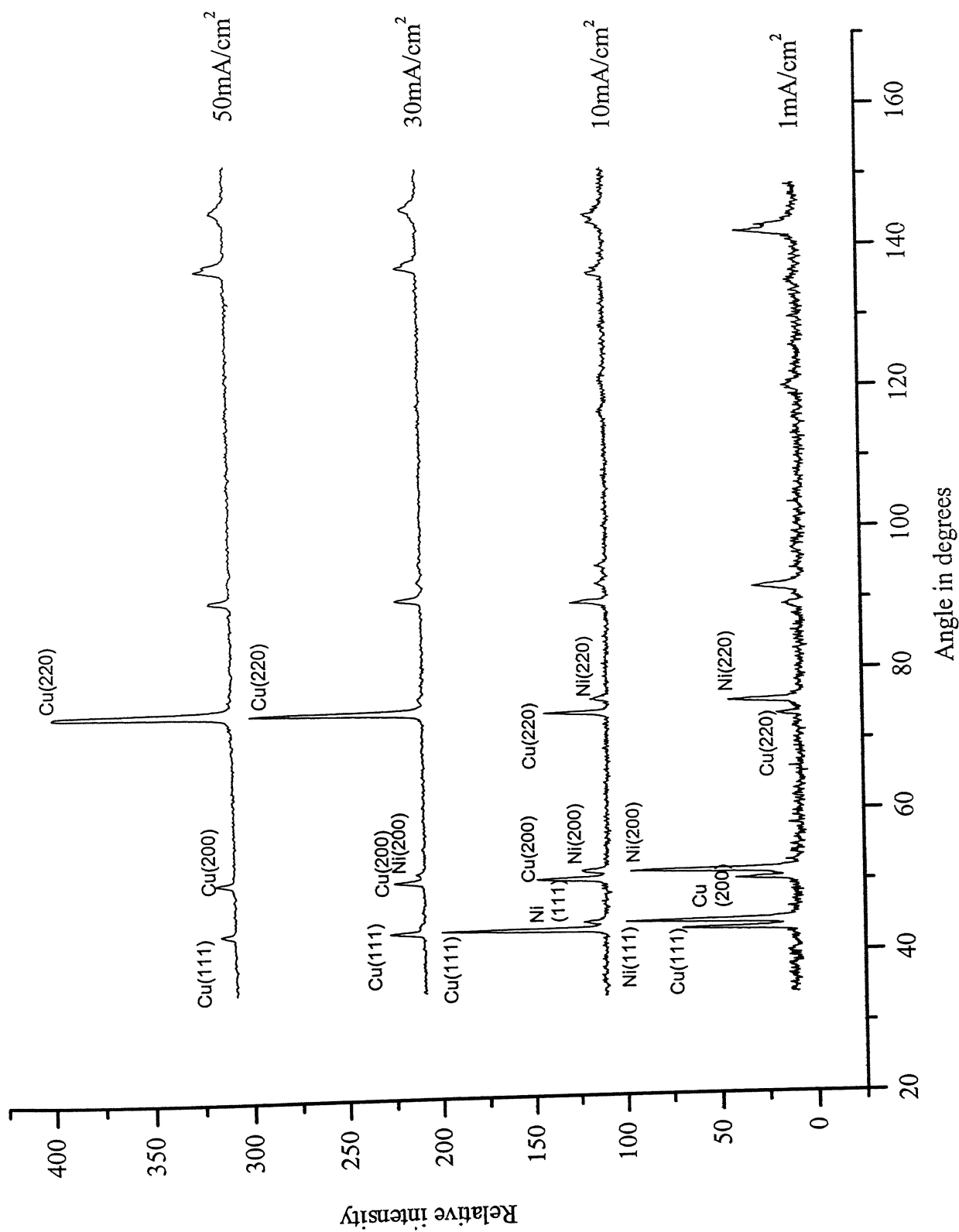
Fig. 4.9. XRD plots of Cu plated annealed Ni-30Co alloy
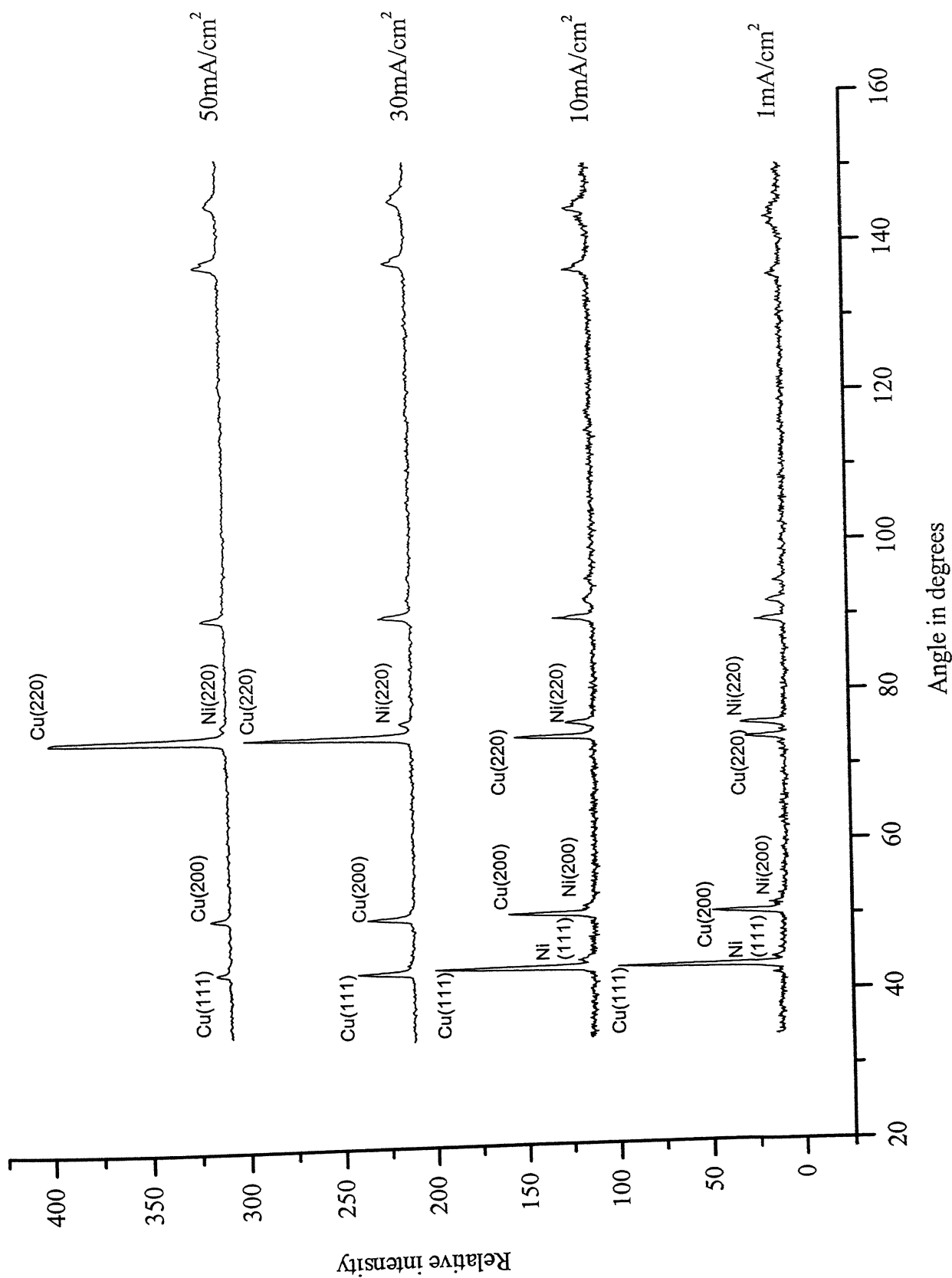
Fig. 4.10. XRD plots of Cu plated annealed Ni-40Co alloy

Fig. 4.11. XRD plots of Cu plated annealed Ni-60Co alloy

4.3. Scanning Electron Microscopy Results

4.3.1. Copper electrodeposits on cold rolled Ni-Co alloys

Fig. 4.12 shows the surface morphologies of copper electrodeposits on cold rolled Ni-10Co alloy substrate with the change in current density, (a) 1 mA/cm^2, (b) 10mA/cm^2, (c) 30mA/cm^2 and (d) 50mA/cm^2.

Fig. 4.13 shows the surface morphologies of copper electrodeposits on cold rolled Ni-20Co alloy substrate at the four different current densities as stated above.

Similarly Fig. 4.14, Fig. 4.15 and Fig. 4.16 show the surface morphologies of copper electrodeposits on cold rolled Ni-30Co, Ni-40Co and Ni-60Co respectively, at the four different current densities.

In all the above cases, the grain size of the copper deposit decreases with the increase in current density from 1mA/cm^2 to 50mA/cm^2.

4.3.2. Copper electrodeposits on annealed Ni-Co alloys

Fig.4.17 shows the surface morphologies of copper electrodeposits on annealed Ni-10Co substrate with the change in current density. The same four current densities were used for deposition of copper, 1mA/cm^2, 10mA/cm^2, 30mA/cm^2 and 50mA/cm^2.

Fig.4.18 shows the surface morphologies of copper deposits on annealed Ni-20 Co substrate with the change in current density. Fig.4.19, Fig.4.20 and Fig.4.21 show the surface morphologies of the copper deposits on annealed Ni-30Co, Ni-40Co and Ni-60Co respectively at the four different current densities.

As the current density increases from 1mA/cm^2 to 50mA/cm^2, the grain size of the copper deposit decreases.
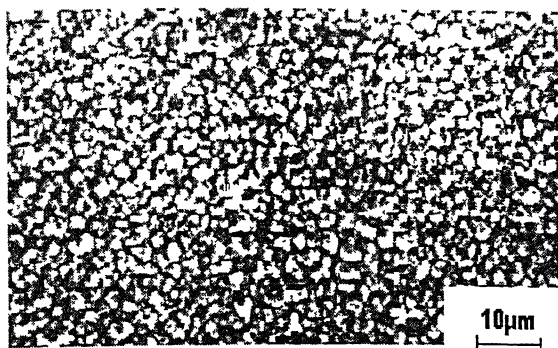
(a) 1mA/cm^2
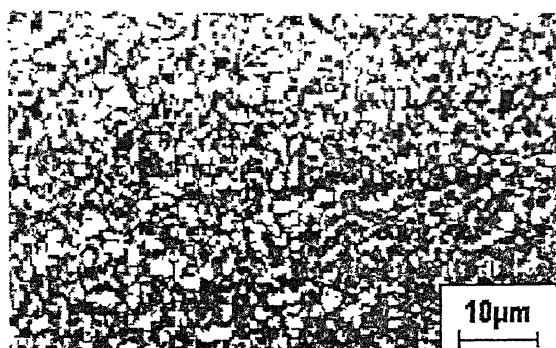
(b) 10mA/cm^2
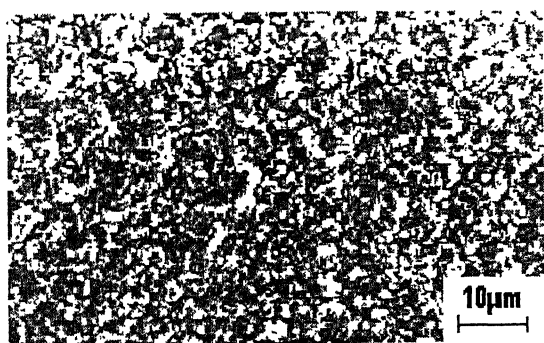
(c) 30mA/cm^2

(d) 50mA/cm^2

Fig. 4.12. SEM micrographs of Cu deposit on cold rolled Ni-10Co alloy substrate at different current densities

(a) 1mA/cm^2

(b) 10mA/cm^2

(c) 30mA/cm^2

(d) 50mA/cm^2

Fig. 4.13. SEM micrographs of Cu deposit on cold rolled Ni-20Co alloy substrate at different current densities.
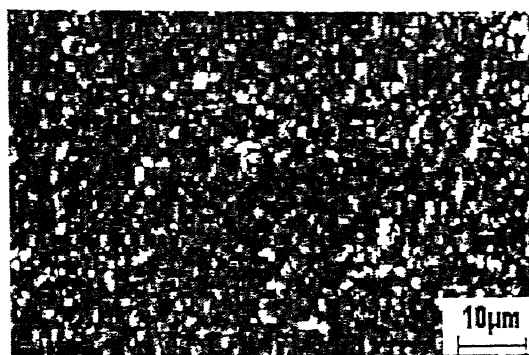
(a) 1mA/cm^2

(b) 10mA/cm^2

(c) 30mA/cm^2

(d) 50mA/cm^2

Fig. 4.14. SEM micrographs of Cu deposit on cold rolled Ni-30Co alloy substrate at different current densities.

(a) 1mA/cm^2
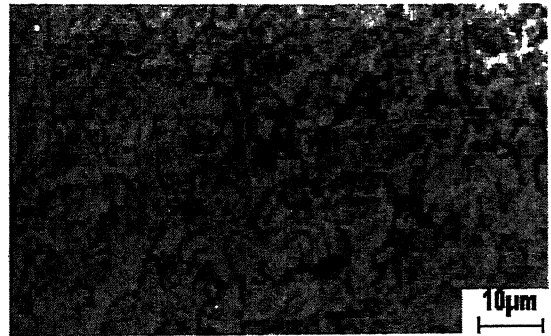
(b) 10mA/cm^2

(c) 30mA/cm^2

(d) 50mA/cm^2

Fig. 4.15. SEM micrographs of Cu deposit on cold rolled Ni-40Co alloy substrate at different current densities.
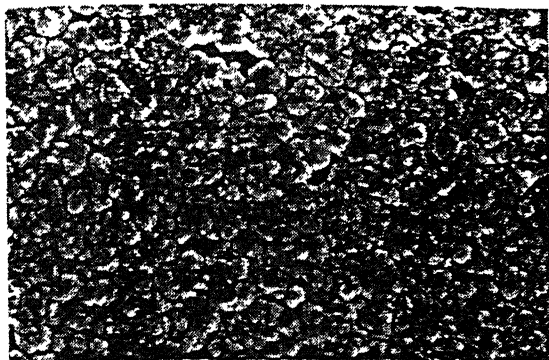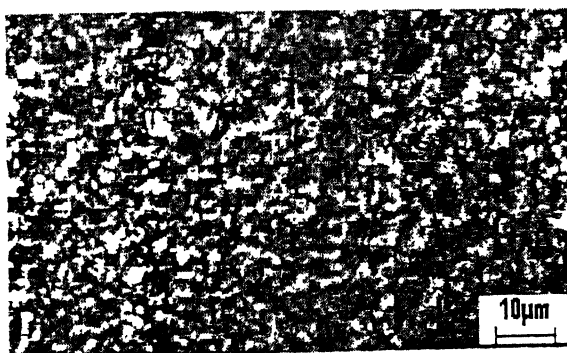
(a) 1mA/cm^2

(b) 10mA/cm^2

(c) 30mA/cm^2

(d) 50mA/cm^2

Fig. 4.16. SEM micrographs of Cu deposit on cold rolled Ni-60Co alloy substrate at different current densities.
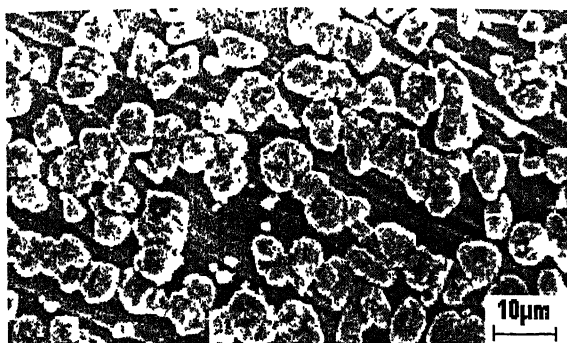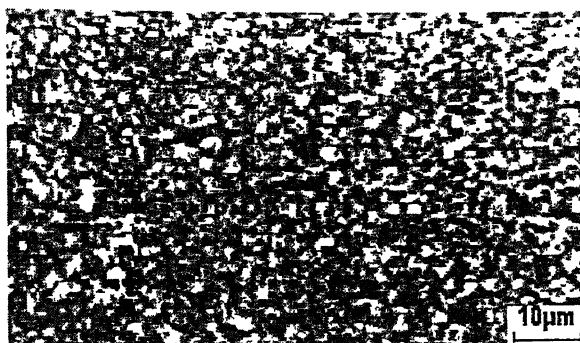
(a) $1mA/cm^2$
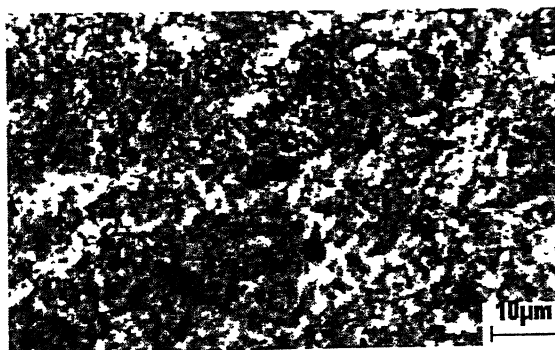
(b) $10mA/cm^2$

(c) $30mA/cm^2$
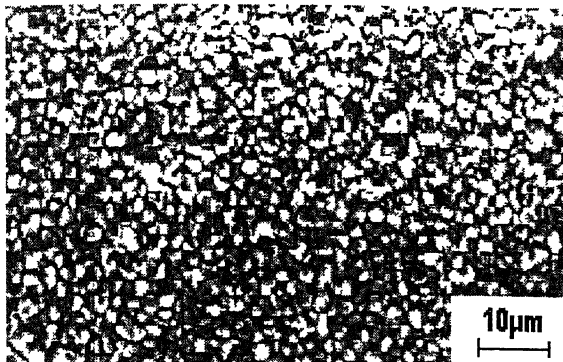
(d) $50mA/cm^2$

Fig. 4.17. SEM micrographs of Cu deposit on annealed Ni-10Co alloy substrate at different current densities.
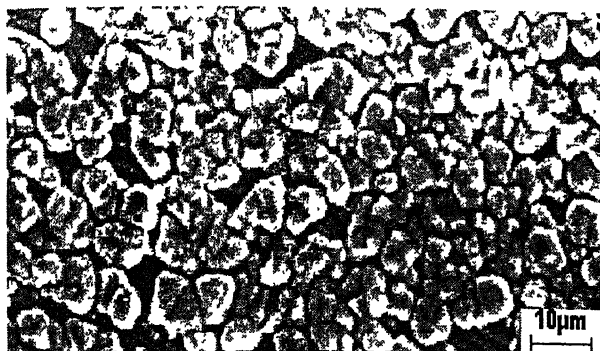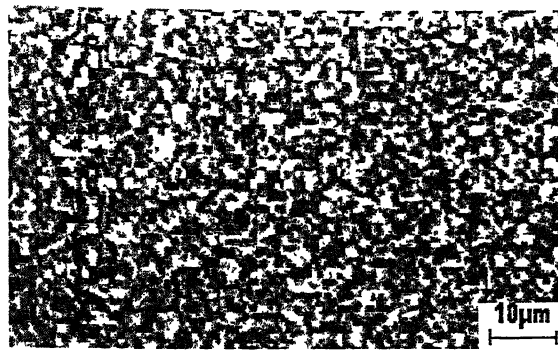
(a) $1mA/cm^2$
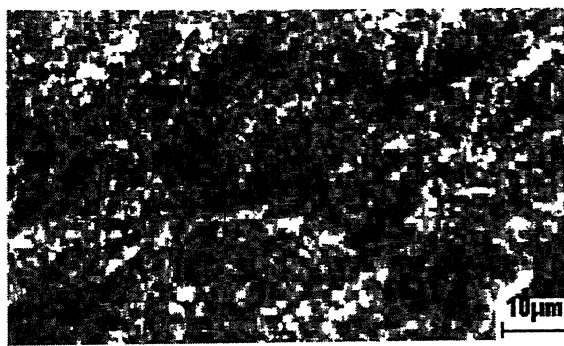
(b) $10mA/cm^2$

(c) $30mA/cm^2$
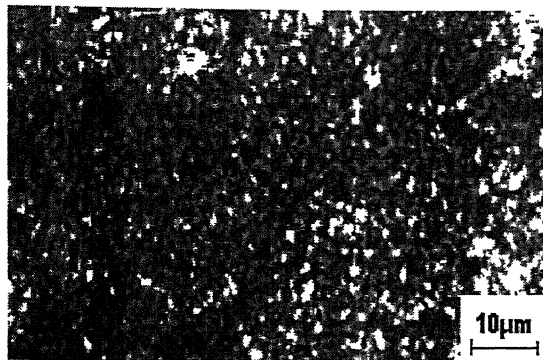
(d) $50mA/cm^2$

Fig. 4.18. SEM micrographs of Cu deposit on annealed Ni-20Co alloy substrate at different current densities.
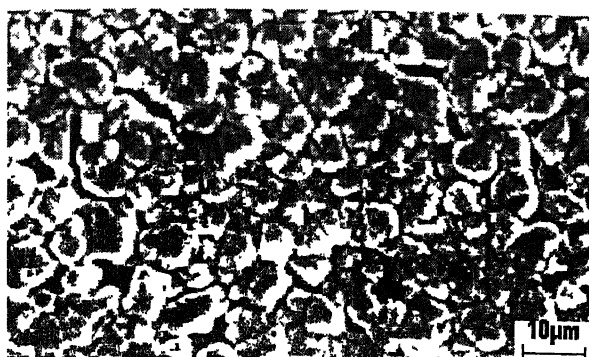
(a) 1mA/cm^2
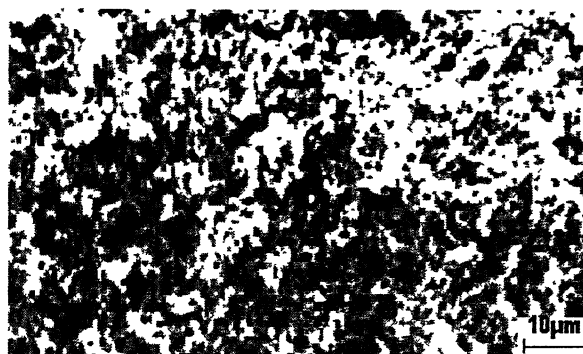
(b) 10mA/cm^2

(c) 30mA/cm^2

(d) 50mA/cm^2

Fig. 4.19. SEM micrographs of Cu deposit on annealed Ni-30Co alloy substrate at different current densities.
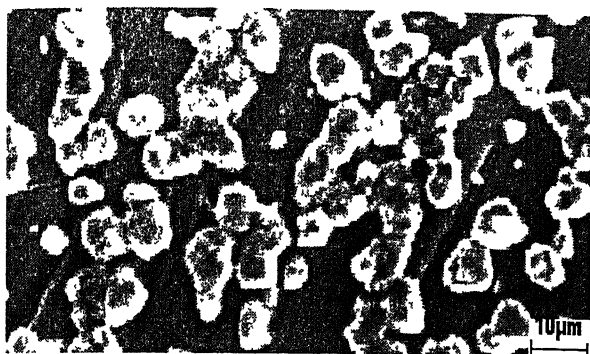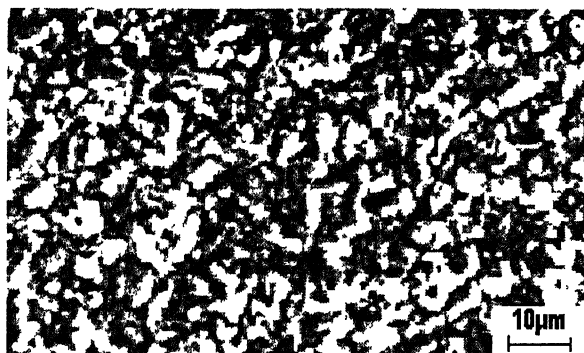
(a) 1mA/cm^2
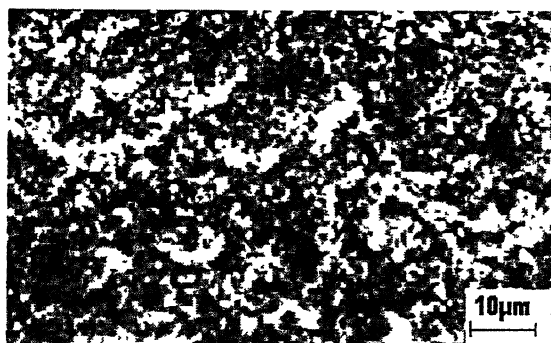
(b) 10mA/cm^2

(c) 30mA/cm^2

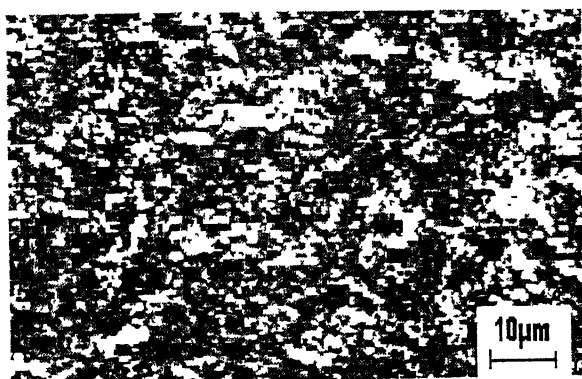**(d)** 50mA/cm^2

Fig. 4.20 SEM micrographs of Cu deposit on annealed Ni-40Co alloy substrate at different current densities.
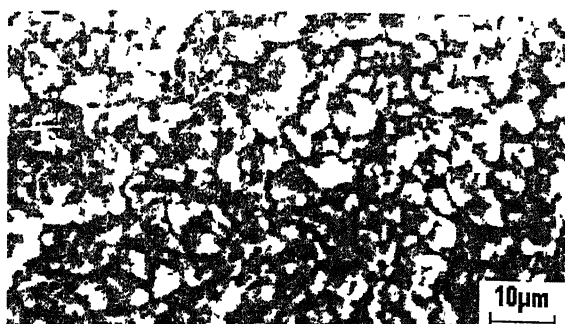
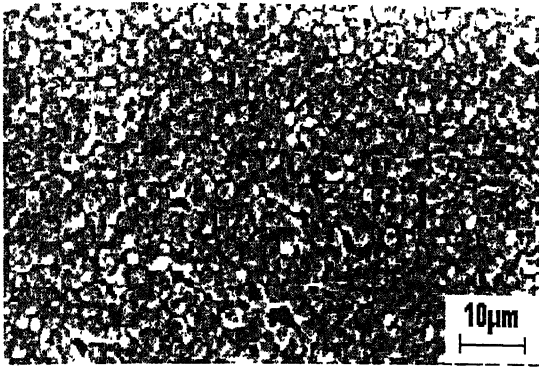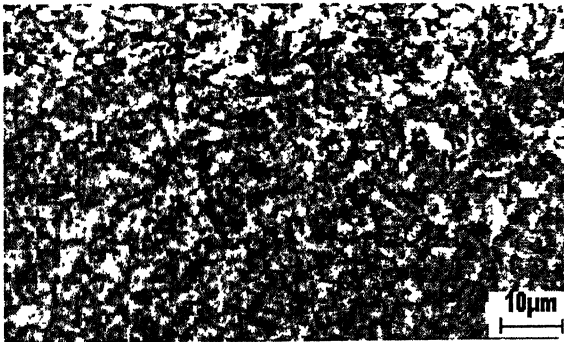**(a)** 1mA/cm^2
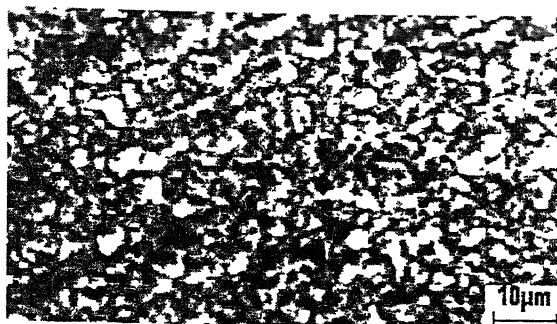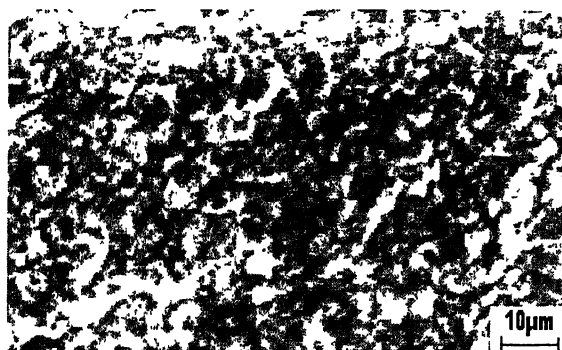
(b) 10mA/cm^2

(c) 30mA/cm^2

(d) 50mA/cm^2

Fig. 4.21. SEM micrographs of Cu deposit on annealed Ni-60Co alloy substrate at different current densities.

4.4. Results of surface roughness measurements

The surface roughness of the electroplated Cu on cold rolled as well as annealed Ni-Co alloys was measured in order to characterize the nature of the electrodeposited copper layer. As already stated, the measurement was carried out in a Fedral Surfanalyzer 5000 surface roughness testing machine. The roughness plots for Cu deposited on cold rolled Ni-10Co and annealed Ni-10Co at 1mA/cm^2 current density are shown in **Fig. 2.22a** and **Fig. 2.22b** respectively. Similarly, the roughness plots for Cu deposited on cold rolled Ni-60Co and annealed Ni-60Co at 50mA/cm^2 current density are shown in **Fig. 2.23a** and **Fig. 2.23b** respectively.

Tables 4.12-4.16 show the three roughness parameters R_a (average value), R_q (root mean square value) and R_y (peak to valley height value) for the cold rolled Ni-Co alloys with copper electrodeposition. **Table 4.12** shows the three roughness parameters at different current densities for Cu plated Ni-10Co alloy. Similarly, **Table 4.13, 4.14, 4.15** and **4.16** are values for Ni-20Co, Ni-30Co, Ni-40Co and Ni-60Co alloys respectively.

R_a, R_q and R_y values for annealed Ni-Co alloy with Cu electrodepostion are given in **Table 4.17-4.21** for different current densities. **Table 4.17, 4.18, 4.19, 4.20** and **4.21** give the three roughness parameters for annealed Ni-10Co, Ni-20Co, Ni-30Co, Ni-40Co and Ni-60Co alloys respectively.

The only parameter of maximum importance is the average roughness value R_a which is given is **Table 4.22** (Cu-plated cold rolled Ni-Co alloys) and **Table 4.23** (Cu-plated annealed Ni-Co alloys). These R_a values are plotted in **Fig.4.24-Fig.4.32**. **Fig. 4.24-Fig. 4.27** give the variation of roughness of the Cu deposit with different current densities for all the cold rolled and annealed Ni-Co substrates. **Fig.4.28-4.32** give the variation of roughness of the Cu deposit with increasing Co concentration in the alloy at different current density values. In each of the figures, B represents cold rolled condition and C represents annealed condition of the substrate.

Fig. 4.24 gives the roughness value, R_a (in μm) at a plating current density of 1mA/cm^2. The two boxes are for Cu-plated cold rolled alloy (box B) and Cu-plated annealed alloy (box C) respectively, as indicated in the figure. The R_a value corresponding to the Cu-plating on each of the five Ni-Co alloys are shown in the figure, both for cold rolled and annealed substrate. The figure shows that the average roughness

of Cu plated on annealed alloys (box C) is higher than that of cold-rolled alloys (box B) at 1mA/cm^2.

On increasing the current density (**Figs. 4.25, 4.26 and 4.27**), the average roughness value of Cu on annealed Ni-Co alloys decreases as compared to cold rolled alloys. At 50 mA/cm^2 it can be clearly seen that R_a is less for Cu-plated annealed Ni-Co alloys in comparison to Cu-plated cold rolled alloys.

Fig.4.28 shows the R_a values plotted for different current densities for Cu-plated Ni10-Co. The figure shows that R_a for C (annealed) is higher than for B (cold rolled). For Ni-20Co alloy substrate, R_a of Cu deposit is almost same for both cold-rolled and annealed condition (**Fig.4.29**). For higher Co concentration of 30% in the alloy substrate, R_a of Cu deposit on cold-rolled and annealed alloys show a wide variation. The average roughness of Cu on annealed Ni-30Co is lower than that of cold-rolled Ni-30Co alloy substrate (**Fig4.30**)

Again, for 40% concentration of Co in Ni, the roughness of Cu deposit is raised for annealed alloy (in comparison to cold rolled alloy substrate). This is shown in **Fig.4.31**. Finally **Fig.4.32** shows that the R_a value decreases for the copper deposit on annealed Ni-Co alloy substrate.

In short, it has been found that there is a general trend of the roughness of the electroplated copper when the substrates are compared.

SURFANALYZER 5000 05/26/2003 00:28

SAVED AS: (FILE NOT SAVED)
Company: FEDERAL PRODUCTS CO.
Part: XXX-YYY
Operator: J. EMPLOYEE

TEST CONDITIONS...
CUTOFF (r)   0.80 mm
CUTOFF (w)   0.80 mm
FILTER   ANSI 2-RC
DRIVE SPEED   0.50 mm/sec
PROBE RANGE   +/-500 Um (L)
PROBE RATIO   1:1
EVALUATION   1.00 mm
TRAVERSE   TL
POLARITY   Normal
HORIZ GRAD   0.1 mm/div
VERT SCALE   +/-25 Um

HORIZ GRAD   0.1 mm/div
VERT SCALE   +/-25.00 Um
                (5.00 Um/div)
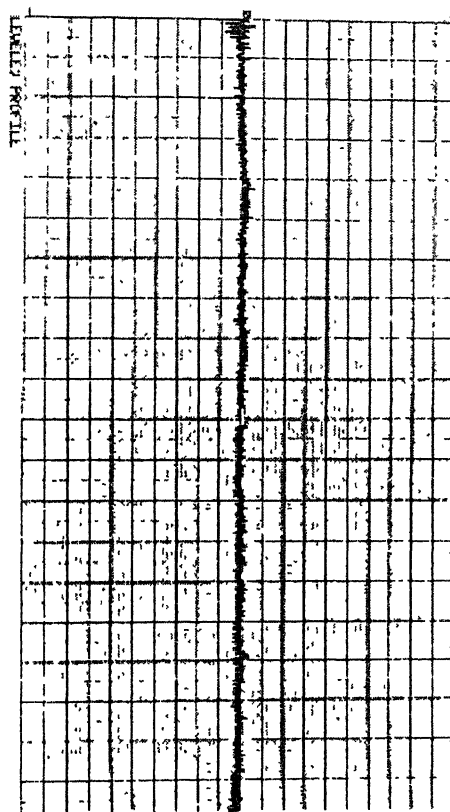
1 div = 1 cm

PARAMETER RESULTS...
PROFILE...
PR=
PRa=
PRq=
Pt=

ROUGHNESS.
R=
Ra=
Rq=

WAVINESS..
W=
Wa=
Wt=

Fig. 4.22(a) Roughness plot of Cu layer deposited on cold rolled Ni-10Co alloy substrate at 1mA/cm^2 current density

SURFANALYZER 5000 05/28/2003 01:18

SAVED AS· (FILE NOT SAVED)

Company: FEDERAL PRODUCTS CO.

    Part: XXX-YYY

Operator: J. EMPLOYEE

TEST CONDITIONS...

CUTOFF (r)	0.80 mm
CUTOFF (w)	0.80 mm
FILTER	ANSI 2-RC
DRIVE SPEED	0.25 mm/sec
PROBE RANGE	+/-50 Um (N)
PROBE RATIO	1:1
EVALUATION	0.66 mm
TRAVERSE	TL
POLARITY	Normal
HORIZ GRAD	0.05 mm/div
VERT SCALE	+/-5.0 Um

HORIZ GRAD	0.05 mm/div
VERT SCALE	+/-5.00 Um
	(1.00 Um/div)

1 div = 1 cm
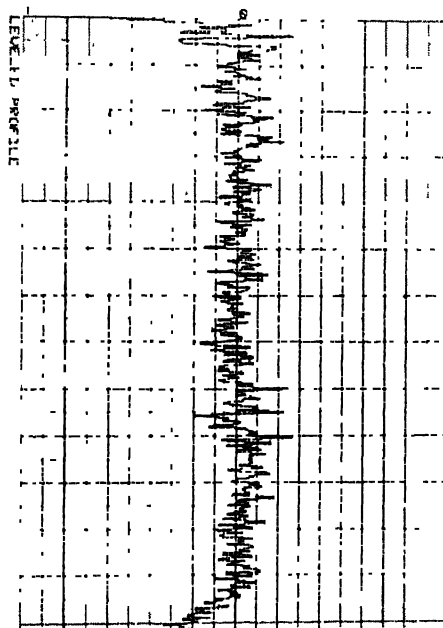
PARAMETER RESULTS...

PROFILE .
PRa	...	Um
PRq	...	Um
Pt	...	Um

ROUGHNESS...
Ra	0.34	Um
Rq	0.47	Um
Rv	4.40	Um

WAVINESS...
Wa	...	Um
Wq	...	Um
Wt	...	Um

Fig. 4.22(b) Roughness plot of Cu layer deposited on annealed Ni-10Co alloy substrate at 1mA/cm^2 current density

SURFANALYZER 5000   05/26/2003   06·17

SAVED AS: (FILE NOT SAVED)

Company: FEDERAL PRODUCTS CO.

    Part XXX-YYY

Operator J EMPLOYEE

TEST CONDITIONS

CUTOFF (r)   0.80 mm
CUTOFF (w)   0.80 mm
FILTER   ANSI 2-RC
DRIVE SPEED   0.25 mm/sec
PROBE RANGE   +/-50 Um (N)
PROBE RATIO   1:1
EVALUATION   0.66   mm
TRAVERSE   TL
POLARITY   Normal
HORIZ GRAD   0.05 mm/div
VERT SCALE   +/-5 0 Um

HORIZ GRAD   0.05 mm/div
VERT SCALE   +/-5.00 Um
                (1.00 Um/div)

1 div = 1 cm

LEVELED PROFILE
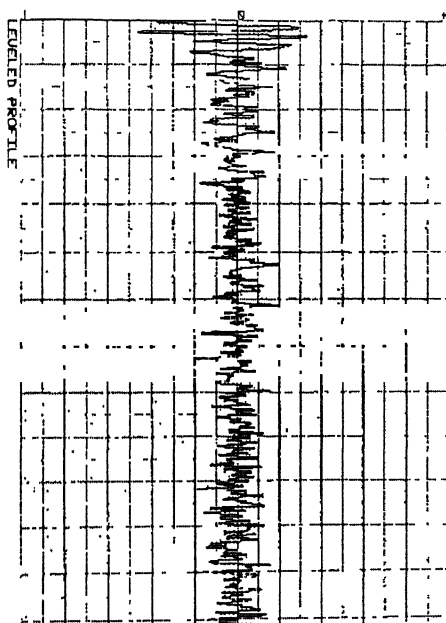
PARAMETER RESULTS ..

PROFILE...
PRa   ...   Um
PRq   Um
Pt   ...   Um

ROUGHNESS.
Ra   0.32   Um
Rq   0.44   Um
Rv   3.95   Um

WAVINESS ..
Wa   ..   Um
Wq   .   Um
Wt   ○   ..   Um

Fig. 4.23(a) Roughness plot of Cu layer deposited on cold rolled Ni-60Co alloy substrate at 50mA/cm^2 current density

FEDERAL®

SURFANALYZER 5000   05/28/2003   01:13

SAVED AS   (FILE NOT SAVED)
 Company: FEDERAL PRODUCTS CO.
    Part: XXX-YYY
Operator: J. EMPLOYEE

TEST CONDITIONS
CUTOFF (r)   0.80 mm
CUTOFF (w)   0.80 mm
FILTER   ANSI 2-RC
DRIVE SPEED   0.25 mm/sec
PROBE RANGE   +/-50 Um (N)
PROBE RATIO   1:1
EVALUATION   0.66   mm
TRAVERSE   TL
POLARITY   Normal
HORIZ GRAD   0.05 mm/div
VERT SCALE   +/-5.0 Um

HORIZ GRAD   0.05 mm/div
VERT SCALE   +/-5.00 Um
                  (1.00 Um/div)

1 div = 1 cm

LEVELLED PROFILE
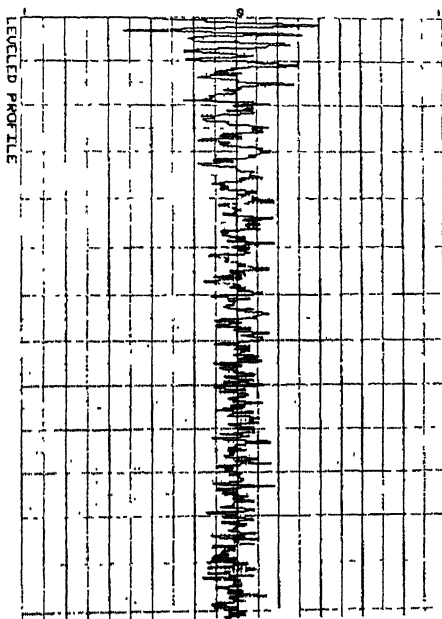
PARAMETER RESULTS...

PROFILE...
PRa   ...   Um
PRq   ...   Um
Pt   ...   Um

ROUGHNESS
Ra   0.36   Um
Rq   0.49   Um
Rv   4.60   Um

WAVINESS...
Wa   ...   Um
Wq   ...   Um
Wt   ...   Um

Fig. 4.23(b) Roughness plot of Cu layer deposited on annealed Ni-60Co alloy substrate at 50mA/cm^2 current density

Table 4.12. Surface roughness of electrodeposited Cu layer on cold rolled Ni-10Co

Roughness parameters(μm)	Current density			
	$1mA/cm^2$	$10mA/cm^2$	$30mA/cm^2$	$50mA/cm^2$
R_a	0.70	0.33	0.39	0.37
	0.30	0.35	0.43	0.40
	-	0.40	0.35	0.44
	-	-	0.34	0.34
R_q	0.90	0.48	0.55	0.49
	0.40	0.51	0.60	0.57
	-	0.55	0.52	0.67
	-	-	0.47	0.52
R_y	0.20	5.45	5.60	4.05
	4.80	5.70	5.60	5.45
	-	5.10	5.60	5.50
	-	-	5.20	5.15

Table 4.13. Surface roughness of electrodeposited Cu layer on cold rolled Ni-20Co

Roughness parameters(μm)	Current density			
	$1mA/cm^2$	$10mA/cm^2$	$30mA/cm^2$	$50mA/cm^2$
R_a	0.30	0.29	0.33	0.37
	0.40	0.47	0.32	0.34
	0.40	0.56	0.44	0.41
	-	0.42	0.39	0.28
R_q	0.40	0.40	0.48	0.54
	0.50	0.60	0.46	0.48
	0.50	0.96	0.40	0.59
	-	0.63	0.49	0.41
R_y	5.00	3.80	5.85	5.30
	4.80	4.45	4.95	5.00
	5.00	12.65	5.95	6.05
	-	6.90	5.45	3.08

Table 4.14. Surface roughness of electrodeposited Cu layer on cold rolled Ni-30Co

Roughness parameters(μm)	Current density			
	1mA/cm^2	10mA/cm^2	30mA/cm^2	50mA/cm^2
R$_a$	0.60	0.31	0.33	0.41
	0.30	0.34	0.33	0.36
	0.70	0.28	0.29	0.31
	-	0.41	0.32	0.34
R$_q$	0.80	0.45	0.48	0.54
	0.40	0.50	0.46	0.46
	1.00	0.43	0.40	0.45
	-	0.58	0.49	0.46
R$_y$	5.80	4.60	5.45	4.55
	4.00	5.95	4.70	3.30
	6.00	5.10	4.15	4.80
	-	4.95	5.70	5.20

Table 4.15. Surface roughness of electrodeposited Cu layer on cold rolled Ni-40Co

Roughness parameters(μm)	Current density			
	1mA/cm^2	10mA/cm^2	30mA/cm^2	50mA/cm^2
R$_a$	0.30	0.38	0.31	0.32
	0.30	0.36	0.29	0.30
	0.30	0.34	0.28	0.31
		0.36	0.33	0.31
R$_q$	0.40	0.53	0.44	0.45
	0.40	0.53	0.42	0.42
	0.40	0.53	0.43	0.42
	-	0.49	0.49	0.43
R$_y$	4.80	5.10	4.95	5.00
	4.60	6.00	4.10	4.60
	5.40	7.40	5.60	4.75
	-	4.85	5.45	4.55

Table 4.16. Surface roughness of electrodeposited Cu layer on cold rolled Ni-60Co

Roughness parameters(μm)	Current density			
	$1mA/cm^2$	$10mA/cm^2$	$30mA/cm^2$	$50mA/cm^2$
R_a	0.30	0.33	0.28	0.32
	0.50	0.33	0.39	0.37
	0.30	0.27	0.31	0.29
	0.30	0.33	0.38	0.34
R_q	0.40	0.50	0.43	0.44
	0.60	0.44	0.54	0.51
	0.40	0.40	0.46	0.42
	0.40	0.45	0.50	0.47
R_y	4.40	6.20	5.40	3.95
	4.60	4.70	5.40	4.55
	4.60	3.95	5.75	4.05
	4.00	4.65	4.55	5.05

Table 4.17. Surface roughness of electrodeposited Cu layer on annealed Ni-10Co

Roughness parameters(μm)	Current density			
	1mA/cm^2	10mA/cm^2	30mA/cm^2	50mA/cm^2
R_a	0.29	0.36	0.46	0.40
	0.34	0.33	0.46	0.30
	0.45	0.32	0.40	0.31
	0.46	0.34	0.33	0.32
R_q	0.46	0.54	0.61	0.54
	0.47	0.52	0.62	0.40
	0.66	0.49	0.56	0.43
	0.58	0.47	0.49	0.41
R_y	4.95	6.25	5.40	4.75
	4.40	6.40	5.80	3.25
	6.15	5.80	5.35	4.50
	4.25	3.80	5.30	2.65

Table 4.18. Surface roughness of electrodeposited Cu layer on annealed Ni-20Co

Roughness parameters(μm)	Current density			
	1mA/cm^2	10mA/cm^2	30mA/cm^2	50mA/cm^2
R_a	0.38	0.44	0.33	0.33
	0.29	0.39	0.31	0.32
	0.46	0.32	0.33	0.39
	0.36	0.33	0.37	0.33
R_q	0.52	0.61	0.49	0.42
	0.40	0.55	0.46	0.43
	0.63	0.49	0.46	0.56
	0.54	0.50	0.49	0.43
R_y	4.85	6.00	5.50	3.20
	4.20	5.35	5.35	3.75
	6.65	5.75	5.30	6.50
	5.90	5.75	4.25	3.80

Table 4.19. Surface roughness of electrodeposited Cu layer on annealed Ni-30Co

Roughness parameters(μm)	Current density			
	1mA/cm^2	10mA/cm^2	30mA/cm^2	50mA/cm^2
R_a	0.34	0.34	0.31	0.29
	0.32	0.28	0.35	0.27
	0.34	0.31	0.33	0.34
	0.33	0.32	0.30	0.29
R_q	0.49	0.49	0.46	0.41
	0.47	0.45	0.47	0.35
	0.48	0.43	0.44	0.45
	0.46	0.46	0.39	0.37
R_y	5.60	5.35	5.25	4.85
	4.95	6.15	4.05	3.10
	4.95	4.80	3.85	3.50
	3.95	5.35	3.10	2.90

Table 4.20. Surface roughness of electrodeposited Cu layer on annealed Ni-40Co

Roughness parameters(μm)	Current density			
	1 mA/cm^2	10 mA/cm^2	30 mA/cm^2	50mA/cm^2
R_a	0.36	0.34	0.28	0.32
	0.36	0.44	0.35	0.31
	0.41	0.41	0.29	0.30
	0.39	0.37	0.29	0.32
R_q	0.49	0.47	0.40	0.45
	0.53	0.57	0.46	0.43
	0.57	0.57	0.40	0.38
	0.52	0.49	0.37	0.40
R_y	4.90	4.50	4.25	5.10
	6.45	4.30	3.65	4.85
	5.95	4.85	4.00	2.80
	4.20	4.30	2.75	3.35

Table 4.21. Surface roughness of electrodeposited Cu layer on annealed Ni-60Co

Roughness Parameters(µm)	Current density			
	1 mA/cm^2	10 mA/cm^2	30 mA/cm^2	50 mA/cm^2
R_a	0.32	0.29	0.48	0.36
	0.29	0.29	0.28	0.30
	0.32	0.33	0.41	0.30
	0.33	0.29	0.28	0.33
R_q	0.48	0.45	0.62	0.49
	0.44	0.41	0.37	0.39
	0.50	0.47	0.58	0.41
	0.47	0.42	0.37	0.46
R_y	4.70	5.50	4.45	4.60
	6.00	4.55	2.80	3.75
	5.65	5.00	6.20	4.10
	5.60	5.30	3.15	4.45

Table 4.22. R_a values of electrodeposited Cu layer on cold rolled Ni-Co alloys

Current density → R_a (μm)	1mA/cm²	10mA/cm²	30mA/cm²	50mA/cm²
Ni-10Co	0.250	0.270	0.3775	0.3875
Ni-20Co	0.275	0.435	0.3700	0.3500
Ni-30Co	0.400	0.335	0.3175	0.3550
Ni-40Co	0.225	0.360	0.3025	0.3100
Ni-60Co	0.350	0.315	0.3400	0.33

Table 4.23. R_a values of electrodeposited Cu layer on annealed Ni-Co alloys

Current density → R_a (μm)	1mA/cm²	10mA/cm²	30mA/cm²	50mA/cm²
Ni-10Co	0.3850	0.3375	0.4125	0.3325
Ni-20Co	0.3725	0.3700	0.3350	0.3425
Ni-30Co	0.3325	0.3125	0.3225	0.2975
Ni-40Co	0.3800	0.3900	0.3025	0.3125
Ni-60Co	0.3150	0.3000	0.3625	0.3225

Fig. 4.24. Plots showing R_a (roughness parameter) values of copper layer on cold rolled and annealed Ni-Co alloy substrates at 1mA/cm^2 current density.

Fig. 4.25. Plots showing R_a (roughness parameter) values of copper layer on cold rolled and annealed Ni-Co alloy substrates at $10mA/cm^2$ current density.

Fig. 4.26. Plots showing R_a (roughness parameter) values of copper layer on cold rolled and annealed Ni-Co alloy substrates at 30mA/cm^2 current density.
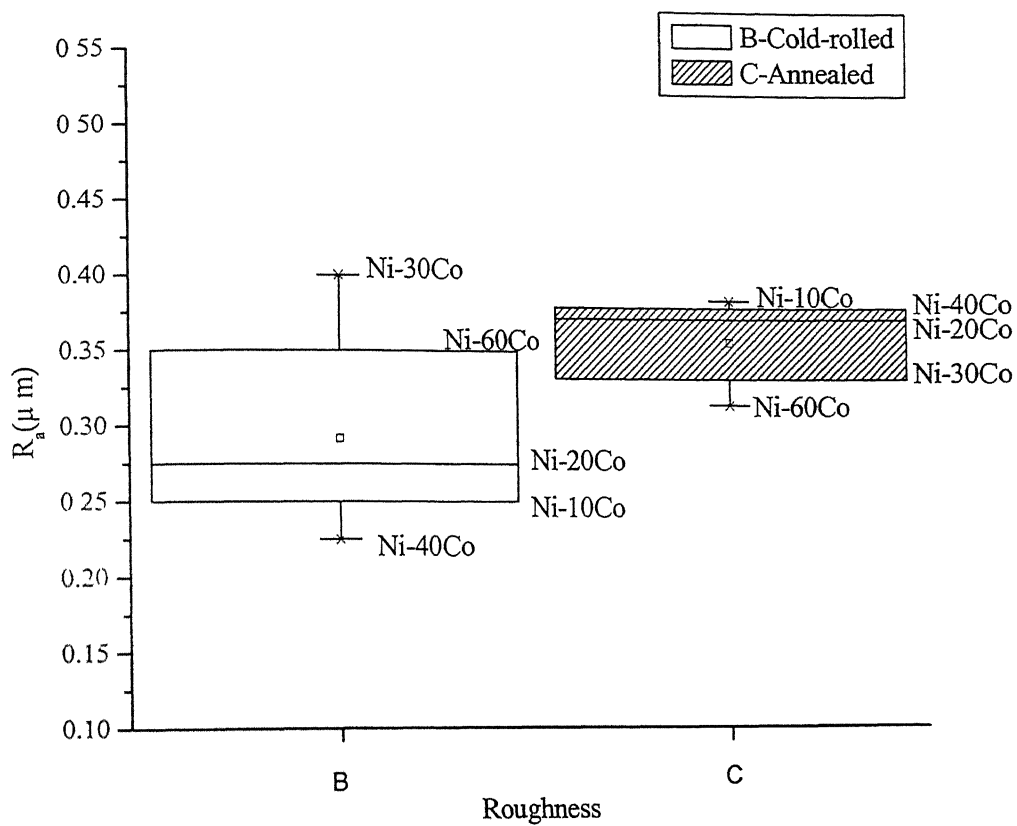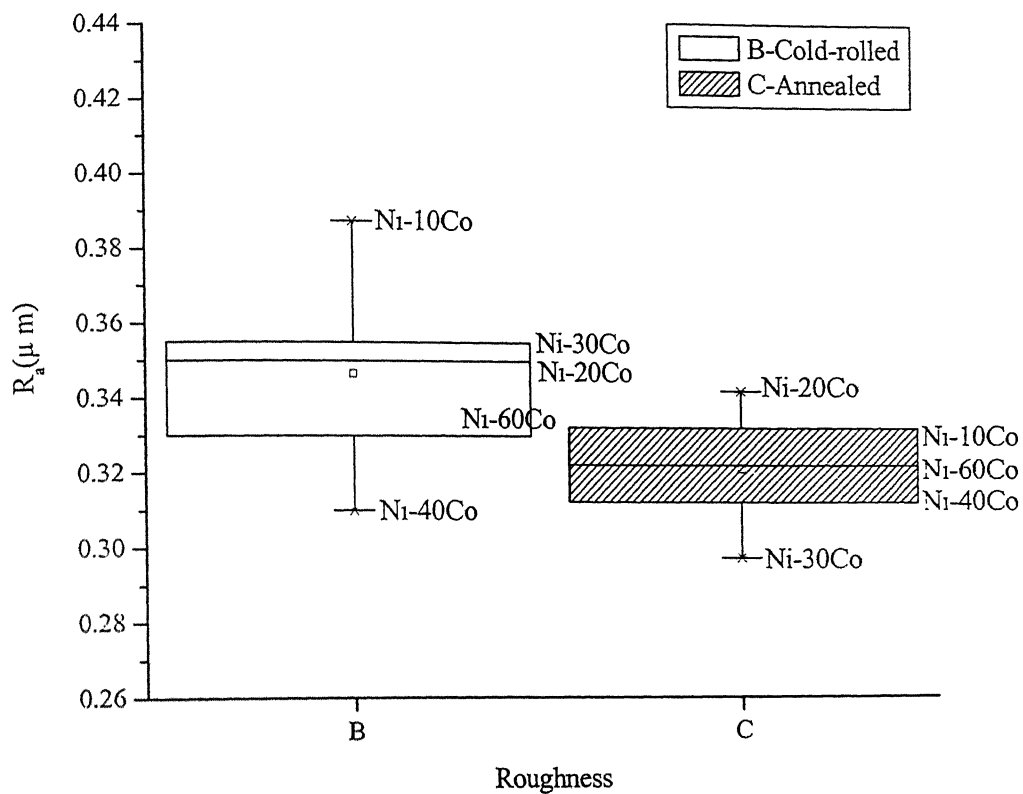
Fig. 4.27. Plots showing R_a (roughness parameter) values of copper layer on cold rolled and annealed Ni-Co alloy substrates at 50mA/cm^2 current density.
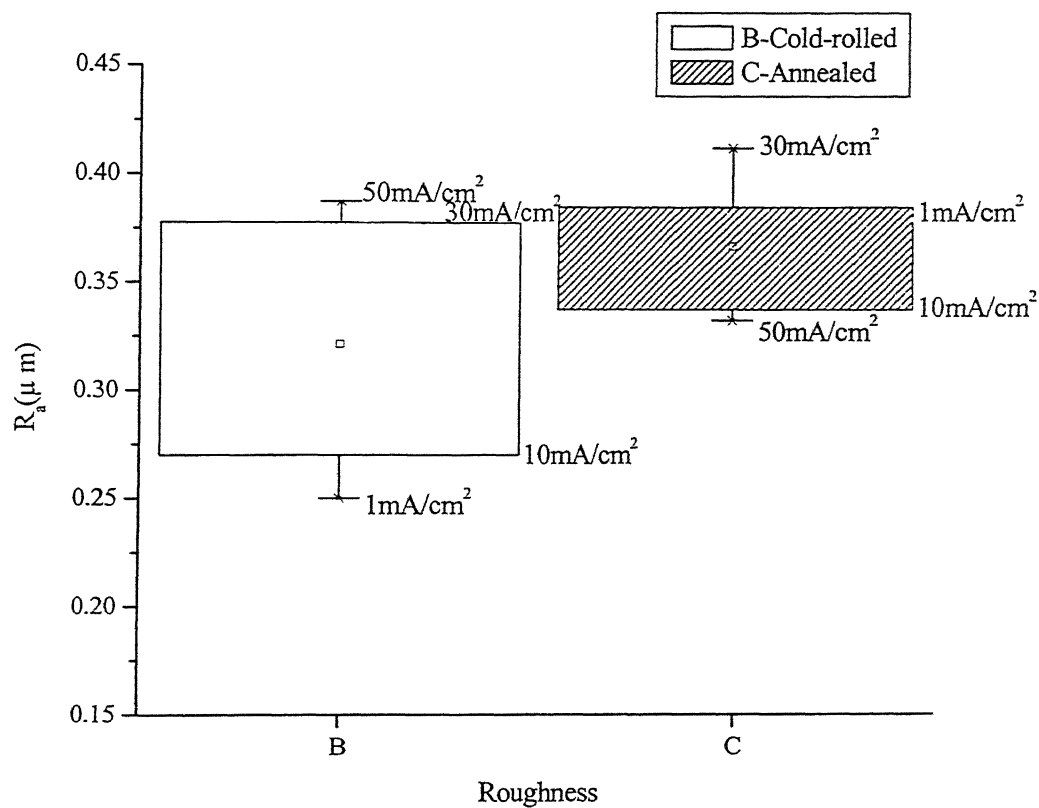
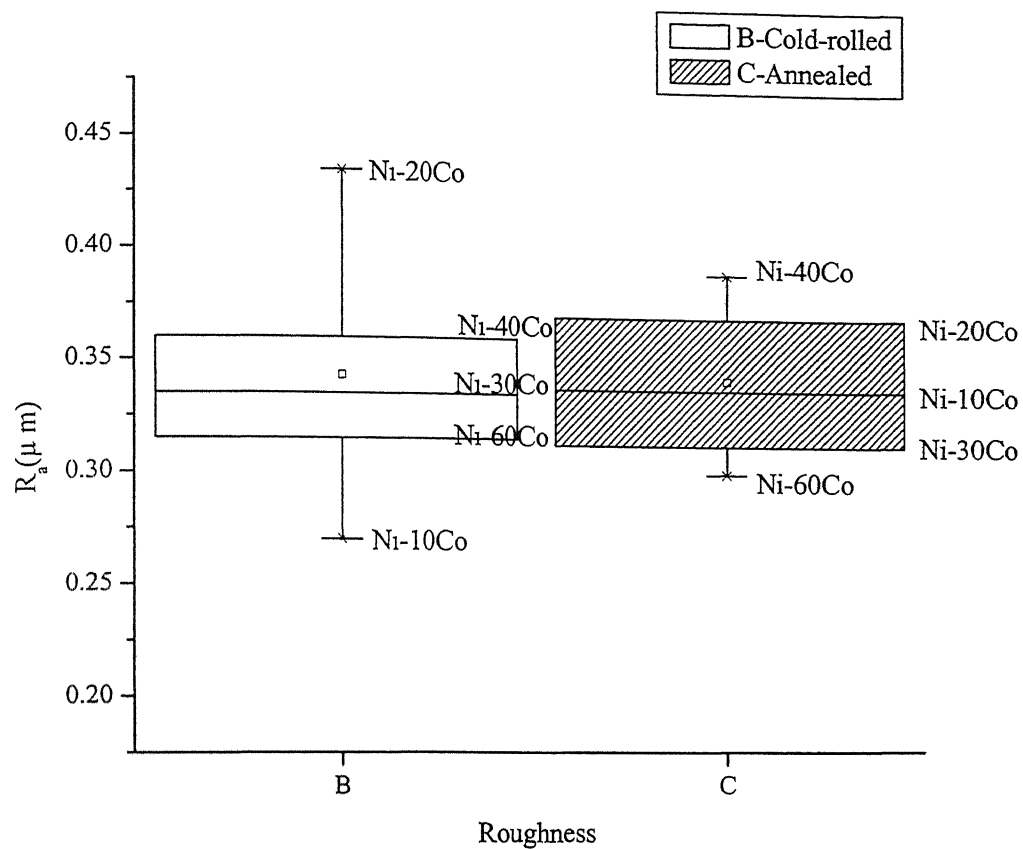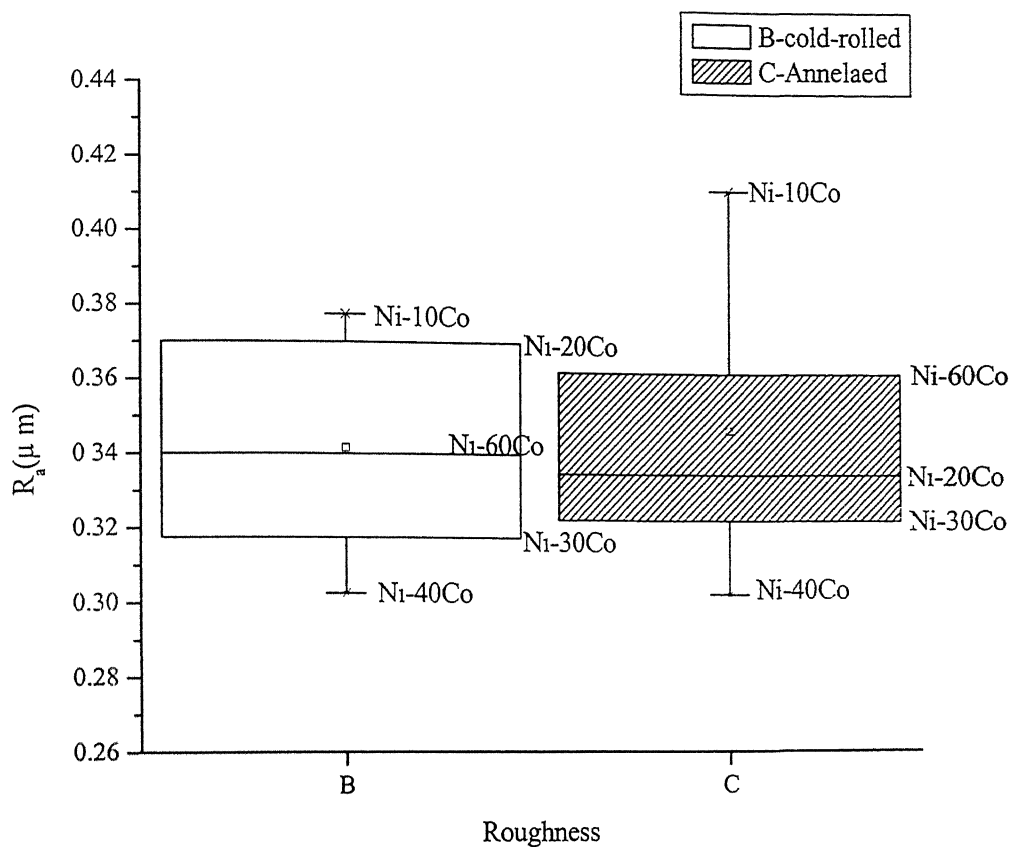**Fig. 4.28.** Plots showing R_a (roughness parameter) values of copper layer on cold rolled and annealed Ni-10Co alloy substrates at different current densities.
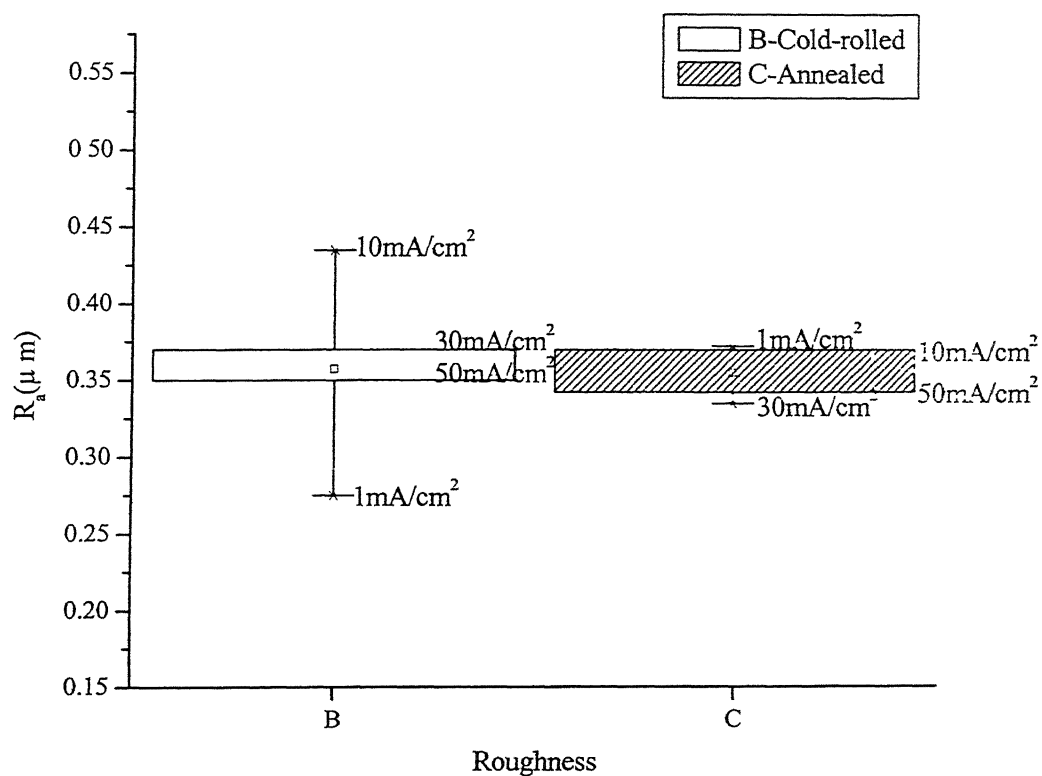
Fig. 4.29. Plots showing R_a (roughness parameter) values of copper layer on cold rolled and annealed Ni-20Co alloy substrates at different current densities.

Fig. 4.30. Plots showing R_a (roughness parameter) values of copper layer on cold rolled and annealed Ni-30Co alloy substrates at different current densities.

Fig. 4.31. Plots showing R_a (roughness parameter) values of copper layer on cold rolled and annealed Ni-40Co alloy substrates at different current densities.

Fig. 4.32. Plots showing R_a (roughness parameter) values of copper layer on cold rolled and annealed Ni-60Co alloy substrates at different current densities.
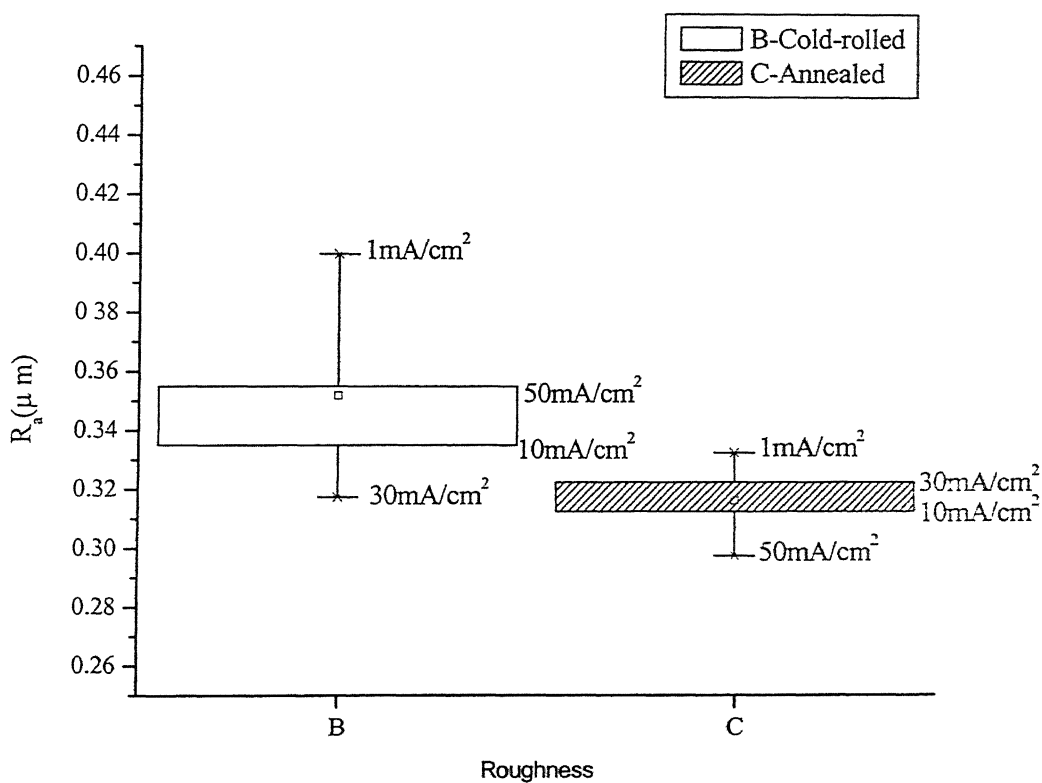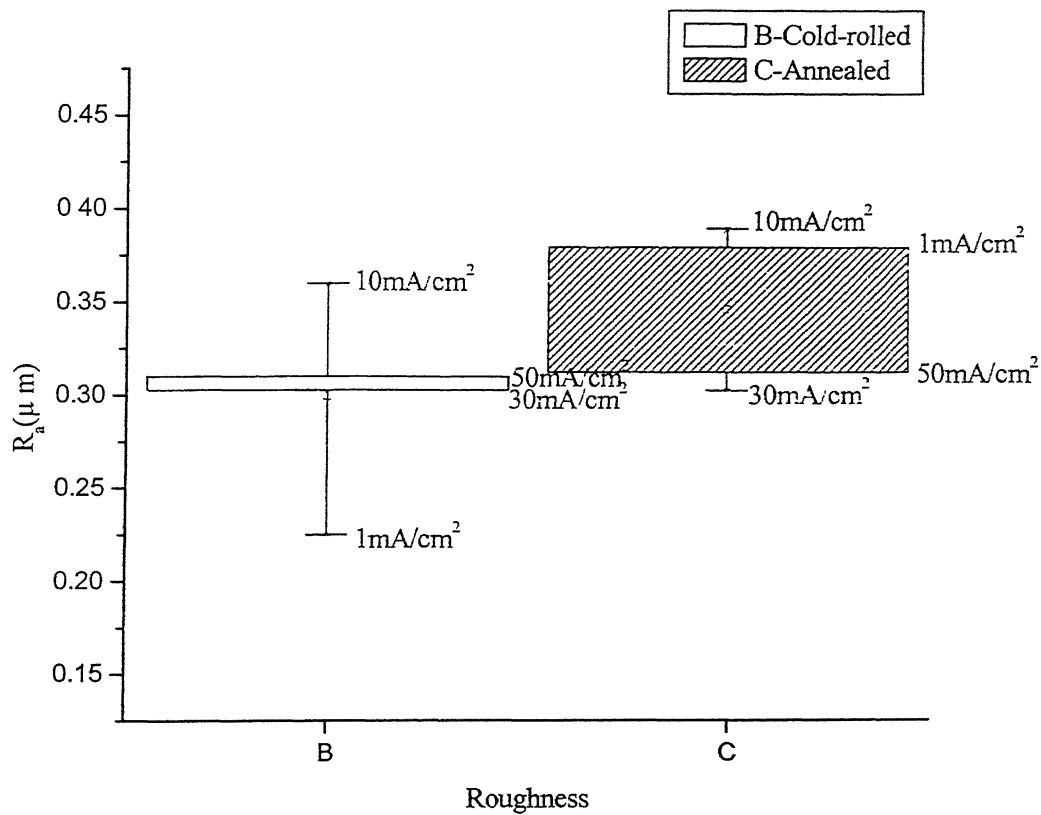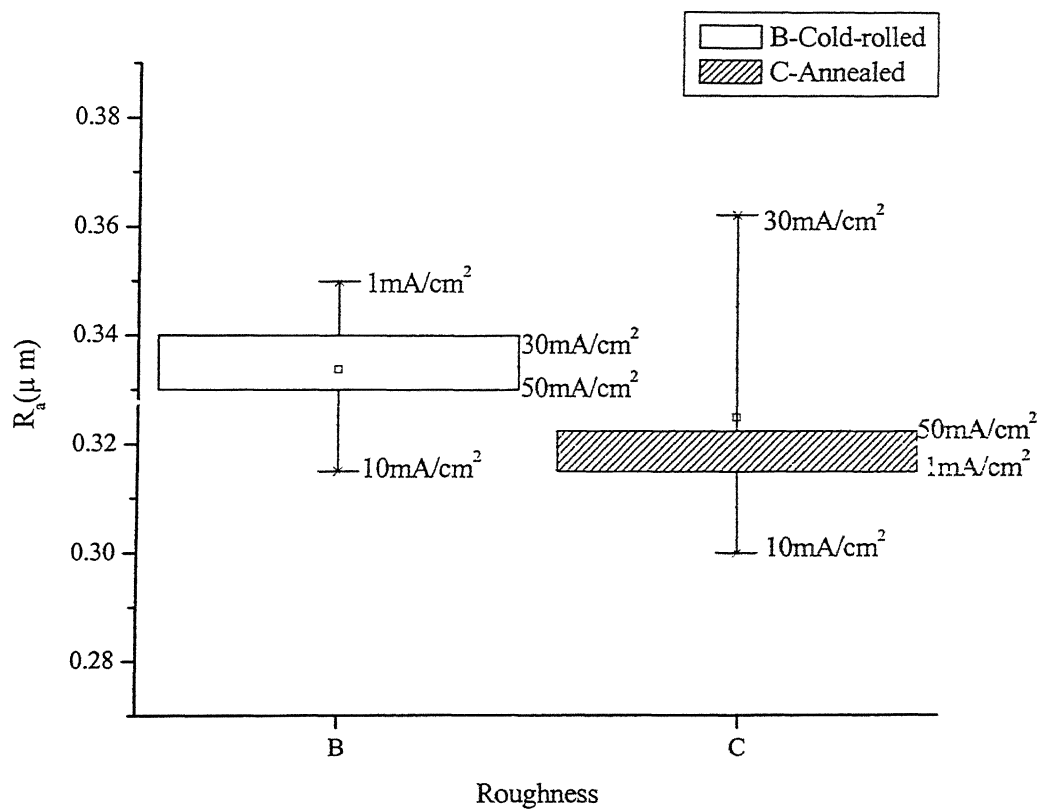
CHAPTER 5

DISCUSSION

In the present investigation, pure Cu was electroplated on Ni-Co substrates, which were initially cold rolled and annealed in order to develop different crystallographic textures. Out of the five cold rolled alloys, Ni-10Co, Ni-20Co and Ni-30Co alloys possessed a typical Cu-type texture, whereas Ni-60Co alloy had a typical brass type texture[40]. In the former, the major texture components were {110}<112>, {112}<111> and {123}<634>, while in the latter, the components were {110}<112> and {110}<001>. In contrast the Ni-40Co alloy showed a mixed type of texture, intermediate between the above two. So far as the cold rolled and annealed alloys are concerned, the major texture component of the alloys Ni-10Co, Ni-20Co and Ni-30Co were the cube {100}<001>, the amount of this component decreased with the Co content. The Ni-40Co alloy contained very little of this component and this was practically zero in the Ni-60Co alloy- the major texture component of the latter being {110}<112>[40]

The thickness of the electrodeposited layer and the course of its development was found to be more or less constant, irrespective of the texture of the substrate. This is clearly evident from this study. The substrate composition also does not seem to have any affect on the thickness of the electrodeposited layer. The thickness has nearly linear relationship with current density.

From the X-ray diffraction patterns of Cu electroplated cold rolled Ni-10Co it is evident that in general, the Cu pattern sharpens and Ni pattern weakens as current density increases. This is quite natural, since with increase in current density the thickness of the Cu layer increases. Cu(111)/Cu(220) ratio decreases with current density. In other words, out of the (111), (200) and (220) peaks of Cu, the Cu(220) peak increases in intensity and the Cu(111) peak decreases in intensity while the Cu(200) peak remains more or less the same in intensity. Initially, Ni(220) is the strongest peak (at $1mA/cm^2$). Finally, at $50mA/cm^2$, Cu(220) is the strongest peak. It strengthens from a current density level of $10mA/cm^2$. The same pattern is found for cold rolled Ni-20Co, Ni-30Co, Ni-40Co and Ni-60Co substrate. From these results it is understandable that with increases in current density there is a definite change in the texture of the electrodeposited layer. Usually in

untextured Cu,(111) is the strongest peak, while the present investigation shows a progressive increase of the Cu(220) peak with the increment in current density. However, strangely enough these textural changes in the Cu deposit seem to be quite independent of the texture as well as the composition of the cold rolled substrate materials.

Similarly for the annealed substrates, the Ni pattern gradually weakens with increase in current density and Cu pattern sharpens. But here, initially the Ni(200) is the sharpest (at $1mA/cm^2$), contrary to that obtained for the cold rolled substrates. This Ni(200) weakens from $30mA/cm^2$ onwards. Finally, Cu(220) is the sharpest, sharpening starts at $30mA/cm^2$ for Ni-10Co and Ni-20Co alloy substrates while sharpening starts at $10mA/cm^2$ for Ni-30Co, Ni-40Co and Ni-60Co substrates. Ni(200) almost vanishes after $10mA/cm^2$ for Ni-40Co. Ni(200) is practically zero right from the beginning in Ni-60Co. Ni(220) is rather sharp initially for Ni-40Co and Ni-60Co. These results again indicate that the texture of electrodeposited layer is more or less independent of the texture of the annealed substrate materials too. The most interesting result is that whether the substrates are in the cold rolled or in annealed conditions (and therefore vary widely in their textures), the Cu(220) peak ultimately becomes the strongest peak of the electrodeposited layer. Thus the electrodeposited layer exhibits a definite strong texture when it finally develops.

In all the above cases the deposited Cu layer did not inherit the texture of the substrate at the lower current densities, and also developed its own texture at higher current densities. Thin electroplated coatings of fcc metals usually have a <111> fiber texture since the (111) close-packed surface in these materials is associated with the lowest surface free energy[40]. This has not been found to be true, however, in the present case.

From SEM study, we find that for both cold rolled and annealed materials, grain size decreases with increase in current density, the role of the substrate texture again does not seem to be important here.

From the roughness results, it is found that the variation of R_a with current density, at a particular composition of substrate is more in cold rolled materials than in annealed materials. However, within each group, variation of R_a with current density does not follow a general trend, it is rather erratic. The same trend is observed when variation of

R_a with composition (at a particular current density) is considered (see **Tables 5.1 and 5.2**).

Table 5.1 Variation of R_a with current density for a particular composition:

Composition of substrate	Cold rolled alloy substrate:	Annealed alloy substrate:
	Variation of R_a(μm)	
Ni-10Co	0.14	0.08
Ni-20Co	0.16	0.04
Ni-30Co	0.10	0.03
Ni-40Co	0.13	0.08
Ni-60Co	0.04	0.06

Table 5.2 Variation of R_a with composition at a particular current density:

Current density	Cold rolled alloy substrate:	Annealed alloy substrate:
	Variation of R_a(μm)	
1mA/cm^2	0.18	0.07
10A/cm^2	0.19	0.09
30mA/cm^2	0.07	0.11
50mA/cm^2	0.08	0.05

These results seem to indicate that the substrate texture could have some effect on the roughness of the electrodeposited layer. The deposited layers are definitely much more smooth in case of the annealed than in the cold rolled Ni-Co alloys. The exact reason for this is not very clear though.

Overall, the crystallographic textures of Ni-Co alloy substrates do not seem to have any tangible effect on the texture and grain size of the electrodeposited Cu layer, whereas the roughness properties of the layers seem to be affected somewhat by the substrate texture.

CHAPTER 6

CONCLUSION

1. The thickness of the electrodeposited layer and the course of its development was found to be more or less constant, irrespective of the texture of the substrate.

2. The substrate composition also does not seem to have any affect on the thickness of the electrodeposited layer. The thickness has nearly linear relationship with current density.

3. From the X-ray diffraction patterns of Cu electroplated on cold rolled and annealed Ni-Co alloys it is evident that in general, the Cu pattern sharpens and Ni pattern weakens as current density increases For annealed substrate, initially the Ni(200) is the sharpest (at $1mA/cm^2$), contrary to that obtained for the cold rolled substrates(where Ni(220) is the sharpest at the lowest current density).

4. In the present investigation a progressive increase of the Cu{220} peak with the increment in current density has been found. However, these textural changes in the Cu deposit seem to be quite independent of the texture as well as the composition of the cold rolled substrate materials. The deposited Cu layer did not inherit the texture of the substrate at the lower current densities, and also developed its own texture at higher current densities. The Cu(220) peak ultimately becomes the strongest peak of the electrodeposited layer.

6. From SEM study, we it was found that for both cold rolled and annealed materials, grain size decreases with increase in current density, the role of the substrate texture again does not seem to be important here.

7. The deposited layers are definitely much more smooth in case of the annealed than in the cold rolled Ni-Co alloys. This was obtained from roughness study.

REFERENCES:

1.Copper Plating, *Metal Finishing, Volume 98, Issue 1, 2000, Page 234* Romualdas "Ron" Barauskas

2. *Electroplating*, F.A. Lowenheim

3. Electroplating science, Gaida, Bernhard

4. Modern Electroplating, Lainer, V. I.

5. Practical electroplating Handbook, Parathasaradhy, N. V.

6. Handbook of Practical Electroplating, Rodgers, Thomas M.

7. Choi et al.(1998) *J. Korean Institute of Metals and Materials*, Vol. 36, No. 10, P1686

8. Gewith et al. J.O. (1998)

9. *TIME* (1997) Vol.6, P72

10. P. Singer, Semicond. Int.Vol. 21 (1998), p.91

11. Kim and Hong, *"Microstructures and textures of copper electrodeposition on the WN diffusion barrier"*, Proc.12th Intl. Conf on Textures of Materials .

12. Jae-Young Cho and Jerzy A. Szpunar, *"The effect of Substrate Texture and Electroplating Conditions on the Texture and Surface Morphology of Copper Electrodeposits"*

13. K.De Blauwe, A De Boeck, J. Bollen and W.Timmermans, *"Influence of Processing Paramaters on the Texture of Pure Zinc Electrodeposited Coatings on Steel"*.

14. Lin, Y., (1992) *"Microstructure of Zinc-based Coatings on Steel Sheets"*, Ph.D. Thesis, Northwestern University, Evanston, Illinois.

15. H.Park and J.A.Szpunar *"The influence of deposition parameters on texture in electrogalvanized zinc coating"*.

16. K. Lüke, Proc. Sixth Int. Conf. Text. Mater. 1, 14(1981)

17. R.K. Ray, Acta Metall.Mater. Vol.43, No.10, 3861-3872, 1995.

18. J.Hirsch and K. Lüke, *Acta metal.* 36, 2863 (1988).

19. K.H. Virnich, *Phd dissertation*, Intitut für Metallkunde, R.W.T.H. Aachen, Germany (1979)

20. P. Singer, Semicond. Int. 21 (1998) 90.

21. P. Singer, Semicond. Int. 17 (1994) 52.

22. K. Sheppard, R. Weil, Semicond. Int. 20 (1997) 67.

24. C. Rye, K. Kwon, A.L.S. Loke, H. Lee, T. Nogami, M. Dubin, R.A. Kavari, G.W. Ray, S.S. Wong, IEEE Trans. Electron Devices 46 (1999) 1113.

25. Anette A. Rasmussen a, Jens A.D. Jensen a,1, Andy Horsewell a, Marcel A.J. Somers , *"Microstructure in electrodeposited copper layers; the role of the substrate"* Electrochimica Acta 47 (2001) 67–74.

26. M. T. Pérez-Prado and J. J. Vlassak, *"Microstructural evolution in electroplated Cu Thin films"*

27. Brongersma SH, Richard E, Vervoort I, Maex K. IEEE. 2000;31-33.

28. Lee H, Lopatin D, Wong SS. IEEE. 2000; 114-116.

29. S. Simon Wong, Changsup Ryu, Haebum Lee, Alvin L.S. Loke, Kee-Won Kwon, Som Bhattacharya, Rory Eaton, Rick Faust, Bob Mikkola, Jay Mucha, and John Ormando, *"Barrier/Seed Layer Requirements for Copper interconnects"*, 1998 International Interconnect Technology Conference.

30. J. Pospiech and J. Jura, Z. Metallkd., 65 (1974) 324.

31. H. J. Bunge, Mathematische Methoden der Texturanalyse. Academic Press, Berlin (1969))

32. R.J. Roe, J.appl. Phys. 36.2024 (1965)

33. J.Jura and J.Pospiech, Textures 3, 1 (1978)

34. W. Truszkowski, J. Pospiech, J. Jura and B. Major, Proc.3 *e* me Coll.Europ '*e* en Surf Text. Pont- 'a-Mousson, France (1973).

35. K.H.Virnich,J.pospiech, A.Flemmer and K.Lü cke, Proc. Fifth Int. Conf.Text.1,129 (1978).

36. J. Hirch and K.Lü cke, Acta metal. 33, 1927 (1985).

37. J.Hirch and K.Lü cke, in Theoretical Methods of Texture Analysis (edited by H.J.Bunge), p.53. D.G.M., Oberursel(1987).

38. J.Hirsch and K.Lü cke, Acta metal. 36, 2863 (1988).

39. K.Lü cke, J.Pospiech, K.H. Virnich and J. Jura , Acta metal. 229, 167 (1981).

40. R.K.Ray : unpublished work